Delft University of Technology

Wind Energy Group, Faculty of Aerospace Engineering,
& Faculty of Electrical Engineering, Mathematics and Computer Science

to obtain the degree of Master of Science in Sustainable Energy Technology at Delft University of Technology

Modelling and Sizing of a Hybrid Power Plant using Airborne Wind Energy

Author:
Sweder Reuchlin

Student number:
4455673

TU Delft day to day supervisor:
Ir. Rishikesh Joshi

TU Delft professor:
Dr.-Ing. Roland Schmehl

TU Delft

An electronic version of this thesis is available at `http://repository.tudelft.nl/`

July 1, 2022

Modelling and Sizing of a Hybrid Power Plant using Airborne Wind Energy

Master Thesis by:	Sweder Reuchlin
Student Number:	4455673
Project Duration:	November, 2021 - July, 2022
Institution:	Delft University of Technology
Thesis Commitee:	Dr.-Ing. Roland Schmehl
	Dr. Hesan Ziar
	Ir. Rishikesh Joshi

Contact information
Author: Sweder Reuchlin
Email: sweder.reuchlin@gmail.com

Source of the picture on the title page: photo composite based on an image of Kitepower B.V.

Preface

This master thesis was written for the Sustainable Energy Technology master at Delft University of Technology. During my master's, I followed the autonomous profile, which includes wind energy, solar energy, and energy storage courses. In this thesis, all three subjects of the autonomous track came together. The topic of this thesis is of interest to anyone interested in one of the use cases of airborne wind energy and hybrid power plants. Readers who are particularly interested to see how the model works will find this in chapter 3. Readers who are more interested in the business case evaluation of the hybrid power plant can find this in chapter 5. The performance and cost data for the kite system are established in collaboration with Kitepower. Since many uncertainties are present in the cost calculations of the airborne wind energy systems, this specific data is not to be published in the MATLAB model; therefore, dummy numbers are provided in the code, uploaded on GitHub.

First and foremost, I would like to thank Roland and Rishi for giving me the opportunity to work on this exciting topic. When I look back on the last eight months, I am delighted to have worked so well together within the airborne wind energy group at the faculty of Aerospace Engineering. I would like to thank Rishi for all the times he was available for me and spar about ideas for improving my model and work, in particular. I had fun working with Rishi, and I enjoyed the last eight months of my study. Roland's enthusiasm about airborne wind energy got me excited about working in this field, which I knew little about a year ago. Moreover, I am looking forward to working with airborne wind energy in the future.

Next, I would like to thank the airborne wind energy group members who helped me develop ideas for my thesis. The biweekly meetings were precious to keep up with what the others were working on and get feedback on my work. The last person I would like to thank from Delft University of Technology is Hesan Ziar, who helped me by supervising my internship and is on my thesis committee. I experienced enjoyable cooperation with him during my internship period, where he helped me balance my internship's academic and business aspects. Moreover, I'm glad that some of my work during my internship is also used in my thesis.

Finally, I would like to thank my friends and family for the support they have given me throughout my time studying at the university. I am very grateful to my parents, who made it possible for me that I could go to university. I should be thankful to my friends for making my time at university such a pleasure, and I look forward to what the future holds.

Rotterdam, July 1, 2022

Sweder Reuchlin

Summary

In this thesis, a framework for modelling and sizing of a hybrid power plant (HPP) consisting of airborne wind energy (AWE) is developed in MATLAB. Much research is done into the development of AWE, but little is known about appropriate use cases. This research aims to investigate the use case of AWE in combination with solar energy, batteries, and a diesel generator. Multiple locations are evaluated to test the HPP. With different load, solar, and wind resource data, the HPP's components are sized accordingly, yielding the optimal levelized cost of electricity (LCoE).

Optimally sizing the combination of the four components of the HPP shows that the LCoE can be significantly decreased as opposed to the stand-alone system. The solar and wind resources complement each other in energy production, resulting in the system's battery capacity being reduced and the individual generating components being less oversized. The analysed location in Marseille shows a LCoE decrease of 42% compared to a HPP consisting only of solar energy and batteries. Comparing the HPP to a HPP consisting of AWE and batteries, the LCoE is reduced by 57%. With the addition of a diesel generator, the renewable status of the HPP is lost. However, the LCoE further decreases from 388 €/MWh to 281 €/MWh, making the HPP very competitive with diesel generators for off-grid situations.

The most significant advantage of AWE over conventional wind turbines is mobility. Since a 100 kW airborne wind energy system (AWES) fits in a 20 ft container, the whole HPP is easily transported and used in locations where temporary electricity is needed. Projects, where electricity is needed for only a few years would never look into using conventional wind turbines, but AWE could be the solution. Three sites in Africa and the Middle East are analysed, and the performance of the HPP is evaluated. AWESs are used at two of the three locations. The LCoE of all projects for the optimally sized HPP ranges between 109 and 169 €/MWh, making it highly competitive with diesel-generated systems.

This thesis lays the foundation for investigating the use of AWE in a HPP. The calculations are based on many assumptions. A sensitivity analysis is done to the most considerable uncertainties to include possible future price in-/decreases. With further research, optimal locations for the HPP can be found and investigated. Moreover, the HPP is now sized for the lowest LCoE, and an investigation into the green premium is done. By investigating more on this subject, other objectives can be set to evaluate the use of AWE in a HPP.

List of Symbols

Abbreviations

AM	air mass	
AOI	angle of incidence	[°]
AWE	airborne wind energy	
AWES	airborne wind energy system	
BoS	balance of system	
CF	capacity factor	
c-Si	crystalline silicon	
cov	covariance	
DGO	diesel generation optimisation	
DHI	diffuse horizontal irradiance	[W/m^2]
DNI	direct normal irradiance	[W/m^2]
ENTSOE-E	European network of transmission system operators for electricity	
FF	fill factor	
GHI	global horizontal irradiance	[W/m^2]
HPP	hybrid power plant	
IRR	internal rate of return	[%]
KPI	key performance indicator	
LCoE	levelized cost of electricity	[€/MWh]
O&M	operation and maintenance	
PV	photovoltaic	
SF	shading factor	
SVF	sky view factor	
STC	standard test conditions	
WS	wind speed	[m/s]

Latin letters

A	area	[m^2]
E	energy	[Wh]
D	demand	[Wh]
G	irradiance on a PV module	[W/m^2]
I	current	[A]
I_t	initial investment	[€]
M_t	annual costs	[€]
n	ideality factor	[-]
P	power	[W]
r	discount rate	[%]
T	temperature	[C]
T	transmittance of the module	[-]
V	voltage	[V]

Greek letters

α	absorption coefficient	[-]
η	efficiency	[%]
θ	tilt angle	[°]
κ	temperature dependency coefficient	[C^{-1}]
ρ	Pearson correlation coefficient	[-]
σ	standard deviation	[-]

Subscripts

a	ambient
dif	diffuse
dir	direct
M	module
mpp	maximum power point
NOCT	nominal operating cell temperature
oc	open-circuit
ref	reflected
sc	short-circuit
sys	system
Tot	total
u	u-direction
v	v-direction

Constants

k_B	Boltzmann constant (1.380649*10^{-23} J/K)
q	elementary charge (1.602*10^{-19} C)

Contents

1 Introduction

Airborne wind energy (AWE) is a method of wind energy generation which aims at reaching altitudes of up to 400 m, quadruple the hub height of the average offshore wind turbine in 2019 [1]. Reaching higher altitudes, the kites experience higher and more constant wind speeds, yielding a potentially higher annual energy production [2],[3]. The kites are connected to the base on the ground (the ground station) by a long tether, which can be used to conduct electricity. There are many different concepts regarding AWE, where the aircraft differ in size, shape, and method of electricity generation. There are two main principles of generating electricity using this new technology.

The first concept is Ground-Gen AWE, where, as the name implies, the electricity is generated on the ground using a generator. With this concept, there are two phases: the reel-out phase, which produces electricity, and the reel-in phase, which consumes electricity. During the reel-out phase, the kite flies in figures of eight higher and higher up in the sky. By gaining altitude, the kite exerts a tension force on the tether and, therefore, on the generator on the ground, see figure 1.1a. Once the kite reaches its highest point, it is reeled towards the base to go through the cycle of reeling out and reeling in again [4]. In this cycle, called the pumping cycle, more energy is generated during the reel-out phase than is consumed during the reel-in phase.

The second concept is the so-called Fly-Gen AWE. Instead of generating the electricity on the ground, the electricity is generated using a/multiple generator(s) attached to the kite in the air. At higher altitudes, the wind is stronger and more consistent, resulting in a higher energy yield than at the hub height of a conventional wind turbine. This electricity is then transmitted to the ground using a special tether which can conduct the generated electricity to the ground [4], see figure 1.1b. A different electricity yield can be achieved by varying the kite's altitude.

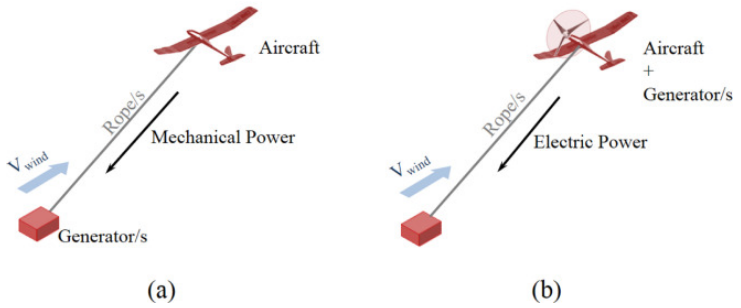

Figure 1.1: Two different concepts of AWE: Ground-Gen on the left (a), Fly-Gen on the right (b) [4].

This fast-developing technology is still in the research and development phase, and AWE's use case is uncharted territory. Moreover, compared to conventional wind turbines, airborne wind energy systems (AWESs) require significantly less material [5]. Another key argument to choose AWESs over conventional wind turbines is that AWESs have significantly higher mobility. This increased mobility makes it possible to generate electricity from wind energy for a relatively short period of time, and could therefore perfectly used in temporary micro-grids.

The daily cycles of the solar and wind resources are (somewhat) complementary worldwide [6]. This motivates the investigation of a hybrid power plant (HPP) consisting of wind and solar energy generation. A HPP aims to balance the strengths and weaknesses of different energy generation sources to have a more constant energy production, and reduce the battery capacity. A photo composite of a HPP using AWE and solar energy is given in figure 1.2. By investigating this concept, this fast-developing technology's use case can be demonstrated.

This research aims to model and size a HPP consisting of AWE and evaluate the results. The model is made using MATLAB and is used to evaluate the sizing of the components of the HPP for different locations with their corresponding wind, solar, and load data. Before the HPP is sized, a location analysis is done to check the (anti-)correlation between the resources and the load. The levelized cost of electricity (LCoE) is calculated for the optimally sized HPP and used to evaluate the use case of a HPP for that specific location. Three business case locations where electricity is currently produced solely by diesel generators are analysed, and the value of the HPP is evaluated.

The report will be presented in the following structure. Chapter 2 provides the problem analysis through a literature study, the research questions, and the methodology. The explanation of how the MATLAB model is developed is given in chapter 3. The results and evaluation of the model are located in chapter 4. The use of the model is given in chapter 5, where three different locations are evaluated in a business case. In the final chapter, chapter 6, the key takeaways of the research are concluded.

Figure 1.2: A photo composite of a HPP plant with solar PV and the Kitepower Falcon on a test site in Aruba [7].

2 Problem Analysis

In this chapter, the research gap is analysed. The first section, section 2.1, is the literature review, explaining the different components of the hybrid power plant (HPP) and its architecture. Following the literature review, the research questions are formulated in section 2.2. Finally, in section 2.3, the methodology of the research is explained.

2.1 Literature Review

In this section, the concept of a HPP and its architecture is first explained, followed by a literature study of the HPP's four components: airborne wind energy (AWE), solar energy, battery storage, and diesel generation.

2.1.1 Hybrid Power Plants

A HPP is a combination of two (often renewable) energy sources, frequently combined with a storage solution. By combining two different energy generating units, cost competitiveness can come from value synergies through shared infrastructure and shared operation & maintenance (O&M) costs. Since a HPP often consists of two renewable energy sources dependent on uncontrollable energy sources, a storage solution in a stand-alone system to cover for the intermittency in electricity generation is needed [8]. When the HPP is connected to the main electricity grid, however, energy storage does not need to be considered because the electricity regulation in the grid can be done by controllable electricity generating units like, for example, a gas-fired power plant.

This research investigates the combination of wind and solar energy resources and a storage solution. In addition, the use of diesel generators will be analysed to see if they can be a valuable component of the HPP. The concept of a HPP is not new, as can be seen by the development of HPPs worldwide [9]. However, to the best of the author's knowledge, a HPP using AWE is not researched before.

The motivation behind combining wind and solar energy as electricity generation resources comes from the fact that there is an anti-correlation between the wind speed and solar irradiance on both a daily and a seasonal scale. Wind speeds tend to be stronger during the winter due to uneven heating of the earth's surface [10], which results in a higher electricity yield from wind energy generation in winter. During the summer, solar irradiance on the earth's surface is stronger and therefore yields a higher electricity generation from solar photovoltaic (PV) modules, see figure 2.1. When the two generating components of the HPP are correctly sized, a more constant electricity power production throughout the year can be expected.

On a daily scale, intermittency in electricity generation is also expected. Electricity generated through solar energy can only be generated between sunrise and sunset. Wind speeds are not constant throughout the day either, and they tend to be the strongest at the height of 10 meters in the early afternoon, while at the height of 200 meters, wind speeds are strongest between midnight and sunrise [11]. The electricity demand can hardly ever follow this intermittency in electricity production. Therefore, using a storage solution will help tackle this generation's intermittency on a daily scale. See figure 2.2 for the daily energy demand and generation with wind and solar as energy sources.

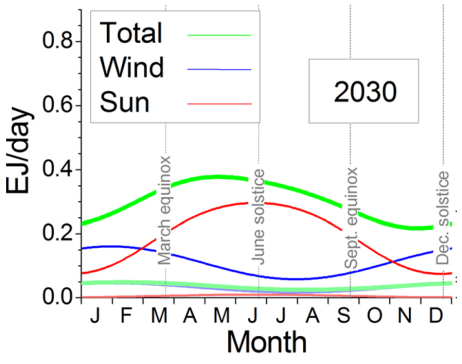

Figure 2.1: Seasonal energy generation variation [12].

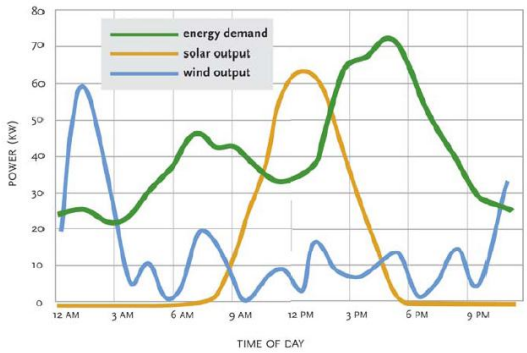

Figure 2.2: Daily energy generation variation [13].

The different components of the HPP are in off-grid applications interconnected in a DC-microgrid. Some of the advantages of using a DC grid over an AC grid are: that the control of the energy in the system generation is more easily done, and the overall costs of the grid are cheaper [8]. DC-loads can be directly connected to the grid, whereas AC-loads first need an inverter. The complete analysis of the best type of grid and configuration is outside the project's scope. For this research, it is assumed that all the different electricity generators generate DC electricity. Which holds for solar PV modules and diesel generators. Because, diesel generators can produce either AC or DC electricity [14], depending on their application. For AWE, it is considered that a converter is used.

An illustration of a HPP architecture is given in figure 2.3. In this figure, within the green square, the different electricity generation types and the battery are illustrated. From left to right and from top to bottom: AWE, diesel generator, solar PV, and battery. A control unit optimises the dispatch of electricity based on the wind and solar as well as the price forecast. The illustration shows the HPP connected to the grid. For an off-grid scenario, the substation and the grid icons would be replaced by the load directly.

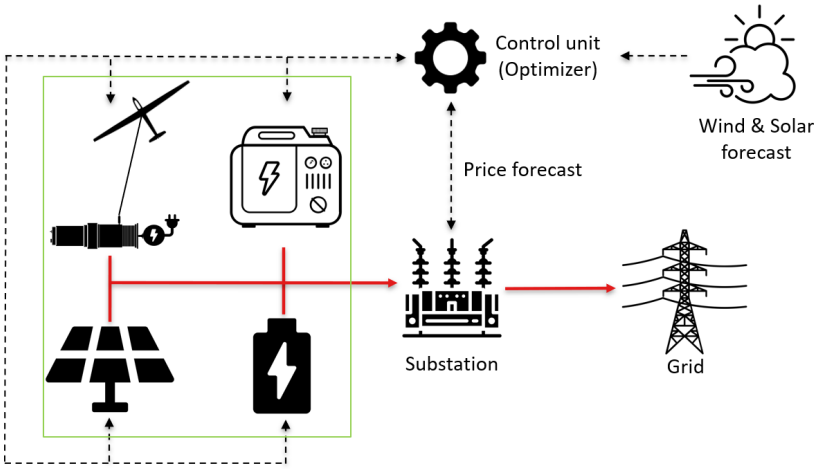

Figure 2.3: A possible architecture of a hybrid power plant. Icons from: [15]

The use of airborne wind energy in a micro-grid is discussed in literature, as done by R. de la Garza Cuevas [16]. The research introduces the idea to use airborne wind energy systems (AWESs) for off-grid communities or camps. The research indicates that one of the key conclusions would be to focus on the sizing of the storage system in the micro-grid. Moreover, it recommends to use superconducting magnetic energy storage as storage solution.

The use-case of HPP in off-grid locations is further expanded in this thesis research. The HPP consists of two more components than just the AWES and storage solution; solar modules and a diesel generator are considered as well. By introducing these two additional electricity generation methods, the whole micro-grid doesn't rely on just one source of electricity generation, making it more robust and driving LCoE further down.

One of the most important focus points is to appropriately size the storage solution. In this research, the trade-off between generated electricity curtailment and the size of the storage solution is carefully evaluated. On the contrary of the recommendation to use magnetic energy storage, this thesis use Lithium batteries as storage solution, which is explained in section 2.1.4. In favour of using Lithium batteries, the storage solution could be used to mitigate long-term energy variations [16].

2.1.2 Airborne Wind Energy

The most commonly used and studied AWESs concept is the Ground-Gen pumping kite power. Therefore, this thesis considers the pumping cycle AWE as the wind resource component of the HPP. There are two types of kites: either a soft kite or a fixed-wing kite. Both types work following the same principle. However, there are a few slight differences. This research uses data from the Kitepower Falcon 100 kW, a soft kite [7] image shown in figure 2.4.

Figure 2.4: The Kitepower Falcon on a test site in Aruba with a couple of wind turbines in the background [7].

Advantages
Unlike conventional wind turbines, AWESs will have a few distinct advantages. The first advantage is that AWESs will have significantly higher capacity factors than traditional wind turbines since the kites can reach higher altitudes and more constant and stronger wind speeds [17]. Adjusting the height of operation for the varying wind speeds makes the kites always find the optimum operation height and can therefore maximise the potential energy yield [2].

The second advantage of AWESs is that the systems will require less material than wind turbines. Not only for the construction of the kite is less material needed, but also fewer bending moments on the foundation are exerted, resulting in less material needed for the foundation [18]. With the rise of the demand for green electricity, more and more steel and concrete are required to build wind turbines. Looking into renewable energy technologies that still use wind energy but require fewer raw materials will be of great importance in the future [19].

The third advantage of AWESs is that the system will be very portable. The Kitepower Falcon [7] is a 100 kW AWES which can fit entirely in a 20 ft container. In contrast to wind turbines, the AWES can be used for some time in one place, quickly packed up and then used at another location. This comes in handy in a stand-alone system set up for locations where temporary electricity is needed, for example, a military camp.

Finally, the lifetime of the kite is 4,000 hours, as can be seen in appendix B. This means that if the AWES is in operation 7,000 - 8,000 hours per year, the kite has to be replaced twice. On the other hand, the lifetime of the ground station is 25 years. At the start of the project, only one kite needs to be bought in order to get the AWES up and running. By replacing the kites over the lifetime of the ground station, the initial investment cost are reduced and the costs for replacing a new kite every two years are discounted.

The value of airborne wind energy
In literature, AWESs are compared to conventional wind turbines to investigate the added value to the electricity system, as done in the research by E. Malz et al. [20]. In this research, the economic value of AWESs in future electricity systems is evaluated. This research concludes that the total share of wind energy is barely affected by the introduction of AWESs since they will replace traditional wind turbines. According to the research, in locations with good wind conditions, the AWESs will not replace the wind turbines in the future. Whereas, the locations with poor wind resource, the research proposes a use for the AWESs.

In this thesis research, a whole different aspect of the use-case of AWE is investigated. Where the research of E. Malz et al. focuses on replacing wind turbines, this thesis gives new insights in the use of AWE as a method of electricity generation in a HPP. More specifically, the AWESs add value to HPPs due to the mobility of the system, resulting in new aspects of use-cases in temporary micro-grids. Wind turbines cannot be considered to be used in temporary micro-grids since the lifetime of the turbines often exceeds the lifetime of the project where the electricity is demanded.

This research proposes to investigate the use-case of AWESs beyond the locations where traditional wind turbines are installed. Locations other than temporary micro-grids that could be considered are sites where the public perception prefers to use AWESs over wind turbines. Moreover, off-shore foundations of decommissioned wind turbines could be of interest for future AWESs. By playing into the above mentioned advantages of the AWESs, future use of AWESs can be expected which will result in significant contribution of AWE in the total share of wind energy.

2.1.3 Solar Energy

The second source of electricity generation in the HPP is done with solar energy. The working principle of this technology is based on the photovoltaic effect, see figure 2.5. A solar PV module consists of two (or more) materials that form a junction. When solar radiation hits a PV module (1), photons are absorbed in the junction where charge carriers, an electron and a hole, are generated (2). The photo-generated charge carriers are then separated in the junction (3). The charge carriers are collected at the terminals of the junction, where the electrons will pass through a circuit (4) and recombine with the holes (5) [21].

Solar radiation comprises three components: direct, diffuse and reflected radiation [22], as illustrated in fig. 2.6. The direct radiation is radiation that directly falls on the solar module. Diffuse radiation comes from sunlight that gets refracted through particles in the air or clouds. The reflected radiation is sunlight that gets reflected off the earth's surface.

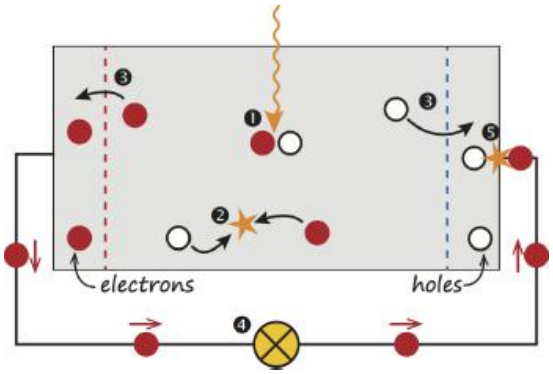

Figure 2.5: A schematic model of a solar cell [21].

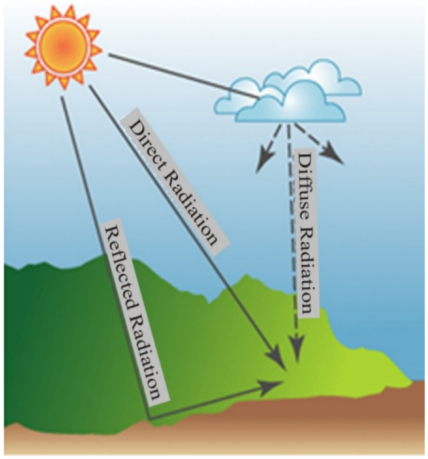

Figure 2.6: The three components of solar radiation [22].

Two main factors affect the efficiency of the solar modules. The first factor is that solar modules are dependent on temperature. The warmer the module becomes, the lower the efficiency of the model. The opposite is valid for when the module becomes colder. A solar module is tested under standard test conditions (STC), which means that the irradiance is equal to 1000 W/m^2, the temperature is 25°C, and a sea-level air mass (AM) of 1.5. The module's efficiency is given for at STC. Therefore, when the modules are colder than 25°C, which often happens during winter, the energy conversion efficiency is higher than at 25°C. Again, the opposite is valid for when the modules are warmer than 25°C. The more in-depth explanation and calculations with this concept are given in section 3.3.3.

The second effect on the efficiency of the solar modules is the effect that the irradiance has on the module. This effect on the efficiency is weaker than the effect of the temperature, but it still needs to be considered. A solar module is tested under STC with an irradiance level of 1000 W/m^2. The irradiance is seldom equal to precisely 1000 W/m^2. Therefore, the efficiency of the module is different at every irradiance level. The concept behind this effect is more complicated than the temperature dependency and will be elaborated on in section 3.3.4.

2.1.4 Battery System

A storage solution has to be considered when the HPP is used in an off-grid configuration. The ancillary services the battery could perform in a grid-connected configuration are outside of this project's scope. Therefore only in an off-grid situation will batteries play a role.

The primary use of the batteries will be to cover the daily intermittency in electricity generation, so-called short-term storage. The goal of the storage solution is to store energy when there is an energy surplus in the system and provide energy to the system when not enough energy is generated to meet demand.

In this research, Lithium batteries are considered because a movement in the industry towards this type can be seen, with for example the Tesla Powerpacks [23]. In this thesis, no specific battery system is considered. The sizing of the battery system is very variable throughout the whole project and is therefore sized as capacity rather than integers of a specific kind of one battery size. The use of superconducting magnetic energy storage, as recommended by [16], is not considered since the HPP will be used in hot environments and refrigeration costs are high [24].

Some assumptions of the battery specifications have been made and are given in table 2.1. NREL estimates the storage cost of the battery as 198 $/kWh (or 182 €/kWh) in 2030 [25]. A conversion rate of dollar to euro of 1:0.92 is considered in this thesis. The year 2030 is considered because AWE technology is still in the research and development phase and is expected to be market-ready by 2030. Typical round-trip efficiencies and state of charge limits for lithium-ion batteries are 90% and 10-100%. The lifetime of such a utility-scale battery storage system is determined to be ten years, which corresponds to a cycle life of 10,000 cycles [26].

Table 2.1: An overview of the battery specifications.

Battery Assumptions	
Type	Lithium-ion
Energy storage cost	182 €/kWh
Round-trip efficiency	90 %
State of charge limits	10-100 %
Cycle life	10,000
Lifetime	10 years

2.1.5 Diesel Generators

In most off-grid locations where electricity is necessary, diesel generators are used. These generators produce electricity by burning diesel in a diesel engine, which drives the electricity generator. This research will be interesting to see how the hybrid power plant can perform against these diesel generators for off-grid locations or if diesel generators could be used to generate electricity as a component of the HPP.

Wind and solar energy are uncontrollable energy resources. This means that generating a specific amount of electricity at a particular time is difficult/near impossible to do without using a battery. Diesel generators are a controllable electricity generation source. This makes it possible that the demand can be very closely matched by ramping up and down the electricity generation when desired.

A diesel generator will use about 0.4 litres to produce one kWh of electricity [27]. The average diesel price in the Netherlands in 2021 was 1.37 €/L [28]. The initial investment cost of diesel generators is around 600 €/kW of installed power [29]. For the investment cost of diesel, no learning curves are applied since the technology is very mature. The expected lifetime of a diesel generator is assumed to be 25 years [30]. Following the simple formula of the multiplication of the energy density by the price per litre, a cost per kWh can be determined of 0.548 €/kWh produced.

The burning of diesel produces carbon dioxide (CO_2) emissions. The European Union has introduced the carbon tax to reduce carbon emissions in Europe. This tax aims to make burning fossil fuels steadily more expensive, making green solutions more attractive, with the final goal to have zero emissions by 2057 [31]. Industrial companies can still burn fossil fuels when they use carbon permits which are traded at the emission trade system (ETS). In 2021, the carbon tax in the Netherlands was 30 €/tonne CO_2 [32].

Over the coming years, the carbon tax is projected to rise to 125 €/tonne in 2030 [33]. This means that not only the cost of fuel but also the cost of CO_2 emission should be considered in the calculation of the electricity price for diesel generation in Europe. With the burning of one litre of diesel, 2.6 kg CO_2 is released into the air [27]. This means that by generating one kWh of electricity, 1.04 kg CO_2 is released into the air, which results in an extra cost of 0.13 €/kWh. The total cost of generating one kWh of electricity becomes 0.678 €/kWh. The diesel price prediction for the future is outside this project's scope. Moreover, the price varies per country and is dependent on how easily the fuel is available. To not over-complicate these factors, the Dutch price of diesel in 2021 is considered for calculations within Europe. However, later in the research, a sensitivity analysis of the diesel price will be done to incorporate potential price increases or decreases.

2.2 Research Questions

Following the literature research, research gap was analyse and five research questions were formulated. All five of these research questions are answered in this research:

1. What are the possible architectures and components of hybrid power plants using airborne wind energy?
2. What is the added value of airborne wind energy in a hybrid power plant?
3. How are wind speed and solar irradiance correlated on an hourly and daily resolution?
4. How are hybrid power plants different for off-grid compared to grid-connected locations?
5. How does the sizing of the components change when setting different objectives?

2.3 Methodology

To answer the research questions, given in section 2.2, a model of the HPP is made in MATLAB. This model uses wind and solar resource data, load data, and diesel generation data to determine the optimal capacity of each of the components of the HPP for the set objective. By making a model in MATLAB, many different configurations are tested, and components of the system can be easily swapped for other components.

After the model is made, different resource data are put in the model. This way, other locations and different load cases can be compared and evaluated. Since most of the model's outputs are based on theoretical formulas, the outcomes have different results than a real-life situation would yield. However, when the assumptions are kept within a certainty range, the results can be interpreted to understand what it would look like in a real-life situation.

To include this uncertainty of the input variables within the model, a sensitivity analysis is made of the HPP model's most important/variable components. This way, results from the model outputs and conclusions are drawn and evaluated.

This research aims to make it possible for the HPP to be tested in any location around the world. Therefore, the model needs to be adaptable for different input variables, which are location dependent. In chapter 3, the structure of the model is explained, based on one location in Europe with high wind and solar irradiance. Chapter 4 will interpret and evaluate the results of the model of chapter 3. To illustrate the use of the model, in chapter 5, real-life cases are tested and evaluated to investigate the use of HPPs in real-life situations.

3 Model Development

This chapter explains how the model is developed and the calculations which lead to the final results. In section 3.1, the flowchart of the model is explained and shown. Before any calculations are done, the location of the HPP is analysed in section 3.2. The performance and cost modelling of the solar and wind energy is done in section 3.3 and section 3.4, respectively. The components of the hybrid power plant (HPP) are sized based on the load data, which is found in section 3.5. When the load data and the annual energy production of the components of the HPP are known, the battery is sized in section 3.6. The final element of the HPP is the diesel generator, analysed in section 3.7. Finally, the HPP is optimally sized using a system optimiser, explained in section 3.8. The MATLAB model will be made available on the author's GitHub page: `https://github.com/SwederReuchlin`.

3.1 Flowchart of the Model of the Hybrid Power Plant

The flowchart of the HPP model, given in figure 3.1, shows how from the input data, the desired output data is acquired. The flowchart consists of two separate calculation flows. The top part represents how to calculate the Pearson correlation coefficients. These coefficients indicate how strong two data sets are correlated, as is explained in section 3.2. The bottom part of the flowchart represents the key performance indicators (KPIs) calculation.

The bottom part of the flowchart is where the performance and cost of the airborne wind energy system (AWES) and the solar photovoltaic (PV) system are calculated based on the wind and solar data. Based on the performance and cost of both methods of generating electricity, the load data, diesel data, and the business case, the capacity of the batteries is sized. Here, there is an iteration loop with respect to the levelized cost of electricity (LCoE). There is a trade-off between the capacity of the batteries and the use of diesel generators. Once the batteries are sized, the model puts out the KPIs to be evaluated.

The calculation of the battery capacity works as follows. The hourly energy generated by the HPP is the sum of the AWES and the solar PV system for each hour. The mismatch between generation and demand is calculated by subtracting the hourly load data from the hourly generation data. When the generation is bigger than the demand, the batteries are charged. The opposite happens when the demand is bigger than the generation. By setting the battery capacity in the beginning to zero, the absolute minimum point in the battery capacity will be the battery's capacity for the next iteration. The battery's capacity is further increased to make sure that the capacity stays above the minimum state of charge for any given hour. Now, the battery capacity will not be lower than the minimum state of charge, resulting in the electricity demand being met at any time point.

It is not always desired to size for the minimum capacity of the battery, i.e. the demand is bigger than the generation for a long period of time. These cases can be very extreme and what will happen is that the battery or other components of the HPP are significantly oversized, resulting in a very high LCoE. By introducing the loss of load, a certain percentage of electricity demand will not be met. For example, if the loss of load is equal to 5%, 95% of the electricity demand will be delivered by the HPP, and 5% is lost.

In an off-grid system, where all demand needs to be supplied by the HPP, the loss of load cannot be zero. The components of the HPP are sized to generate all the demanded electricity. Since both generation methods rely on uncontrollable energy sources, the HPP's components are sized to supply the peak in electricity generation mismatch. Oversizing the components means that a lot of power is curtailed and the battery capacity is sized for the most extreme period in which the demand is cumulatively greater than the supply, for a substantial time period. To prevent oversizing the components of the HPP, a diesel generator is used to generate the electricity for these extreme periods. The diesel generator is used when the mismatch is less than zero, while the renewable generation methods of the HPP are used when the mismatch is greater than zero. What follows is that there is now a trade-off between the size of the diesel generator and the size of the batteries, which is again iterated.

The HPP is optimised using a loop which puts in new values for the AWE capacity (the number of kites), the solar PV capacity (the number of modules), and the loss of load. This is done by setting, in a different script, discrete variables for the inputs of the model. In every loop, the LCoE of a different combination of the three variables is calculated and stored. Once all variable combinations have been through the model, the optimal capacity of the components of the system with the corresponding LCoE is found.

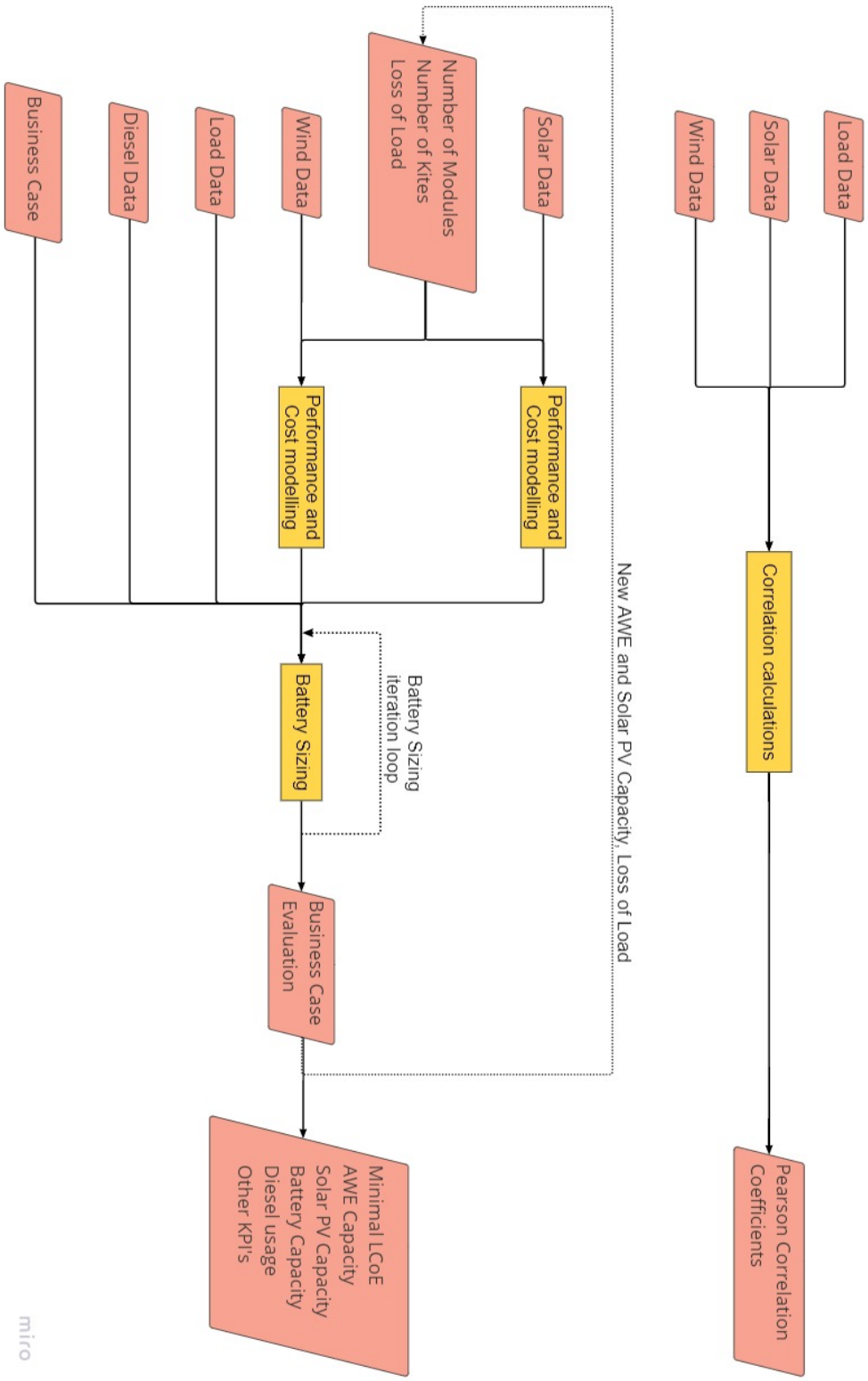

Figure 3.1: The flowchart of the hybrid power plant model.

3.2 Resource Analysis

The solar and wind resources are analysed in this section. First, a location analysis is done by evaluating the wind and solar resources and picking suitable locations for the HPP in Europe. Then, the Pearson correlation coefficients are calculated for the resources and the load data of the specific locations.

3.2.1 Location Analysis

As was illustrated in the flowchart of section 3.1, the first step in modelling and sizing the HPP is to find suitable locations by comparing the Pearson correlation coefficients. To illustrate how the locations are evaluated for a real-life case, four different locations throughout Europe are chosen. The reason locations in Europe are chosen is that the wind and solar resources and load data can be easily acquired.

The optimal location for a HPP, consisting of both wind and solar energy, is a location with high wind speeds and solar irradiance. Locations with high wind speeds at 200 meters and high solar irradiance are the locations of interest, so-called hot spots. Moreover, hot spots should also show a strong anti-correlation between the two resource data sets. As the first step in finding these hot spots, both the map of the global solar atlas [34] and the map of the global wind atlas [35] are investigated; see figure 3.2 and figure 3.3 respectively.

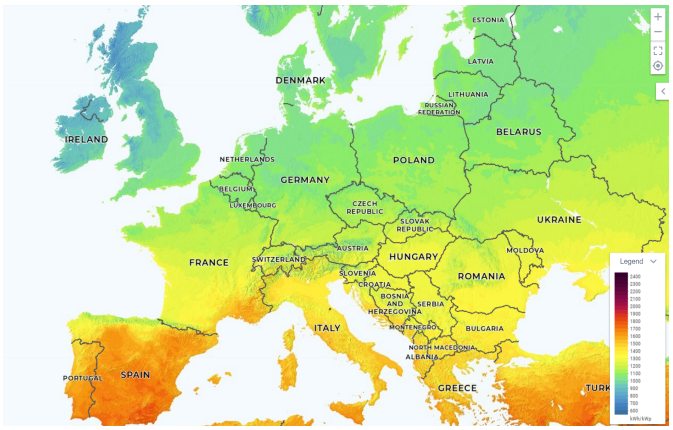

Figure 3.2: The map of Europe showing the solar radiation [34].

From figure 3.2, it can be seen that in the south of Europe, there is the highest solar radiation intensity. Especially the more inland regions in Spain and Turkey have very high solar irradiance. Concerning the wind speeds in figure 3.3, it can be seen that in coastal areas, the wind speeds are the strongest.

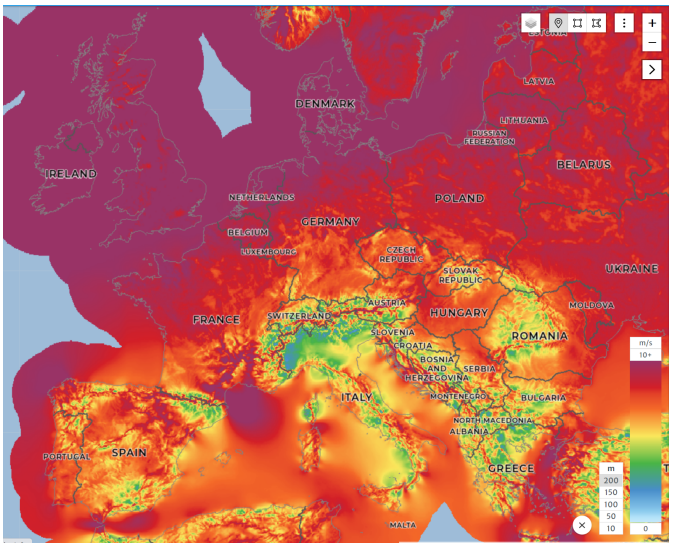

Figure 3.3: The map of Europe showing the wind speeds at 200 m altitude [35].

To test the model, different locations with different characteristics are chosen. These chosen locations act as extreme conditions, combining both high and low irradiance and/or wind speed. This results in four possible combinations of low-low, high-low, low-high and high-high wind speed and irradiance. By overlaying the maps of the global wind and solar atlas, these locations with a different combination of wind speed and irradiance are picked. The following four sites are selected and shown in figure 3.4:

- A: Salzburg, Austria
- B: Dublin, Ireland
- C: Granada, Spain
- D: Marseille, France

Figure 3.4: The map of Europe showing the five chosen locations.

In table 3.1, the location, wind speed and the global horizontal irradiance (GHI) are given for the four sites. As can be seen, each location has a different combination of high or low wind speed and solar irradiance. In the next section, the Pearson correlation coefficients will be calculated to evaluate the correlation between the wind speed, irradiance, and load data of each location.

Table 3.1: Location, wind speed and Global Horizontal Irradiance data.

	Wind	**Solar**	**Location**	**Latitude**	**Longitude**	**Wind Speed [m/s]**	**GHI [kWh/m^2/year]**
A	low	low	Salzburg	47.8	13.0	4.92	1175.7
B	high	low	Dublin	53.3	-6.26	9.37	952.8
C	low	high	Granada	37.2	-3.58	3.02	1879.7
D	high	high	Marseille	43.3	5.37	8.26	1619.0

3.2.2 Pearson Correlation Coefficients

For each of the four locations, chosen in section 3.2.1, the hourly wind speed, GHI, and load data for the years 2017-2019 are acquired. Before calculating the Pearson correlation coefficients, the trend lines of the corresponding data are created. These trend lines are produced using the long-term trend of the additive decomposition function of MATLAB, trenddecomp. This function breaks the data into a long-term trend, a seasonal or oscillatory trend, and a remainder. The addition of these three components returns the original data set.

The trend lines of the four locations for the wind speed are given in figure 3.5. As expected, it can be seen, that the wind speed in Dublin and Marseille are high, and the wind speed in Salzburg and Granada are meagre. Moreover, it is clear from the locations with higher wind speeds that the trend shows that the wind speeds are higher during the winter than during the summer on a seasonal resolution.

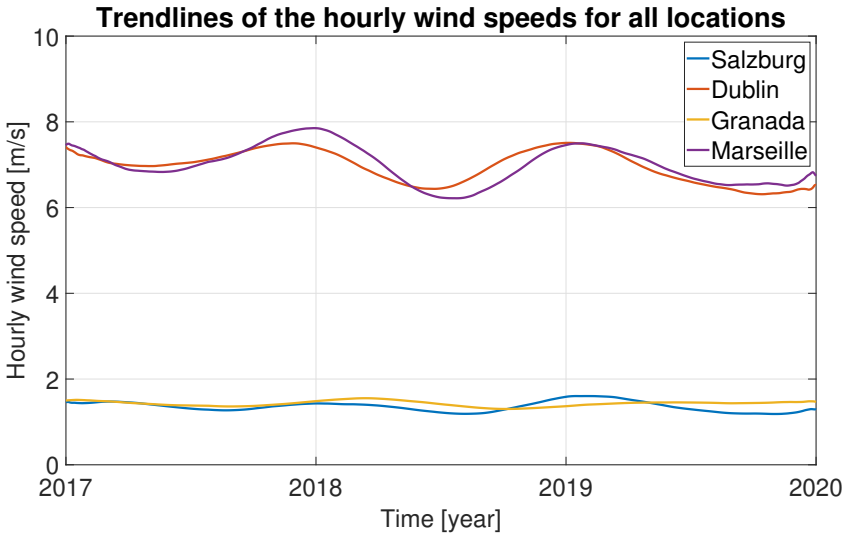

Figure 3.5: The trend lines of the hourly wind speed for all four locations.

When looking at the GHI of the four locations, it can be seen that the trend lines in figure 3.6 are closer together. This is because, as opposed to the strong dispersion in the wind data, the solar data in Europe are still relatively close to each other. Although the four data sets are close to each other, it can still be seen that there are two locations with high solar irradiance (Granada and Marseille) and two locations with low irradiance (Salzburg and Dublin). Moreover, what follows from the figure is that for all four locations, a clear seasonal trend is shown. This trend shows peaks in the GHI during the middle of the year (i.e. summer) and dips during the winter periods.

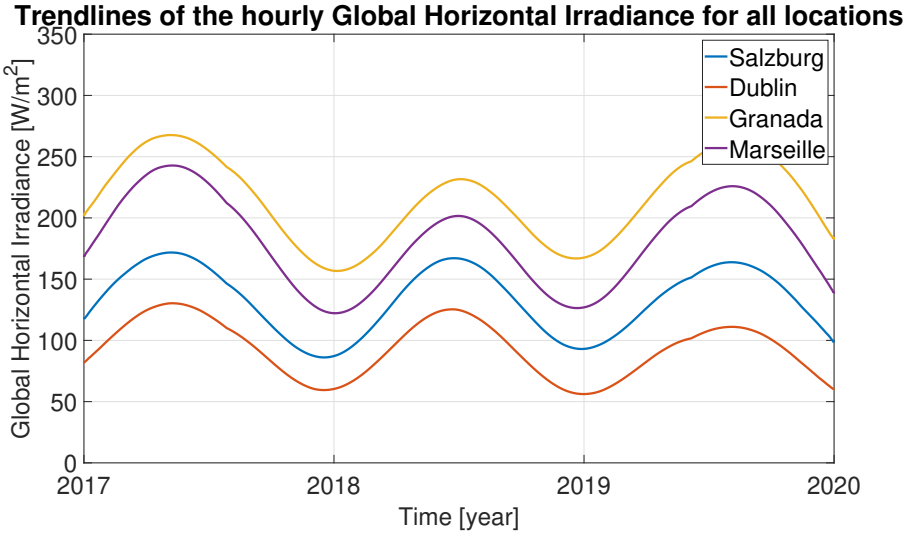

Figure 3.6: The trend lines of the hourly global horizontal irradiance for all four locations.

The (anti-)correlation between the wind and solar resource for all four locations is shown graphically in figure 3.7. The scales on the y-axis for both the wind speed (WS) and the GHI differ from site to site. What can be seen is that, especially in Marseille, there is, graphically, a strong anti-correlation between wind and solar resources on a yearly resolution. It is essential to first look at the long-term trends in the resource data sets to get a feeling of what the numbers represent before calculating the hourly and daily Pearson correlation coefficients.

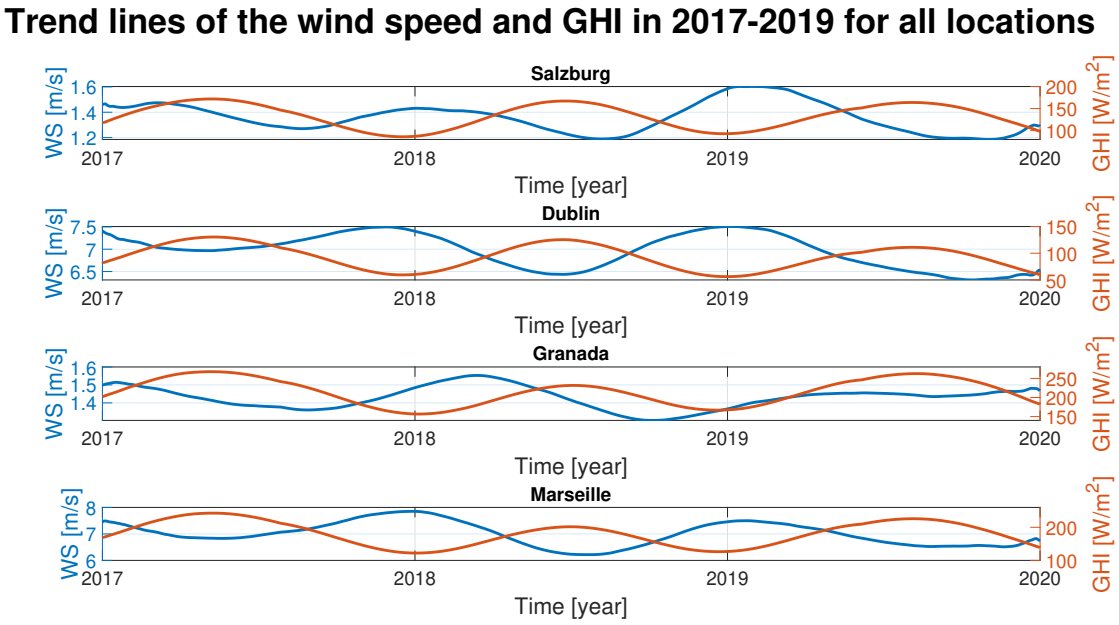

Figure 3.7: Trend lines of wind speed and global horizontal irradiance in 2017-2019 for all four locations.

The Pearson correlation coefficient (ρ) measures the correlation between two data sets and ranges from -1 to 1. A perfect anti-correlation between the two sets of data is equal to -1, whereas a perfect correlation has a value of 1. For the HPP, a strong anti-correlation between the two different resources is desired. Moreover, a strong correlation is desired when looking at the resource and the load. This way, the renewable energy generator would supply a significant part of the load directly without using big batteries.

The Pearson correlation coefficient is calculated using equation (3.1). The covariance (cov) of data sets X and Y are divided by the standard deviation of both X and Y, σ_X and σ_Y, respectively.

$$\rho = \frac{cov(X,Y)}{\sigma_X \sigma_Y} \tag{3.1}$$

The Pearson correlation coefficient is calculated for all the locations on an hourly and daily resolution. For the hourly correlation coefficients, the hourly data is used in equation (3.1). The Pearson correlation coefficients for the daily resolution are calculated by using the summation of the data of each hour of the day. First the resource data is summed up per 24 hours. This yields, for example, the total irradiance during a day, indicating the irradiance level of that day compared to the other days in the three year period. The same is done for the wind resource and the load data. A day with a lot of wind, is indicated by the summation of the wind speeds of that day compared to the other days. The Pearson correlation coefficients for the daily resolution are then calculated using the daily summed up resource and load data, which is used in equation (3.1).

The results of the calculations are given in table 3.2. What stands out is the strong anti-correlation between wind and solar on a daily resolution in Dublin. This means that the battery can be smaller sized over a more extended period. Moreover, Granada and Salzburg have a similar anti-correlation daily between wind and solar. Granada's correlation between load and solar is noticeable on an hourly resolution. This probably has to do with air-conditioning being used during the day, which consumes much electricity. Marseille's strongest anti-correlation is on a daily resolution between load and solar. This means that on days that there is a lot of solar irradiance, not much electricity is used and the other way round. Resulting in a need to oversize the solar modules or use more kites and a bigger battery capacity.

In contrast to what was seen on the trend of the yearly resolution in figure 3.7, the anti-correlation between the wind and solar resources on an hourly and daily resolution isn't as strong as expected. This means that for shared infrastructure, these locations are not ideal. Moreover, the resources do not complement each other as strongly, resulting in the oversizing of the components later on in the HPP.

Table 3.2: Table showing the Pearson correlation coefficients for all four locations on an hourly and daily resolution.

Location	Resolution	Load & Solar	Load & Wind	Wind & Solar
Salzburg	hourly	0.08	-0.01	-0.08
	daily	-0.01	-0.01	-0.31
Dublin	hourly	-0.08	-0.04	-0.12
	daily	0.07	-0.05	-0.39
Granada	hourly	0.32	0.19	0.15
	daily	-0.12	0.05	-0.33
Marseille	hourly	-0.08	0.17	-0.13
	daily	-0.65	0.20	-0.21

In this section, different locations were identified and chosen based on their availability of resources. It can be seen that although the resources show very different strengths in resource availability, their (anti-)correlation was still disappointing. However, in this research, Marseille is chosen as the location to do further calculations. Marseille is the most sensible choice considering the high availability of wind and solar resources. Moreover, the load data for locations in Europe is easily accessible. Finding the optimal hot spots for a HPP is outside the scope of this research.

3.3 Solar Energy - Performance and Cost Modelling

This section analyses the performance and cost of the solar energy component of the HPP. After the system's energy production and cost are evaluated, the LCoE is calculated for a grid-connected case. This section concludes with a reflection on the calculations regarding solar energy. The data sheet of the used solar module can be found in appendix A.

3.3.1 Annual Energy Production

The AEP is the first step in indicating the performance of an energy system. The AEP shows how much energy is yearly produced by the system, which later is used to determine the LCoE. The first step in calculating the AEP for solar energy is downloading the irradiance data. Next, solar modules depend on temperature and irradiance intensity which influence the efficiency and, therefore, the overall energy yield. When the energy produced by one module is determined, the energy produced by a whole system of thousands of modules needs to be determined next. This is done by multiplying the number of modules in a system and considering the system's efficiency. The AEP for a solar energy system is determined when this is done.

3.3.2 Irradiance Calculations

To calculate the three irradiance components mentioned in section 2.1.3, the diffuse horizontal irradiance (DHI), direct normal irradiance (DNI), and the global horizontal irradiance (GHI) need to be downloaded. The data can be found and downloaded for any location in Europe from 2017-2019 from the NREL database [36].

The three different hourly solar irradiance components are given for the second of January in figure 3.8 and the second of August figure 3.9. As can be seen from these figures, the irradiance on the day in summer is stronger and more constant than the irradiance during the winter. Moreover, in contrast with the figure on the right-hand side, the solar irradiance on the left-hand side is not smooth. This has to do with the fact that the second of January was a very cloudy day, whereas there was a clear sky on the second of August.

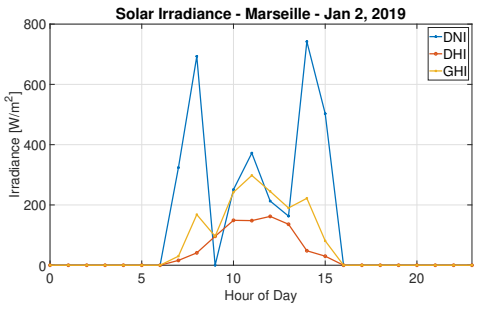

Figure 3.8: Solar Irradiance on January 2, 2019.

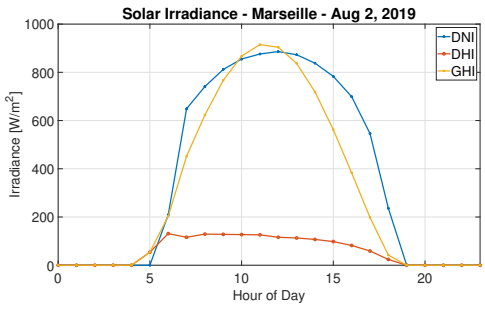

Figure 3.9: Solar Irradiance on August 2, 2019.

Before the direct, diffuse, and reflected irradiance on the module can be calculated, the shading factor (SF), sky view factor (SVF), and angle of incidence (AOI) need to be determined. The optimal tilt angle (θ_M) for solar modules in France is found in the literature to be around 30°[37]. By placing the solar modules at this angle, the yearly energy yield increases by about 4%. However, since the modules will be put in multiple rows and columns, inter-shading between the different modules causes a decrease in energy production if the modules are not placed far enough apart. Increasing the distance in-between the modules results in a reduction of power produced per area since the increase in energy produced is limited while the area increases. Adding the optimal tilt angle will significantly increase the complexity of the energy production estimations for only a slight increase in energy yield. Moreover, the optimal tilt angle would need to be determined and adjusted for each location. Therefore, finding and using the optimal tilt angle and distance in-between the solar modules is considered outside the scope of this thesis, although it is adjustable in the MATLAB model.

It is assumed that the hybrid power plant will be built in an open field with no buildings in the area. Therefore, the shading factor imposed on the solar modules by obstacles can be neglected. The soil of the open field is grass which means that the albedo necessary to calculate the reflected irradiance equals 0.19 [38]. The SVF is the fraction of the visible sky seen by the module. A SVF of 1 means that the solar module lies flat on the surface, facing the whole sky. A SVF of 0.5 would mean that the module is vertically mounted and would only face half of the sky. The SVF is calculated using equation (3.2).

$$SVF = \frac{1 + cos(\theta_M)}{2} \tag{3.2}$$

The AOI is the angle between the surface normal of the solar module and the incident direction of the sunlight. The AOI is necessary to calculate the direct irradiance on the solar modules. Using the toolbox provided by Sandia National Laboratories [39], the AOI for each hour is determined.

Direct Irradiance

The first component to calculate the total irradiance on the solar module is the direct irradiance (G_{Dir}). To calculate the direct irradiance, first, the AOI and the SF must be determined. Once the two values are determined, the direct irradiance can be computed using equation (3.3). Since the DNI is given hourly, the direct irradiance is calculated for each hour.

$$G_{Dir} = I_{DNI} \times cos(AOI) \times SF \tag{3.3}$$

Diffuse Irradiance

The second irradiance component is the diffuse irradiance (G_{Dif}), calculated by equation (3.4). The DHI, which is given per hour, is multiplied by the SVF, resulting in an hourly diffuse irradiance component.

$$G_{Dif} = I_{DHI} \times SVF \tag{3.4}$$

Reflected Irradiance

The third irradiance component is the reflected irradiance (G_{Ref}), calculated by equation (3.5). The global horizontal irradiance is multiplied by the albedo (a), which equals 0.19 for grass areas [38] and (1-SVF). As can be imagined, when the SVF equals one, the amount of solar irradiance reflected from the ground on the solar modules is zero.

$$G_{Ref} = I_{GHI} \times a \times (1 - SVF) \tag{3.5}$$

Now that the three different irradiance components are calculated, again, the second of January and August are given in figure 3.10 and figure 3.11 respectively. As can be seen in both figures, the reflected irradiance is zero for all hours. This is because the modules are mounted flat on the earth's surface, resulting in no reflection from the ground that reaches the surface of the modules. The direct irradiance is the most substantial irradiance component on the summer day, whereas the diffuse irradiance component is more or less as strong during the day in winter. This has all to do with the AOI during the different seasons. The sun doesn't get as high up in the sky as it does during the summer, during the winter. This means that the *cos(AOI)* term in equation (3.3) is minimal, resulting in a low direct irradiance component.

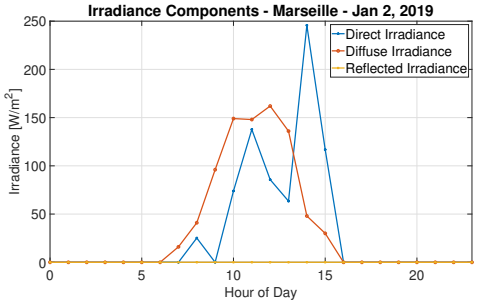

Figure 3.10: Irradiance components on January 2, 2019.

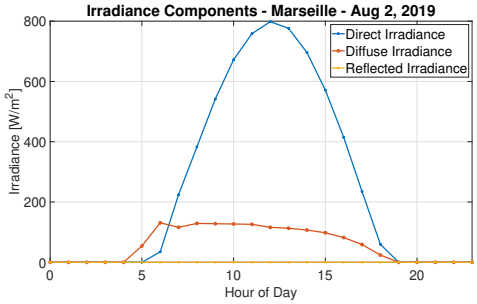

Figure 3.11: Irradiance components on August 2, 2019.

To calculate the total irradiance (G_{Tot}), the three different irradiance components are summed up, see equation (3.6). On a seasonal resolution, the total irradiance is expected to be stronger during summer than during winter. Moreover, as can be seen in figure 3.8 and figure 3.10, clouds have a powerful effect on the irradiance.

$$G_{Tot} = G_{Dir} + G_{Dif} + G_{Ref} \tag{3.6}$$

Once the hourly total irradiance is determined, every 24 hours are summed up to get the daily irradiance levels. In figure 3.12, the total daily irradiance is given in Marseille throughout 2019. What was expected were the high irradiance levels in summer and the low irradiance levels in winter. Moreover, throughout the whole year, there are days when the irradiance drops severely with respect to the yearly trend. This has to do that during those days, many clouds were present, influencing the irradiance levels.

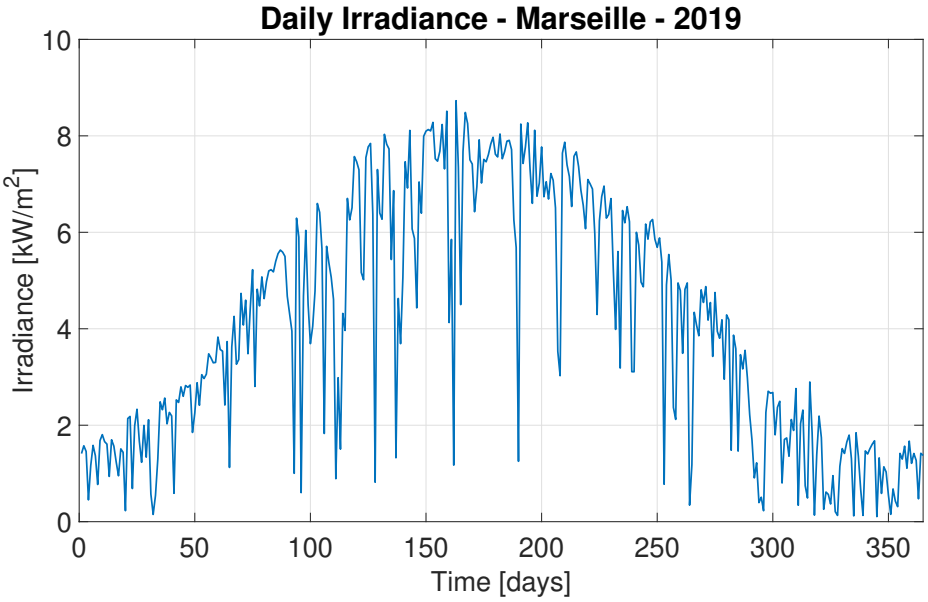

Figure 3.12: Daily total irradiance levels throughout 2019 in Marseille.

3.3.3 Temperature Dependency

Solar modules are tested at a module temperature of 25°C. The modules reach usually higher temperatures when in operation. Solar energy is, in a sense, paradoxical. On the one hand, sunlight is necessary to generate electricity, but on the other hand, the sunlight heats the module, resulting in a decrease in efficiency, sometimes reaching an efficiency decrease of 10-25%. When the module is heated up, the voltage produced decreases significantly while the current is only increased a little. Voltage times current equals power; therefore, heating the module, compared to the tested temperature, negatively affects the efficiency and the energy produced. This concept works both ways, meaning that cooling down the modules increases the overall efficiency.

Two main components affect the module temperature: the ambient temperature T_a and the wind speed v. These variables are together with the three irradiance components downloaded from the NREL database [36]. The wind speed is measured at 10 m and is adjusted for the module height using the log law. The module temperature (T_M) is calculated in equation (3.7), where T_{NOCT} is the nominal operating cell temperature (equal to 45°C), η_{cell} the efficiency of the module, and T and α the transmittance and absorptivity of the module are. The product of $T\alpha$ gives the fraction of the light absorbed by the module and is assumed to be 0.9 [21].

$$T_M = T_a + \frac{T_{NOCT} - 23}{800} G_{Tot} \left(\frac{9.5}{5.7 + 3.8 \times v} \right) \left(1 - \frac{\eta_{cell}}{T \times \alpha} \right) \tag{3.7}$$

3.3.4 Irradiance Dependency

The efficiency of the solar modules is also dependent on the irradiance levels. Modules are tested under STC with an irradiance level of 1000 W/m^2. In real life, the irradiance levels rarely exceed the STC levels, which affects the efficiency of the modules. The efficiency at these lower irradiance levels is different from the module's efficiency given on the datasheet. In equation (3.8), it can be seen that the efficiency (η) is dependent on the irradiance on the module (G_{Tot}) for a constant temperature of 25°C. This efficiency is the power produced at maximum power point (P_{mpp}) divided by the incident irradiance times the area of the module A_M.

$$\eta\left(25°\mathrm{C}, G_{Tot}\right) = \frac{P_{\mathrm{mpp}}\left(25°\mathrm{C}, G_{Tot}\right)}{G_{Tot} A_M} \tag{3.8}$$

To calculate the power produced, first, the short-circuit current (I_{sc}) and the open-circuit voltage (V_{oc}) need to be determined in equation (3.9) and equation (3.10) respectively. As can be seen in equation (3.9), the short circuit current for different irradiance levels is calculated by taking the STC short circuit current ($I_{sc}(STC)$) multiplied by the fraction of the total irradiance divided by the STC irradiance (G_{STC}).

$$I_{\mathrm{sc}}\left(25°\mathrm{C}, G_{Tot}\right) = I_{\mathrm{sc}}(\mathrm{STC})\frac{G_{Tot}}{G_{\mathrm{STC}}} \tag{3.9}$$

To calculate the open-circuit voltage, equation (3.10) is used. In this equation, n represents the ideality factor, k_B the Boltzmann constant, T the room temperature of 298 K, and q the elementary charge.

$$V_{\mathrm{oc}}\left(25°\mathrm{C}, G_{Tot}\right) = V_{\mathrm{oc}}(\mathrm{STC}) + \frac{nk_BT}{q}\ln\left(\frac{G_{Tot}}{G_{\mathrm{STC}}}\right) \tag{3.10}$$

Now that the short-circuit current and the open-circuit voltage have been found, the power at the maximum power point (P_{mpp}) can be found. In equation (3.11), the fill factor (FF) is multiplied by the open-circuit voltage and the short-circuit current. This FF is the ratio between maximum obtainable power and the product of the open-circuit voltage and the short-circuit current. This FF is not irradiance dependent and is different per type of material used for the module.

$$P_{\mathrm{mpp}}\left(25°\mathrm{C}, G_{Tot}\right) = FF \times V_{\mathrm{oc}}\left(25°\mathrm{C}, G_{Tot}\right) I_{\mathrm{sc}}\left(25°\mathrm{C}, G_{Tot}\right) \tag{3.11}$$

3.3.5 Effect on the Power Production

Throughout a year in Marseille, the average module temperature is higher than the 25°C under STC for the times when the module is producing most of the energy. Moreover, irradiance levels are lower than under STC, resulting in a negative effect on the power produced. Combining the two effects on the power produced will give a new efficiency ($\eta\left(T_M, G_{Tot}\right)$) which is now dependent on both the varying module temperature and the light intensity, given in equation (3.12). The first component of the equation corresponds with the light intensity given in equation (3.8). The second component is a fraction used to determine the effect of the module temperature. Typical values for temperature dependency coefficient (κ) are -0.0035/°C for crystalline silicon (c-Si) modules [21].

$$\eta\left(T_M, G_{Tot}\right) = \eta\left(25°\mathrm{C}, G_{Tot}\right)\left[1 + \kappa\left(T_M - 25°\mathrm{C}\right)\right] \tag{3.12}$$

Once the hourly variable efficiency is determined, the hourly produced power (P_{hourly}) by one module can be calculated following equation (3.13) and is simply the product of the hourly efficiency, the total irradiance and the area of the module (A_M).

$$P_{\mathrm{hourly}} = \eta\left(T_M, G_{Tot}\right) G_{Tot} A_M \tag{3.13}$$

The daily energy production produced (E_{daily}) by one module is simply the integral of the hourly power produced with respect to one day, given in equation (3.14). Since the time step of the power produced is one hour, the daily energy yield calculation can be simplified to just the summation of the hourly power production over one day.

$$E_{\mathrm{daily}} = A_M \int_{\mathrm{day}} G_{Tot}(t)\eta(t)\mathrm{d}t \tag{3.14}$$

Figure 3.13 gives an impression of the amount of daily energy produced for the year 2019 in Marseille. What can be seen is the seasonal trend in energy production, with high energy production in the summer and lower energy production in the winter, as was the case with the irradiance levels in figure 3.12.

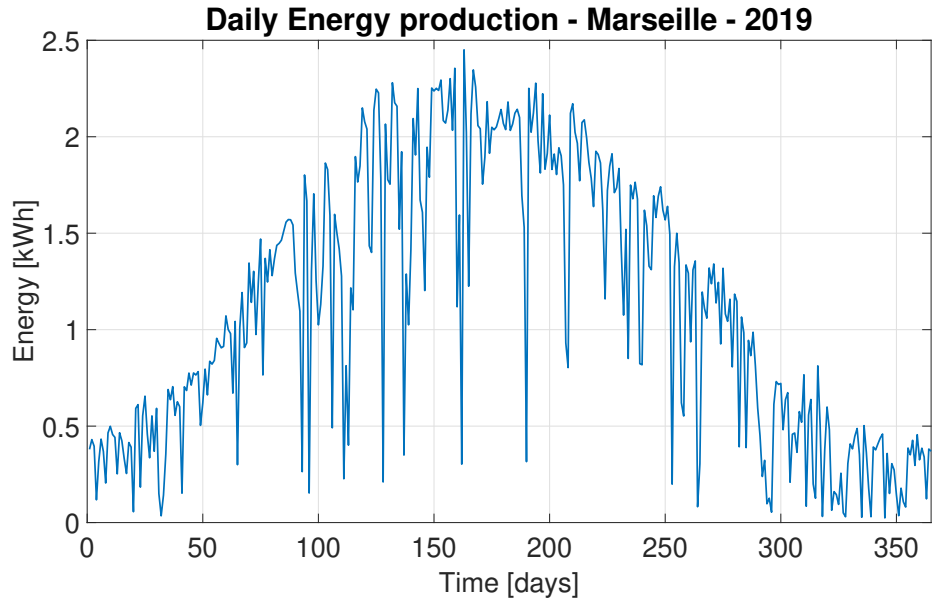

Figure 3.13: The daily energy produced by one solar module in Marseille in 2019.

The effect of the module temperature and the light intensity on the daily energy produced is shown in figure 3.14. It can be seen that the temperature and irradiance have a negative effect on the energy produced by a solar module almost every day throughout the year. Moreover, the figure shows that the effect is stronger during the summer than in the winter. This phenomenon makes sense since the ambient temperature, and therefore the module temperature, is higher during summer, resulting in a more substantial negative effect on the power produced. In total, 4.9% of energy is lost due to the effect of the module temperature and irradiance. Different module types respond differently to an increase/decrease in cell temperature, resulting in a different effect on the energy yield. Investigation of the optimal solar module type for each location is outside the project's scope, and therefore, only one type of solar module (c-Si) is considered for the calculations.

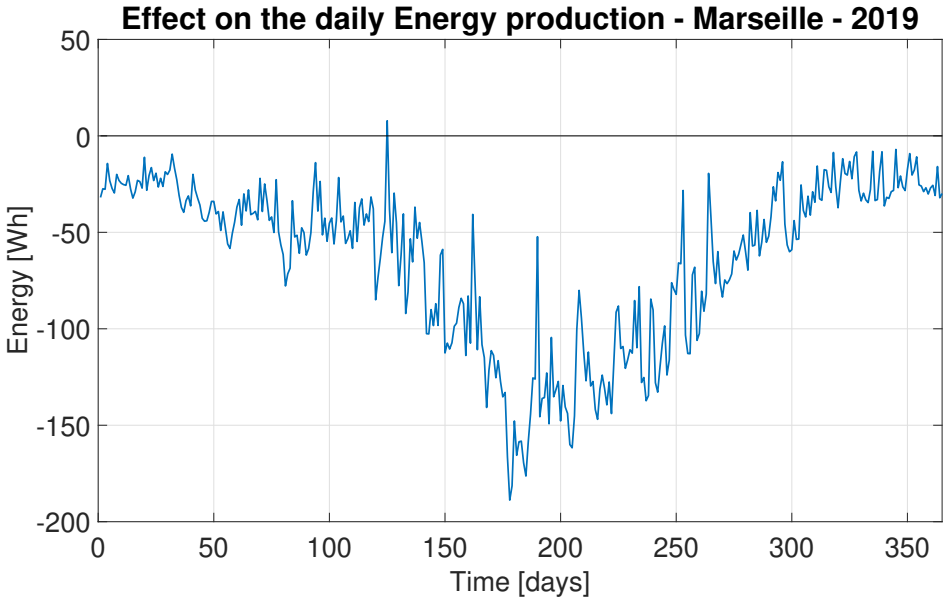

Figure 3.14: The effect of the temperature and the irradiance on the daily energy produced by one solar module.

3.3.6 System's Energy Production

Once the energy production by the modules is determined, the overall system energy production can be determined. The system has three main components that affect the system's energy production. The product of these different component efficiencies will yield the total system efficiency. When the total system efficiency is multiplied by the energy production by the modules, the energy delivered by the system can be determined.

Degradation
The first efficiency considered is the degradation of the solar modules themselves. Over time, the power produced by a module decreases, resulting in gradually lower energy outputs. The degradation rate of a typical c-Si module is around -0.5% per year [40]. This means that the average degradation of the module throughout its lifetime of 25 years equals 0.88 of the original power output, which has a significant impact on the yearly energy produced.

Cabling losses
The second considered efficiency is the efficiency loss due to cabling. Through DC cables, the solar modules are interconnected and connected to the (micro-)grid. Depending on the size and the current and voltage in the cables, some energy is lost. In-depth research on the loss of energy in the cables is outside of this project's scope. However, based on the literature, a loss of about 1.5% is estimated [41].

Module mismatch
The final component of the system efficiency is module mismatch. Module mismatch occurs when two or more solar modules are interconnected. All the modules experience slightly different conditions, like a difference in incident irradiance or ambient temperature. This means that each interconnected module produces a slightly different amount of power. Since they are interconnected, the voltage and/or the system's current need to match, resulting in the worst producing modules, which determines the energy output of the whole interconnected array. Even though the differences are very marginal, a decrease in total energy production by the system is experienced. The losses corresponding to this concept are 0.7% [41].

The inverter's efficiency is not considered at this phase of the research yet since the solar modules will be connected to DC-microgrid. Once the purpose of the HPP and the grid type it will be connected to is determined, the use of an inverter is considered. An overview of the total average system efficiency over its lifetime is given in table 3.3.

Table 3.3: The system efficiency components and the total.

System Efficiency	
Average module degradation over its lifetime	0.880
Cabling efficiency	0.985
Mismatch efficiency	0.993
Total system efficiency	**0.861**

Now that the system efficiencies have been found, the AEP can be calculated. The calculation of the AEP is the same as equation (3.14) but now integrating for a whole year and multiplying it with the system efficiency (η_{sys}), as can be seen in equation (3.15).

$$E_{\text{yearly}} = \eta_{sys} A_M \int_{\text{year}} G_{Tot}(t)\eta(t)\mathrm{d}t \tag{3.15}$$

The annual energy produced by one solar module in Marseille, including the system efficiency, is 406 kWh. When increasing the number of solar modules so that 1 MW is installed, the area needed is 5,000 m^2, and the number of modules is 3,000. A solar farm like this would produce, on average, 1,213 MWh annually. The capacity factor (CF) of the system is calculated using equation (3.16), in which $P_{nominal}$ denotes the nominal power of the system. For this system, the capacity factor is determined to be 13.8%, which can be expected for a utility-scale solar PV farm in France [42].

$$CF = \frac{E_{yearly}}{P_{nominal} \times 365 \times 24} \tag{3.16}$$

3.3.7 Cost

The cost function has two components: the initial investment costs and the O&M costs. The initial investment needs to be paid at the beginning of the project's lifetime. The project's lifetime is 25 years, which is the lifetime of the solar modules. For the solar part of the project, no replacement of the solar energy system components is deemed necessary, and will therefore not be considered. The O&M costs are costs that occur at the end of each year over the whole lifetime of the project. There are four categories in which the initial investment costs of a solar energy system can be divided:

1. Balance of system (BoS) hardware
2. Installation costs
3. Modules
4. Soft costs

BoS hardware
The first category is BoS hardware. This category includes all the costs related to the hardware of the system except for the module and inverter costs. These costs include racking and mounting, grid connection, cabling/wiring, safety and security, and monitoring and control costs. Out of the different components, grid connection costs are the highest. In a hybrid power plant, these costs could be partially shared between the plant's wind and solar energy components to reduce the costs of the whole system. The total cost of the BoS hardware is 276 €/kW [43].

Installation costs
The installation costs are the second category. Three components make up the installation costs: mechanical installation, electrical installation, and inspection. The total installation costs are 163 €/kW [43], where the most expensive mechanical installation costs make up about 75% of the installation costs.

Module
The cost of the module is given separately from the BoS hardware costs because the cost of the module can vary a lot between different types and is considered a separate component of the system. Depending on the type and size of the module, the costs can vary. For this project, the cost per kW of the module is assumed to be 218 €/kW [43].

Soft costs
The final category is the soft costs. These costs consist of margin, project financing, system design, permitting, incentive application, and customer acquisition costs. The total soft costs are 187 €/kW [43].

The total initial investment costs are given in table 3.4. The total cost per kW installed of the solar energy system is 835 €/kW. This cost estimation will be used throughout the project, and when looking at other sources for the cost of utility-scale solar, this estimation seems acceptable [44], [45].

Table 3.4: An overview of the total CAPEX costs of the solar module system [43].

Catergory	**Cost [€/kW]**
BoS hardware	276
Installation	163
Module	218
Soft costs	178
Total	**835**

Operation and Maintenance Cost
The O&M costs are costs related to, as the name entails, the operation and maintenance of the solar plant. The solar modules and the system need to be well maintained to guarantee both the electricity produced and the lifetime of the components. For example, cleaning the modules regularly will help produce more energy without having losses related to soiling. Regular checks need to be performed on the system to check if the system is still safe to operate. The costs associated with the O&M of the system are assumed to be 5 €/kW installed [46].

3.3.8 Levelized Cost of Electricity

An important concept to compare different energy generating systems is the LCoE. This concept will be used as the main objective for sizing the HPP. Once the LCoE is found, the objective can be relaxed to find more solutions that could satisfy different objectives. In the numerator of equation (3.17), the cost-related factors are the initial investment costs (I_t) in year t. The O&M costs for year t are represented in the equation by (M_t). The yearly energy yield (E_t) is given in the denominator. Over the lifetime of a project, the costs and energy yields are summed up, discounted with a discount rate (r) of 5%.

$$\text{LCoE} = \frac{\sum_{t=1}^{n} \frac{I_t + M_t}{(1+r)^t}}{\sum_{t=1}^{n} \frac{E_t}{(1+r)^t}} \tag{3.17}$$

For the solar project, the investment cost only happens in the year zero and is not discounted. Only the O&M cost will be discounted throughout the lifetime of the project. When calculating the yearly energy yield, the degradation of the modules is considered. This means that over the lifetime of the solar modules, the energy produced decreases. Considering these factors, the LCoE is equal to 49 €/MWh. Comparing this value with literature sounds acceptable for utility-scale solar farms [47], [48], [49].

3.3.9 Reflection

With the performance and cost modelling, some assumptions have been made. In this subsection, the most critical assumptions are discussed and reflected upon.

Energy yield calculation
The yearly energy yield is calculated for one location for one year. After looking at resource data over more extended periods, the resource data for the year 2019 is deemed presentable for longer periods. The GHI in 2019 in Marseille was 1,484 kWh/m^2 which is similar to the long-term average of 1,620 kWh/m^2 [34]. This similarity means that the year 2019 is considered an average year compared to the long-term average. Moreover, by choosing one specific year, extreme cases, that would have been averaged out by taking the average of multiple years, are still included in the data. This simplification made it possible to focus more on the essence of the project, getting an estimation of the system's energy production. Moreover, the data for multiple years is not averaged because extreme peaks in the data would have been lost this way. The solar irradiance varies from second to second. However, the data is on an hourly resolution. This resolution is deemed specific enough to get presentable numbers for the estimations of the yearly energy yield.

System efficiency
The system efficiency of the solar energy system is based on literature. The values found in the literature differ per module or other system component type. However, the values found in the literature give a good enough estimation of the true system values. Estimates for cable losses, for example, can differ because it is very dependable on the size and length of the cable. However, the project requires an estimate for these numbers, and therefore literature is consulted.

Cost estimations
The cost estimations are also based on literature and, therefore, will, in any case, not be the actual values of the project. Basing the cost on literature does give a good indication of the actual cost. However, it will not represent the true value of the project. Initial investment and O&M costs are different for every country/region and can differ quite a lot. In the business case research, the cost of solar energy is decreased by a fraction because the initial investment is cheaper in the business case locations than the location in Marseille.

The estimates of the cost involved in this project are costs from recent years. This means that there is no learning curve applied to the cost related to the project. The learning curve to the cost is not applied anymore because even though solar energy is still developing, and the costs related to the project decline over the years, it is decided that solar energy is at a mature enough phase to not account for the learning curve anymore.

3.4 Airborne Wind Energy - Performance and Cost Modelling

A similar approach as in section 3.3 was made to determine the performance and cost of the AWES. After the system's AEP and cost function are determined, the LCoE is calculated for a grid-connected system. Concluding this section, assumptions and estimations are reflected upon.

3.4.1 Annual Energy Production

To calculate the AEP by an AWES, both the wind speed at a specific location and the power curve of the AWES need to be known. As mentioned in section 2.1.2, there are different types of AWESs. In this project, the Falcon 100 kW from Kitepower [7] is chosen as the AWES because of the close collaboration between the Technical University Delft and Kitepower. Moreover, Kitepower supplied both the power curve, see appendix B, and the cost data related to the Falcon system [50].

3.4.2 Wind Speed Data

The wind speed data is downloaded from ERA5 at the height of 975 hPa [51], which equals an altitude of 320 m above sea level. For the year 2019 in Marseille, the hourly wind speeds are downloaded. The location is filled in by using coordinates. ERA5 uses reanalysis data, which means that observations from the past are combined with today's weather model to make a complete picture of the conditions for a specific location and time. The wind speed data is as close to reality as possible, even though no measurements may have taken place for a specific period or location.

ERA5 provides both the wind speed (WS) in the u- and v-direction, ${ws_u}^2$ and ${ws_v}^2$ respectively. To find the combined wind speed, the square root of the sum of two terms squared is taken, as can be seen in equation (3.18).

$$WS = \sqrt{{ws_u}^2 + {ws_v}^2} \tag{3.18}$$

As can be seen in figure 3.15, the wind speed is very variable. However, it can be seen that there is a minor trend on an annual basis, showing slightly stronger wind speeds in winter than in summer. The mean of the wind speed in Marseille is equal to 7.2 m/s.

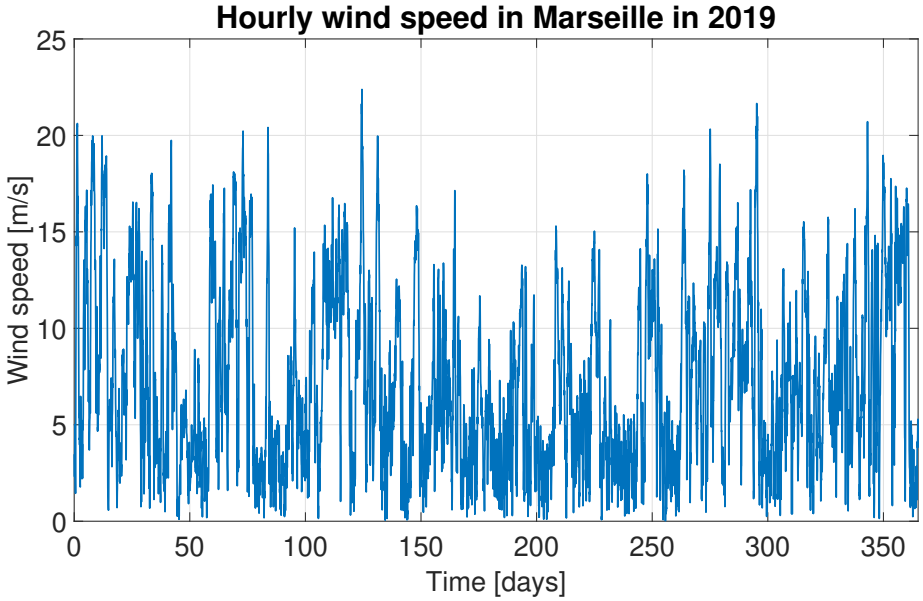

Figure 3.15: The hourly wind speed in Marseille in 2019.

3.4.3 Power Curve

Kitepower provided the power curve of the Falcon that is used for the calculations. The power curve has been reproduced in MATLAB, and a curve fit has been fitted to do calculations with the power curve. In figure 3.16, the data from Kitepower (blue line) and the curve fit (orange line) are given. The cut-in wind speed of the system is 2 m/s, the rated wind speed is 10 m/s, and the cut-out wind speed is 25 m/s. In the figure, it can be seen that the cut-out wind speed provided by Kitepower is 15 m/s. This is true for how the system is at the moment. However, in the future, the system is expected to have a cut-out wind speed of 25 m/s. Therefore, the MATLAB power curve is validated using a quasi-steady model (QSM) [52], and the cut-out wind speed is extended to 25 m/s.

AWE is still very much in the research and development phase. Therefore, no operational data is available to validate the assumptions corresponding to the power estimations of the AWES. The QSM simulation is used to validate the estimated power curve and calculate the AEP [53]. The QSM simulation is a compromise between using a simple single drag coefficient for characterising the flight of the kite, and solving the computationally expensive coupled partial differential equations for determining the kite's flight trajectory [54].

It is interesting to see that below cut-in wind speed, the system costs electricity. This has to do with the fact that it is better to stay in the air for these wind speeds, costing some energy rather than having to launch and land the kite every time the wind speed drops below the cut-in wind speed.

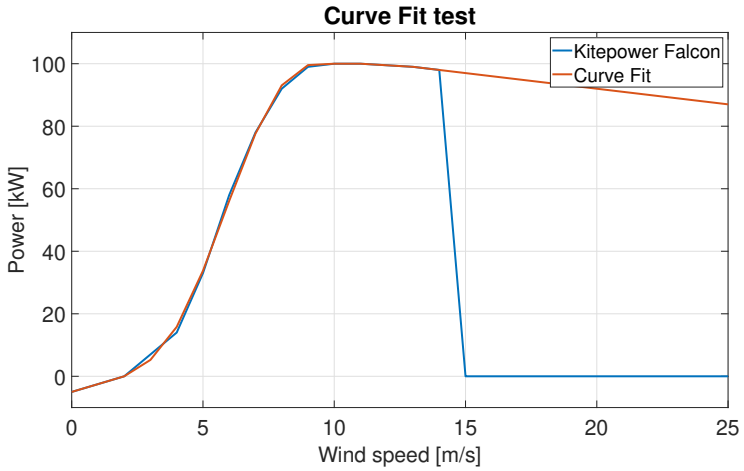

Figure 3.16: Kitepower power curve and fitted power curve data.

Now that both the wind speed data and the power curve have been determined, the hourly produced power by the system can be calculated. The power produced at time t is determined by looking at the wind speed at time t and seeing where it intersects with the power curve. This way, the hourly power production is determined, which is given in figure 3.17.

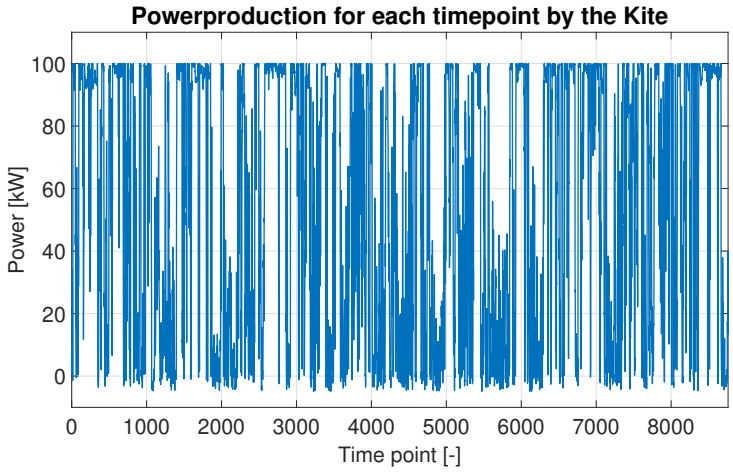

Figure 3.17: The power produced by one Kitepower Falcon 100 kW in Marseille in 2019.

The power production figure in figure 3.17 is challenging to read due to the scattering of the data and, therefore the power production. When the data is sorted, as in figure 3.18, the original power curve can be seen again. There is a little jump at the cut-in wind speed where the curve fit wasn't smooth for this line section, but the power curve's overall estimate seems acceptable.

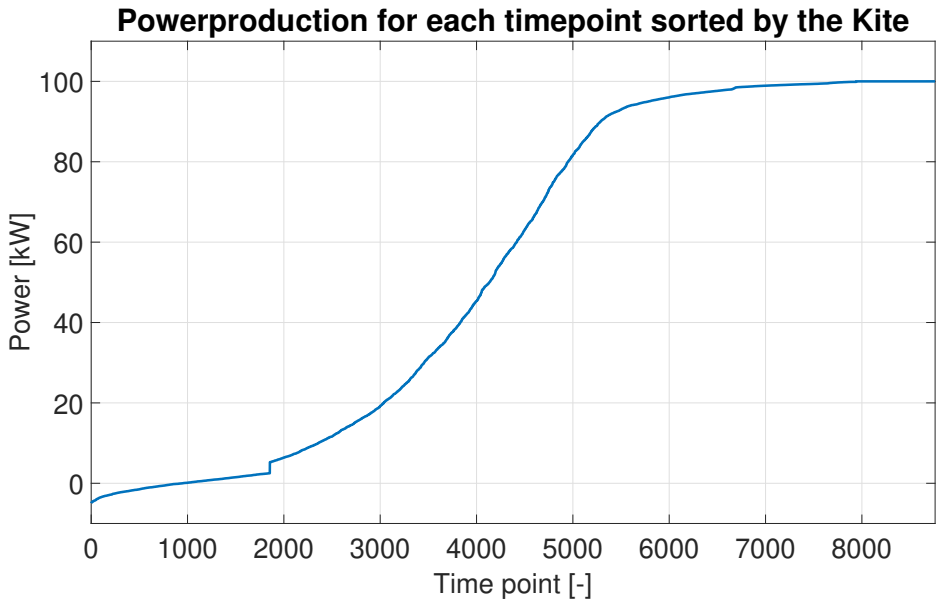

Figure 3.18: The sorted power produced by one Kitepower Falcon 100 kW in Marseille in 2019.

The AEP is calculated by taking the integral of the hourly power produced with respect to time. Similar to the solar energy calculations, the time step of each power production is one hour. Therefore, the AEP is equal to the sum of the power production over one year. The annual energy production by the system in Marseille in 2019 is 472 MWh, which is comparable to what Kitepower says on its website [7].

To put this into perspective, a 100 kW wind turbine placed at a location with an average wind speed of 7 m/s will yield an AEP of 346 MWh [55]. When the average wind speed is 7.5 m/s, the AEP equals 382 MWh [55]. This suggests that the AWES has a higher AEP. However, many more factors take part in the wind speed data other than the average.

The capacity factor is calculated using equation (3.16). For the Falcon, the nominal power is 100 kW, and the calculated capacity factor is 53.9%. Compared to the capacity factor of the solar energy system, it is very high. The capacity factor of other pumping kite systems is found in the literature to be 52% for a kite with an area of 100 m^2 [56].

3.4.4 Cost

The AWES consists of four components: the ground station, tether, kite control unit, and the kite, which are given in 3.19. Over the lifetime of the ground station, which is 25 years, the kite and tether need to be replaced twice per year, see appendix B.

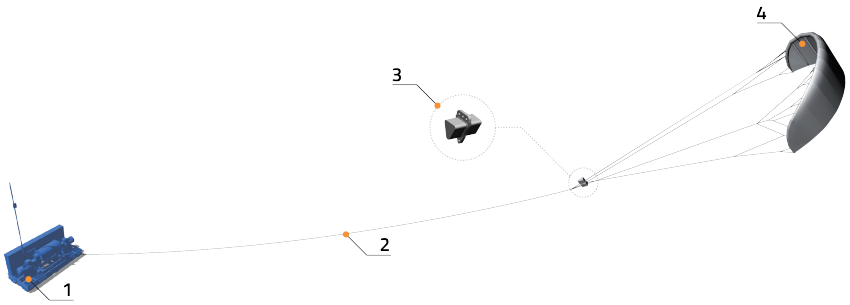

Figure 3.19: The four components of an AWES are; 1. Ground station; 2. Tether; 3. Kite Control Unit; 4. Kite [7].

Kitepower provided the cost related to each component of the system [50]. The cost of the ground station makes up the vast majority of the total cost. However, the lifetime of the ground station is 25 years. This means that for the lifetime of the whole project, only one ground station is necessary. On the contrary, the lifetime of both the kite and the tether is 4,000 hours. For simplicity, it is assumed that every year, the kite and the tether need to be renewed twice. Finally, the kite control unit is assumed to have the same lifetime as the ground station.

The cost estimations provided by Kitepower are not market-ready prices. Therefore, a learning curve has been applied to the components to get the (lower) cost projections due to experience [57]. This learning curve applies to all components of the AWES. A similar learning rate that was observed for wind turbines is applied to the AWES, which is equal to 12% [58]. By applying the learning curves to the system's components, the system's market-ready price is estimated for 2030.

The estimations of the AWES don't include other costs of realising the project. These costs include transport and installation cost, cabling and grid connection cost, permitting and financing costs, and project development cost. These additional costs are given in table 3.5. The total of these additional costs is 24,100 €/unit.

Table 3.5: An overview of the additional cost.

Component	**Cost [€/unit]**
Transport and installation [56]	1,000
Cabling and grid connection [43]	17,100
Permitting and Financing [43]	3,300
Project development [56]	2,700
Total	**24,100**

The replacement kites and tethers will not be bought at the beginning of the project but at the end of each year. This means that similar to how the O&M costs are discounted, the cost of replacing the kites and tethers twice a year will be discounted as well. The O&M for an AWES depends on multiple location-dependent factors and range between 20,000-60,000 €/unit per year. In this project, the O&M costs are 40,000 €/unit per year.

3.4.5 Levelized Cost of Electricity

The LCoE of the AWE project is calculated similarly to the solar project, again using equation (3.17). In this case, the initial investment cost is the cost of the ground station, the tether, the kite control unit, the kite, and the additional cost. The yearly costs are the O&M costs with the cost of two new kites and tethers. The discount rate is again 5%. The annual energy production is constant over all the years, there is no degradation of the system considered. The LCoE of the AWE project is equal to 162 €/MWh, which is significantly more compared to the solar project (49 €/MWh). Comparing the LCoE to literature, a difference can be found (245 €/MWh) for a similar-sized kite [56]. It should be kept in mind that the AWES are still very much in the research and development phase. In the evaluated case, the learning curves have been applied to the costs of the AWES.

3.4.6 Reflection

Wind speed data
Similar to the case for the solar data, the wind speed data is only considered for the year 2019. By choosing to evaluate only one specific year, rather than averaging the wind speeds of multiple years, the peaks in the data are kept. Moreover, the yearly energy yield of multiple years is not evaluated for the simplicity of the computations, but rather, the outcomes are compared with literature. For the business case locations, a three-year period is chosen to increase the reliability of the calculations.

The wind speed data is downloaded for a pressure level of 975 hPa for all locations throughout this research. This corresponds to an altitude of about 320 m above sea level. However, the kites operate at varying altitudes and experience varying wind speeds. Only one operational altitude is considered for the simplicity of the model.

The resolution of the wind speed data is again on an hourly resolution, as was the case for solar irradiance. An investigation on a higher fidelity of the resource data, like a ten-minute resolution, is determined to be a too-high resolution for the simplicity of this research. The hourly resolution is deemed presentable enough to determine the AEP of the AWES.

Finally, the wind speed data is based on reanalysis data. This means that the data used for a specific location and time still estimates the actual value. For this research, this reanalysis data is deemed presentable enough. When, in the future, exact locations are analysed for a business case, local measurements regarding wind speed and solar irradiance need to be conducted.

Power curve estimations
The power curve of the AWES is based on the power curve provided by Kitepower in their brochure, see appendix B. The power curve used in calculating the AEP gives a good approximation of the real energy yield it would give during operation, but it is not the true value. To validate the power curve estimations, the used power curve is validated with a QSM of the same kite system in [52]. The QSM looked very similar to the estimated power curve based on Kitepower's brochure and therefore, the MATLAB power curve is used in the estimations of the AEP.

Cost estimations
Kitepower has provided this research with cost estimations for the Falcon 100 kW system [50]. After a discussion with Kitepower, a learning curve has been applied to the current cost function of the system to make the cost more presentable for 2030. The cost function and the learning curve are not published in this research. Rather, dummy numbers are used in the model on GitHub. Since there is much uncertainty regarding the cost of the AWES, a sensitivity analysis of the LCoE of the HPP to these cost estimations is done in section 4.2.3.

Power gap
The power gap caused by the reel-in and reel-out phase of the pumping cycle AWES needs to be solved [16]. In this thesis, the power gap is not considered explicitly. However, future research could investigate how to mitigate the gap between energy production and the system costing energy. Ways to solve the power gap could be to have multiple kites in operation that are synchronised to reel-in at different moments. Moreover, the battery could be used to cover for the power gap.

3.5 Load data

A real-life case is simulated to analyse the performance of the different HPP configurations. The resource data (both solar and wind data) will be taken for Marseille in 2019. The real-life case will simulate a military camp for training near Marseille. The military camp is very mobile and a temporary military base, meaning that wind turbines cannot be used as renewable energy generators. This motivates the use of an AWES since the kite systems are easily transported.

The load data will be based on different components. For recent military missions, the average energy consumption of one person is 9 kWh/day [16], which equals 3.285 MWh/year. As was calculated in section 3.4.1, the annual energy production of one Kitepower Falcon kite system is equal to 430.4 MWh/year. This would mean that if all the energy generated by the Falcon is used, it will supply enough electricity for 1,300 military personnel.

To discretise the number of kites in this hypothetical army base, an annual energy demand of 430.4*10 = 4,304 MWh/year (or ten kites) is assumed. This would mean that the army base would have around 1,300 personnel. However, there is no accurate load profile of the full electricity use of military camps available. Therefore, a combination of the real-life yearly load data in France and theoretical load data is used to estimate the year-round energy demand.

The real-life load data is the same as used in the resource analysis of section 3.2. This data is downloaded from the ENTSO-E [59] website. This website gives the total load of France in the year 2019, which is equal to $4.678*10^8$ MWh. Scaling down this value with the factor $4{,}304/(4.678*10^8)$ gives how the energy usage would look throughout the year if the military camp had the same electricity use profile as the average load profile of France.

The graph of this hourly electricity demand is given in figure 3.20. As can be seen, there is a stronger use in the electricity demand during the winter than during the summer. Moreover, there are here and there some extreme peaks in the demand on a more hourly level.

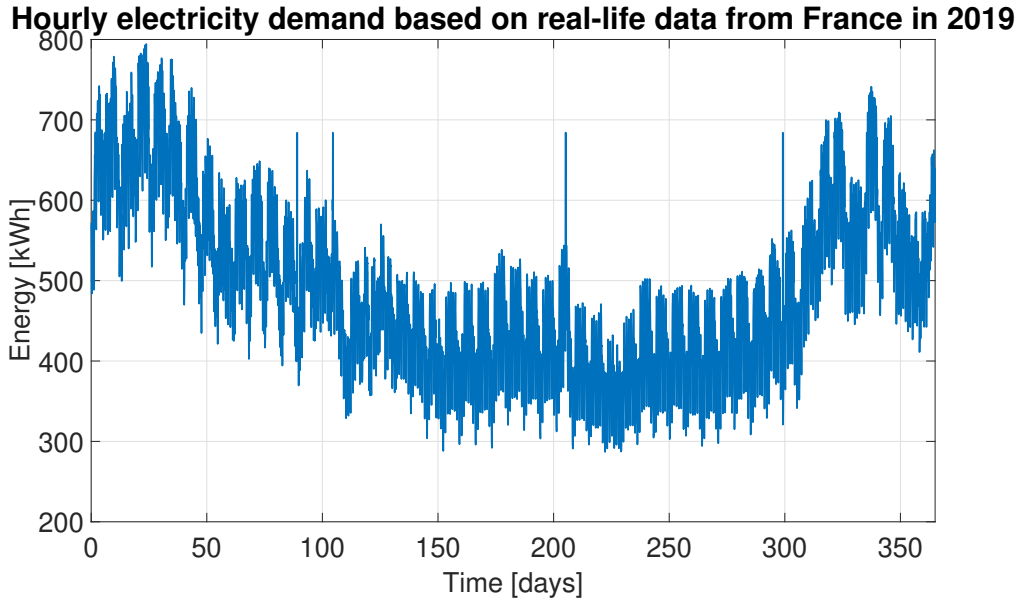

Figure 3.20: The hourly electricity demand for a military camp of 1,300 personnel, based on the load data of the whole of France in the year 2019.

Now that the hourly demand based on the French electricity load profile has been determined, it is time to look at the demand profile based on a theoretical approach [12]. In equation (3.19), the yearly energy demand (E_{yearly}), which is 4,403 MWh, is divided by 365 and multiplied by two fractions. These two terms E_{summer} and E_{winter} make the daily energy use curve of which the values can be found in the supplementary information of [12]. E_{total} is again the yearly electricity demand, which is estimated in this equation and t is the time step in full days. Finally, the function $A(t)$ approximates the variation for the peak in winter and a lower peak in summer, given in equation (3.20).

$$E_{\text{total}}\ (\text{t}) \approx \frac{E_{yearly}}{365}\left[E_{\text{Summer}}\left(\frac{1}{2}+\frac{1}{2}\cos\left(\frac{2\pi(t-172)}{365}\right)\right)\right. \\ \left.+E_{\text{Winter}}\left(\frac{1}{2}-\frac{1}{2}\cos\left(\frac{2\pi(t-172)}{365}\right)\right)\right]A(t) \tag{3.19}$$

$$A(t) = (1+0.075\cos(4\pi(t-217)/365))(1-0.045\cos(2\pi(t-217)/365)) \tag{3.20}$$

Using equation (3.19) and equation (3.20), the hourly electricity demand graph is created. It can be seen that this yearly demand curve is very smooth, see figure 3.21. Moreover, comparing the figure to figure 3.20, it can be seen that the extreme peaks are completely gone. The effect of the *A(t)* term in equation (3.19) can be seen with a strong peak in winter and a slightly weaker peak in summer.

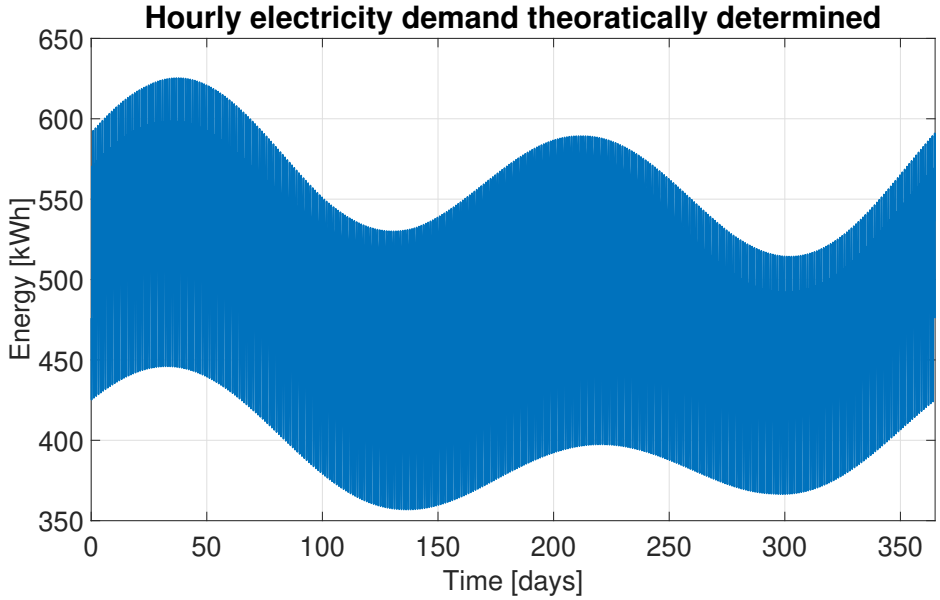

Figure 3.21: Theoretically determined hourly electricity demand for a military camp of 1,300 personnel.

When comparing the load data on a daily resolution for January the second, it can be seen that the shapes of figure 3.22 and figure 3.23 are very similar. However, as was clear from the figures on a yearly resolution, the real-life data electricity demand turns out to be higher than the theoretical demand. Moreover, the theoretical demand curve is smoother than the real-life case.

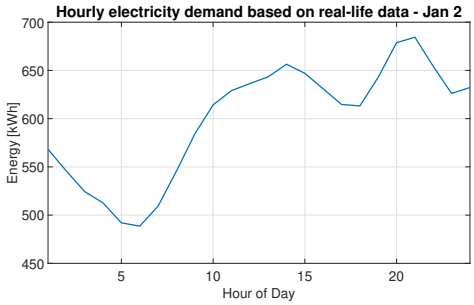

Figure 3.22: Real-life data for January 2.

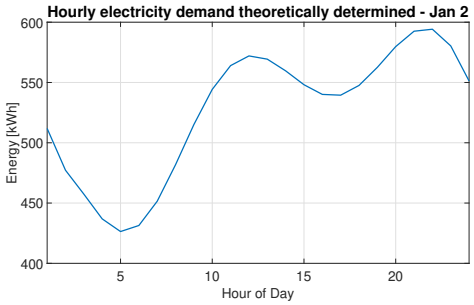

Figure 3.23: Theoretical data for January 2.

Now, looking at the daily demand curves for a day in summer, August the second, it can be seen that the shapes are slightly less similar, see figure 3.24 and figure 3.25. Moreover, the electricity demand is lower for the real-life case than for the theoretical one. A demand curve is expected to have in summer, an afternoon peak and a dip during the night [60], which can be seen in both the real-life and theoretical curves.

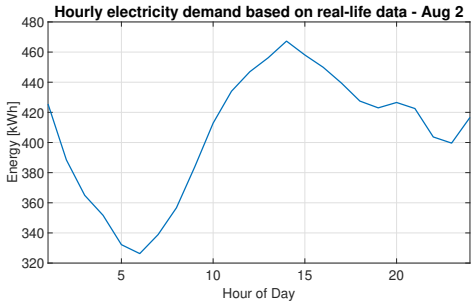

Figure 3.24: Real-life data for August 2.

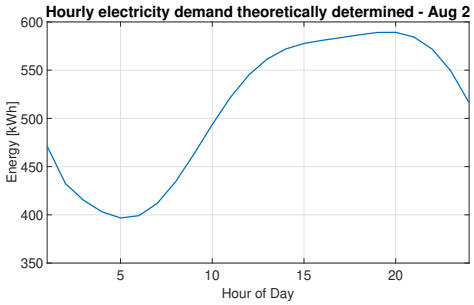

Figure 3.25: Theoretical data for August 2.

After comparing the real-life demand and the theoretical curves, it can be seen that the shape on the yearly resolution (except for the peak in summer) and the shape on the daily resolution are more or less similar. Both data sets have a similar mean: 491 for the real-life data and 494 for the theoretical data. Moreover, the standard deviation of the real-life data is significantly higher than the theoretical data, 104 and 68, respectively. This means that the data for the real-life case is more spread out from the mean than in the theoretical case, which can be seen in the yearly graphs.

The electricity demand of a military camp will probably not follow the average electricity demand in France, nor will it follow the theoretical curves. Therefore, it was decided to add a bit of both demand functions in constructing the demand of the military camp. This way, the forthcoming trends on a yearly and daily resolution will be provided by the smooth functions of the theoretical demand functions. Moreover, as was seen in the real-life case, the demand function is not only smooth. Therefore, adding the real-life demand case to include some "random" peaks in the demand curve will make the overall demand function more realistic.

To calculate the demand for the military camp (D_{camp}), both the real-life demand ($D_{real-life}$) and the theoretical demand ($D_{theoretical}$) have an equal contribution, as can be seen in equation (3.21). As can be seen in figure 3.26, the demand curve is now made more generic since it is not based on the electricity demand of a country for just one year. The mean is now 493, and the standard deviation is 74.

$$D_{camp} = \frac{D_{real-life} + D_{theoretical}}{2} \tag{3.21}$$

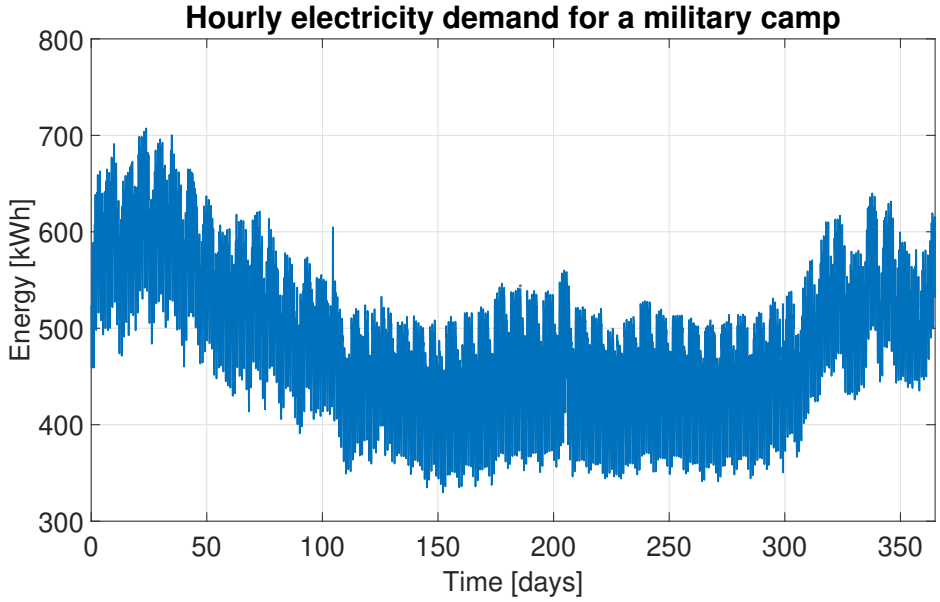

Figure 3.26: The hourly electricity demand for a military camp of 1,300 personnel.

Figure 3.27 and figure 3.28 illustrate the new demand curve on a daily level. Now, the demand curve of the military camp does not depend on the average load data of the whole country, nor does it solely depend on theory. This way, theory and practice come together to make a suitable demand curve.

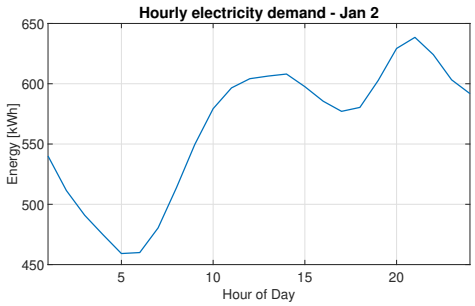

Figure 3.27: Electricity demand for January 2.

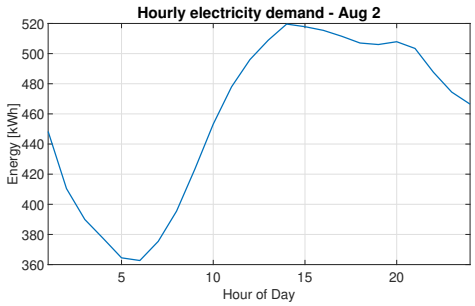

Figure 3.28: Electricity demand for August 2.

For most locations, no empirical annual load profiles are available. In this research, different ways are shown how the load data can be estimated. The first method is to use the data from the ENTSOE-E database to estimate the load function of the specific location. In the second method, the load function is estimated using theoretical formulas. The final way to estimate the load function is to assume a constant load, as was done in the business case chapter. Neither these estimations nor a combination of multiple estimates will give the true load profile. Estimating the load profile as close to the real data is important since the component sizing heavily depends on it. However, for this research, the approximations are deemed well enough to use for the calculations.

3.6 Battery Capacity

Once the performance of both the AWES and solar energy system is known, the total hourly energy generated by the HPP is calculated. At each time point, the demand of that hour is subtracted, this value is called the mismatch between supply and demand. If the total generation is greater than the demand, there is an electricity surplus to charge the batteries with. When the mismatch is smaller than zero, the HPP does not generate enough electricity to meet the demand. What follows is that a battery is necessary to provide the rest of the electricity.

The battery capacity (Capacity(i)) is sized with respect to the maximum amount of necessary electricity. The capacity of the battery for the next time point ($i+1$) is calculated using equation (3.22) when the mismatch (Mismatch(i)) is greater than zero. When the mismatch is smaller than zero, equation (3.23) is used. Here, the round-trip efficiency of the battery $\eta_{round-trip}$, equal to 90%, is accounted for when discharging the battery.

$$Capacity(i+1) = Capacity(i) + Mismatch(i) \tag{3.22}$$

$$Capacity(i+1) = Capacity(i) + Mismatch(i)/\eta_{round-trip} \tag{3.23}$$

The elapsed time for the sizing of the battery capacity is three of the exact same years in a row, both for the resource and load data. This is done because possible extremes can be overlooked when they happen at the turn of the year. To illustrate the steps into the sizing of the battery capacity, a hypothetical situation is created. In this situation, 100,000 solar modules are used, as in section 3.3, and the load is the same as in section 3.5. There is no AWES used in this case, and there is no loss of load.

The hourly battery capacity is given in figure 3.29. As can be seen, the battery's capacity does not exceed zero. The battery capacity is, at this point, still equal to zero. Hence, the maximum that the battery can be charged is equal to the battery's maximum capacity. The figure clearly shows that the system consists of only solar modules due to the substantial dips in battery charge during winter.

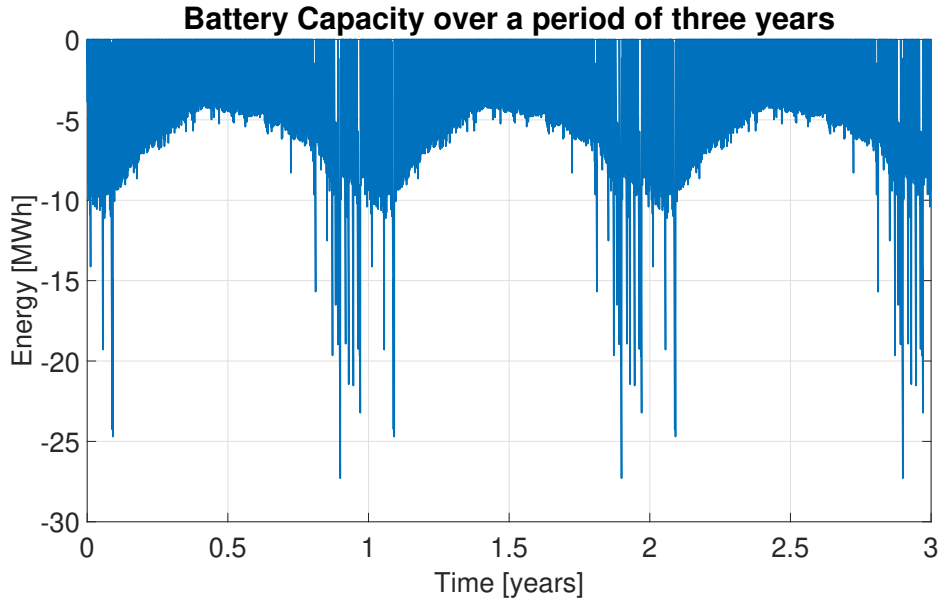

Figure 3.29: Hourly battery capacity before the battery is adequately sized.

The state of charge limits of the battery are accounted for, which are equal to 10-100%. The size of the battery now becomes the absolute of the minimum battery capacity of the previous step plus an extra 10% to account for the state of charge limits, see figure 3.30. What can be seen in the figure is that the battery is sized to supply the whole load, even though most of the battery capacity is not used. This way, the battery capacity is not optimally used.

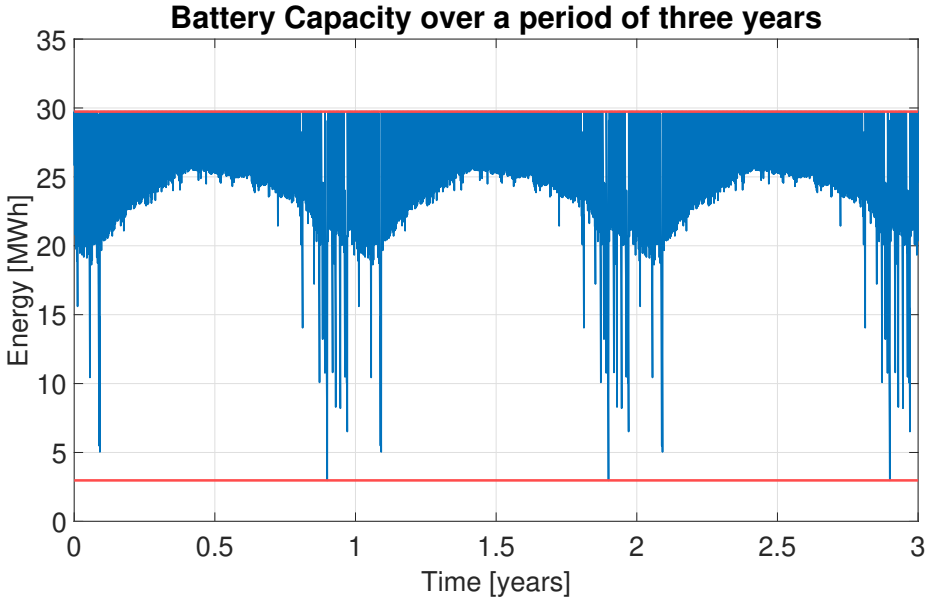

Figure 3.30: Hourly battery capacity with an appropriately sized battery.

The loss of load is introduced to reduce the oversizing of the generation components and the battery capacity of the HPP. What the loss of load does, is it accepts a certain percentage of times in which demand is not met. This means that there are moments in which a power outage is created. In figure 3.31, the loss of load is 5%. As a result of this small decrease in the times that the load is supplied, the battery is decreased by almost two-thirds of the original capacity. This reduction in battery capacity has a significant effect on the LCoE of the HPP. Moreover, the generating components of the system need to be oversized less. Further research on the sensitivity of the loss of load on the LCoE will be investigated in section 4.2.1.

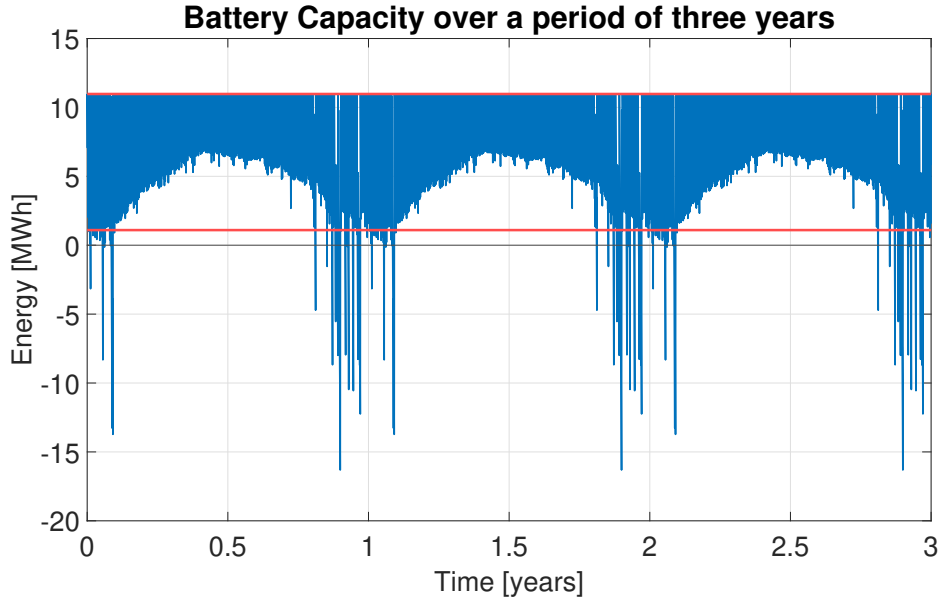

Figure 3.31: Hourly battery capacity with a properly sized battery and a loss of load of 5%.

3.7 Diesel Generation

In an off-grid situation, power outages caused by allowing a load loss are unacceptable. Therefore, there must be another way to supply the load without significant oversizing of the generating or storage components of the HPP. A controllable electricity generation source in the form of a diesel generator is the solution. By adding this diesel generator to the HPP, the battery can still be the same size as was the case without the diesel generator, but now the load is not lost.

To decrease the battery capacity, a diesel generation optimisation (DGO) is introduced. In this new set-up of the HPP, the diesel generator only generates the electricity when the battery capacity of the next hour would have dropped below the minimum state of charge limit of 10% if there was not a diesel generator, like in the case of section 3.6. Moreover, the mismatch of the current hour has to be less than zero (demand > supply). By adding this second condition, the generator jumps in only when the renewable components of the HPP cannot generate electricity above the minimum state of charge. When the mismatch is greater than zero, but the battery capacity still less than the minimum state of charge, the renewable generation methods will provide the electricity.

By introducing the diesel generator and therefore the DGO, part of the electricity will be generated by a diesel generator, which is indicated by a percentage of the total electricity demand. Since most of the time when the battery capacity is about to go under the minimum state of charge, the mismatch is less than zero. Moreover, the generator is not used to charge the batteries, only to supply the electricity. The diesel generator will kick in when the renewable generating components and the battery cannot deliver the load, and is sized to deliver the maximum mismatch. The introduction of the diesel generator results in the fact that the load is not lost, but generated by the diesel generator and other renewable generating methods of the HPP. This way, the individual components capacities are significantly reduced, resulting in a decrease in LCoE.

In figure 3.32, the plot of the electricity stored in the battery is given. Compared to figure 3.31, the capacity does not drop below the minimum state of charge anymore, and the maximum capacity is still the same. This shows how a controllable electricity generation method can add much value to the HPP.

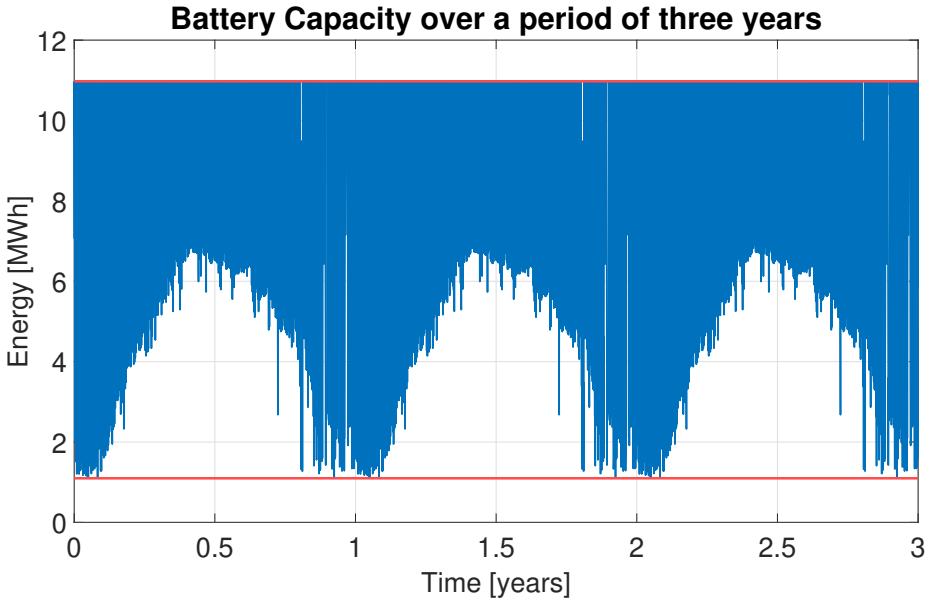

Figure 3.32: Hourly battery capacity with an appropriately sized battery and a loss of load of 5%, which is generated by the diesel generator.

With the addition of the diesel generator, the optimal amount of electricity that is generated by diesel is calculated to minimise the LCoE of the HPP. The big drawback of diesel generation is that it is polluting the environment. Therefore, if set as an objective of the model, the loss of load can also, either be zero or lost completely (meaning that it would not be generated by the diesel generators). Another way to deal with the loss of load would be demand-side management. This is considered outside the scope of this project and therefore demand is considered a strict constraint that always should be met.

The cost functions of the AWES and solar energy systems are already reflected upon. A similar line of thinking goes for the cost function of the batteries and diesel generators. In this research, the battery capacity price is based on estimations by NREL [25]. Since these are approximations, time will tell whether they represent the actual battery price. The diesel generator price is assumed to be mature and will not change a lot between now and 2030. However, the diesel price is super volatile, and it is challenging to determine what it will be in 2030. To include the uncertainty of the future component costs and diesel price, a sensitivity analysis of each component and the diesel price is done in section 4.2. This analysis will make the research more robust to future changes in the current approximations.

3.8 System Optimiser

To find the minimal LCoE of the HPP, an optimiser is made. This optimiser works by putting in discrete variables for the three optimisation components and running the model. The following three variables are optimised:

- Number of solar modules (solar capacity)
- Number of kites (AWE capacity)
- Loss of Load / DGO

Three arrays with different values (usually ascending with a linear slope) are created for the three variables. Each possible combination is put in the model, and the LCoE is calculated. After, the minimum LCoE of the three-dimensional matrix is evaluated. The minimum LCoE and the corresponding component sizing are displayed. The surface plot in figure 3.33 illustrates how the LCoE changes depending on a different number of modules and kites. In this case, the loss of load is kept at zero, and the LCoE has been normalised. The red mark indicates the minimal LCoE.

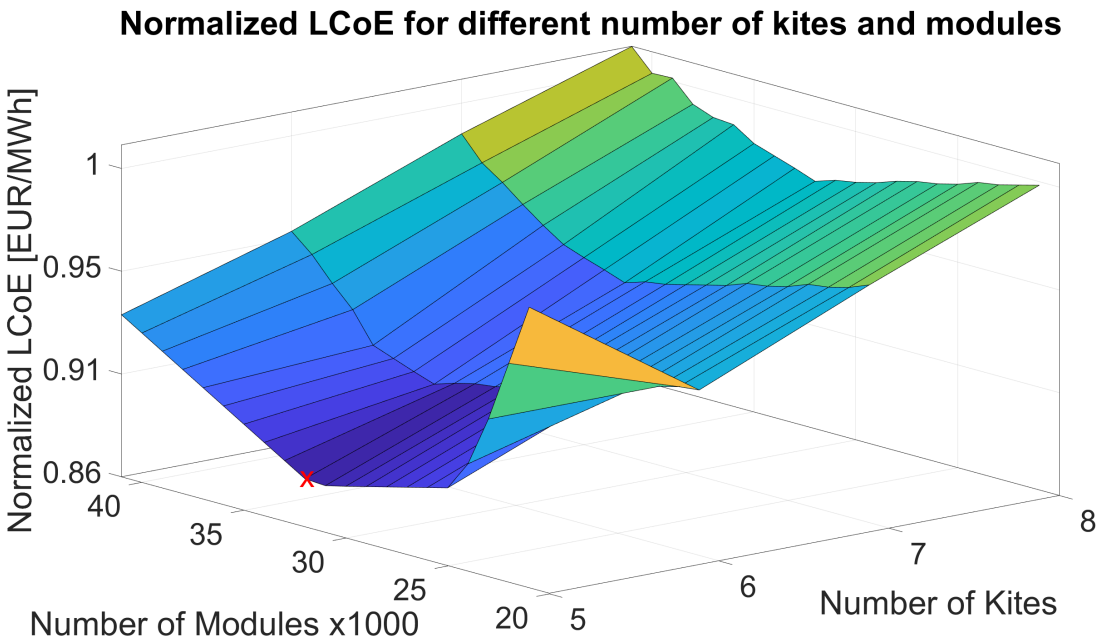

Figure 3.33: A surface plot of the LCoE, dependent on a different number of kites and modules.

In this chapter, the HPP objective of the optimiser was to size for minimal LCoE. However, the HPP can also be sized for other objectives like maximising power per area or security of supply. These different objectives of the HPP can be put in the model, and the optimiser will find the optimal solution with the corresponding sizing of the components.

4 Results and Evaluation

Now that all the performance and cost modelling have been analysed, the model results are evaluated in this chapter. This chapter investigates the use-case of a stand-alone system with the performance and cost modelling of solar energy and airborne wind energy system (AWES) and the load case data given in chapter 3 of Marseille. The most relevant data is summarised in table 4.1.

Table 4.1: An overview of the most important information of the data of chapter 3.

Marseille key information		
Average hourly demand	0.5	MWh
Average wind speed	7.2	m/s
Equivalent sun hours	4.0	kWh/m^2/day
Diesel price	1.37	€/L
Carbon tax	0.125	€/kg

The hybrid power plant (HPP) is built up by adding a component at every step, starting with solar energy and batteries in section 4.1. Then the case of airborne wind energy (AWE) and batteries is investigated, after which the combination of the three components is assessed. To complete the HPP, the diesel generator is added and evaluated. In section 4.2, the sensitivity of the levelized cost of electricity (LCoE) of the HPP with respect to the security of supply, diesel price, and component costs is analysed.

4.1 Hybrid Power Plant configurations

Before investigating the concept of combining two different renewable energy sources, each renewable energy component will be investigated separately to see their performance for a stand-alone configuration. What is different for a stand-alone compared to a grid-connected configuration is that not all the energy generated will be used. This has a significant impact on the LCoE. Moreover, the load needs to be supplied at all times. For all evaluated cases, the load profile of the military camp of section 3.5 is used. Later in this chapter, in section 4.2.1, a sensitivity analysis will be done to investigate the effect of the loss of load.

4.1.1 Solar Energy + Batteries

The first HPP that will be investigated is the combination of solar energy and storage. Since electricity is demanded throughout the day and night, solar energy without storage is not an option. Moreover, more solar energy is produced on a yearly scale during summer than during winter. As is determined in section 3.5, the demand is higher during winter than during summer. Therefore, there is a trade-off between oversizing the solar modules, which results in curtailment of the excess electricity, and the battery capacity. The LCoE is calculated on the consumed electricity by the load, not on the total generated electricity by the system. Loss of load is not considered in this analysis.

As can be seen in figure 4.1, when the nominal power of the solar energy system is increased, the need for a high battery capacity decreases. Moreover, even though the nominal power increases with constant increments of 5 MWp, the battery capacity does not decrease linearly. The reason is that solar energy is not generated every hour of every day. No matter how immense the system's nominal power is, there will always be a need for storage. When looking at the LCoE, it can be seen that there is a sweet spot in the trade-off between the oversizing of the system's nominal power and the battery capacity. The optimal component sizing for this configuration is 30 MWp installed solar power and a battery capacity of 37 MWh, which yields a LCoE of 666 €/MWh.

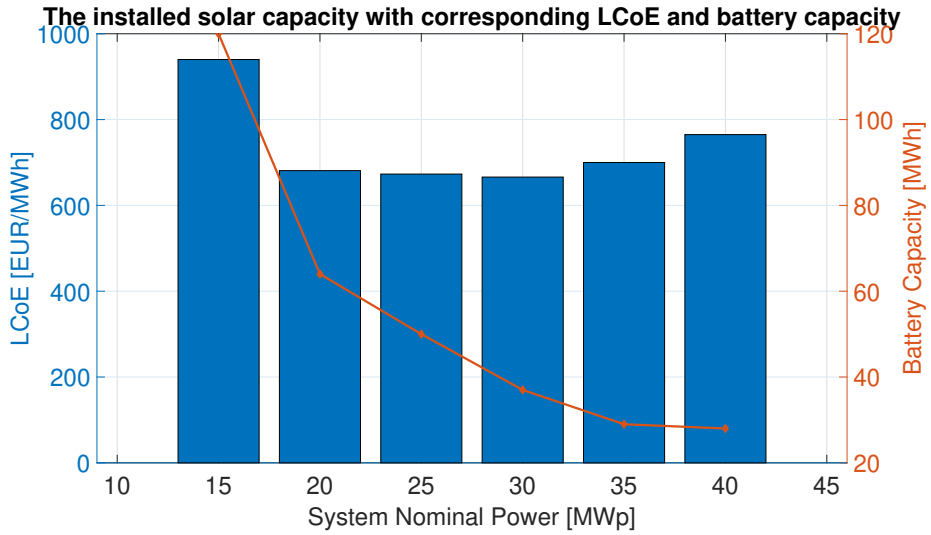

Figure 4.1: A bar plot of the LCoE and battery capacity of increasing installed solar capacity.

The figure in figure 4.2 shows the hourly battery capacity for an optimised HPP containing solar energy and batteries. As can be seen, the peaks are contained in the summer, and the clear pattern that much electricity is generated during that period is visible. This figure looks very similar to figure 3.30, the only difference being that there are about 10,000 solar modules less in the system. This results in the battery being slightly bigger for this case.

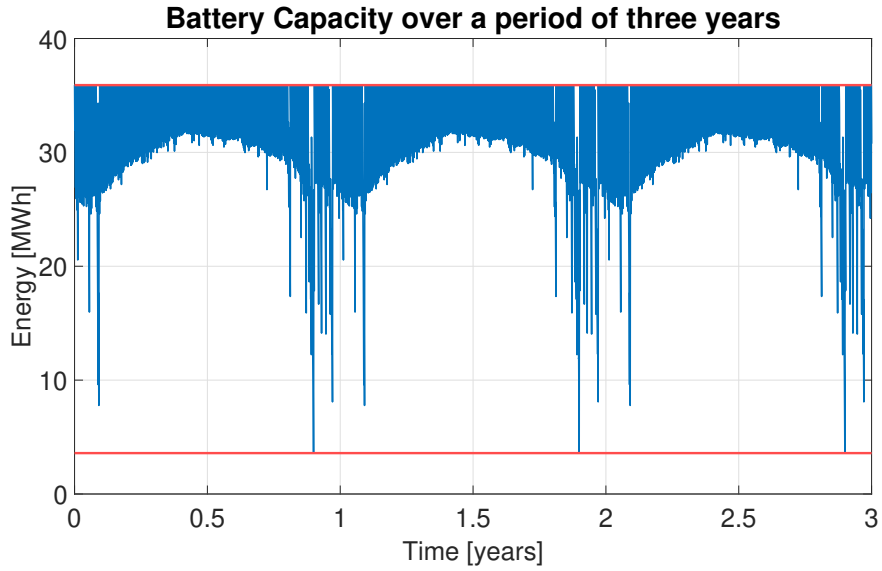

Figure 4.2: The hourly battery capacity for an optimised HPP containing solar energy and batteries.

4.1.2 Airborne Wind Energy + Batteries

Similar to how the optimal LCoE was determined for the HPP consisting of solar energy and batteries, the LCoE is determined for a HPP consisting only of AWE and batteries. Again, an off-grid situation is simulated, which results in a trade-off between oversizing the installed kite power, having to curtail the generated electricity, and the battery capacity.

The kite power is increased with increments of 0.5 MW installed power, which is equal to five kites. What can be seen in figure 4.3 is that the optimal size of the components is 2 MW of AWE and 92 MWh of battery capacity. This results in a LCoE of 899 €/MWh, significantly higher than the HPP containing only solar energy. Moreover, the installed power is significantly less. This has to do with the fact that the capacity factor of AWE is higher than solar energy. Finally, the size of the batteries is bigger, which drives up the LCoE significantly.

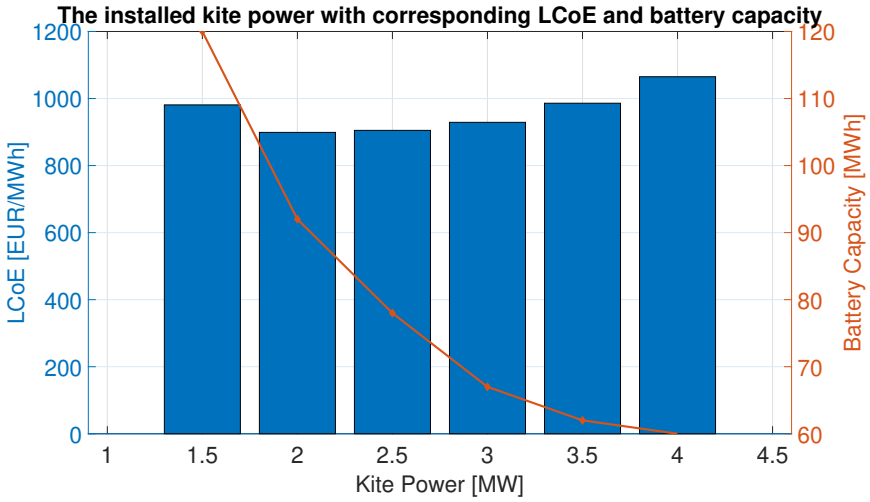

Figure 4.3: A bar plot of the LCoE and battery capacity of increasing installed kite power.

Sizing a HPP with AWE and batteries results in a very different hourly battery capacity plot than in the case with sizing with solar energy, see figure 4.4. What is clear is that in summer, not the most electricity is produced but rather in winter. Moreover, the scattering of the data on the plot is way higher. This means that the system is less oversized, as was the case with the solar plots. This is because AWE is more expensive, to begin with.

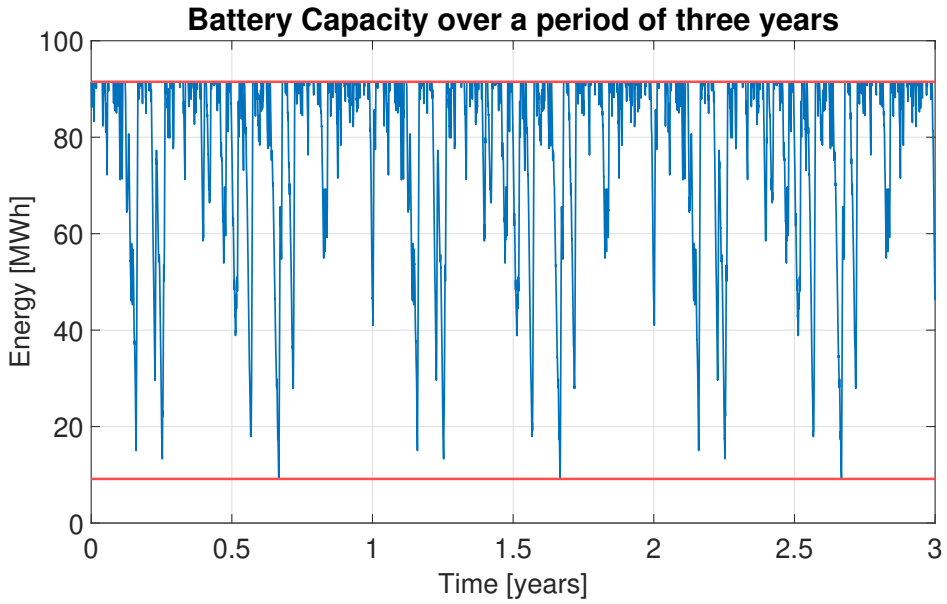

Figure 4.4: The hourly battery capacity for an optimised HPP containing AWE and batteries.

4.1.3 Solar Energy + Airborne Wind Energy + Storage

The next step in designing a HPP is to combine the two different resources with the batteries. Based on the anti-correlation between solar and wind resources, the cost reduction is calculated for the shared use of infrastructure. However, the infrastructure cost of both systems is a tiny percentage of the cost. Therefore, the cost reduction in sharing the infrastructure has barely any effect on the LCoE of the system.

In table 4.2, the component sizing of the two stand-alone resources is given in the first two rows. In the third row, the HPP is sized by combining the two different resources and the battery. As can be seen in the table, the LCoE drops significantly when the two resources are combined, which makes a strong case for the HPP. The ratio between the installed capacity of the two-generation methods is 20:1, solar to wind power, respectively. The battery capacity is smaller compared to the two stand-alone systems. The solar power capacity is 10 MWp, the wind power is 0.5 MW, and the battery capacity is 25 MWh, which yields a LCoE of 388 €/MWh.

Table 4.2: An overview of different capacities of Solar Energy, AWE and Batteries with the corresponding LCoE.

Solar Power [MWp]	Wind Power [MW]	Battery capacity [MWh]	LCoE [€/MWh]
30	0	36	668
0	2	92	899
10	0.5	25	388

With the decrease of installed generation capacity for the HPP, the power that is curtailed for the two stand-alone generation methods significantly decreases. Even in the case of the HPP consisting of AWE and solar PV, the

The hourly battery capacity of the HPP is given in figure 4.5. The effect that the modules have on the system is still very clearly visible, with the depletion of the battery happening in the winter. However, the battery capacity is not as big as in the solar + battery HPP, nor is the installed solar capacity. By introducing the diesel generator, the LCoE can be further minimised.

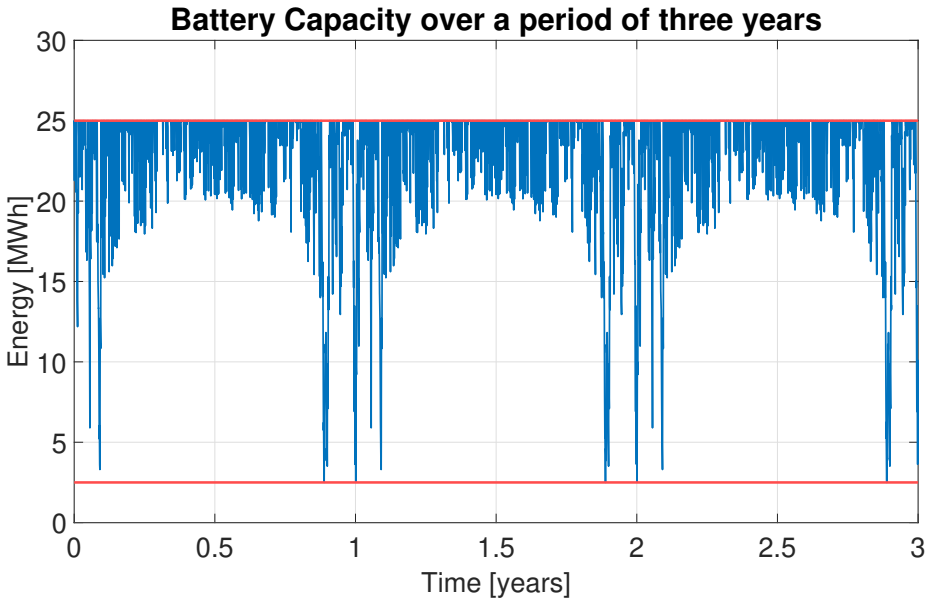

Figure 4.5: The hourly battery capacity for an optimised HPP containing solar energy, AWE and batteries.

4.1.4 Addition of Diesel Generators

Looking at figure 4.5, it is evident that the battery is still not optimally used. The battery capacity is sized in order to be able to supply all the load. Diesel electricity is generally more costly than solar or wind electricity generation [61]. However, in off-grid situations where the load needs to be 100% supplied, the batteries need to have sufficient capacity to store all the necessary electricity. A battery capacity of this size significantly drives the cost and the LCoE up. Therefore, by using diesel generators to supply part of the load (through the means of diesel generation optimisation (DGO), explained in section 3.7), the battery capacity can be decreased. In the evaluated case, the litre price of diesel is 1.37 €/L, and the carbon tax is 0.125 €/kg emitted, as in section 2.1.5.

In table 4.3, the HPP configuration of the previous section and the configuration which allows for diesel generation are given. In the case for allowing for DGO, the load is not lost, but it is provided by the diesel generators when the mismatch is smaller than zero. When the mismatch is greater than zero, the renewable electricity generators of the HPP itself will provide the electricity. The diesel generator has a power rating of 688 kW.

With 7% diesel generation, the solar modules are significantly less oversized; the solar power is decreased by a factor of two, from 10 to 5 MWp installed. This means that less solar power is curtailed. The installed wind power is slightly increased, from 0.5 to 0.6 MW (equal to the addition of one Falcon Kite). The most significant change happens in the battery capacity, which is decreased from 25 to 7.2 MWh. By generating part of the load (7%) by diesel generators, the LCoE drops from 388 to 281 €/MWh. In the LCoE calculations, the denominator (the load) is constant for all LCoE calculations since only the used electricity by the load is regarded. This means that, although less power is curtailed in the case of a HPP with a diesel generator, power curtailment is observed.

Table 4.3: A comparison in the component sizing between a system with zero and optimal diesel use with corresponding LCoE.

Solar Power [MWp]	Wind Power [MW]	Battery Capacity [MWh]	Diesel Generation [%]	LCoE [€/MWh]
10	0.5	25	0	388
5	0.6	7.2	7	281

As can be seen in figure 4.6, the battery is way smaller than in previous HPP configurations. The seasonal trend of summer electricity generation by the solar modules is not as visible as previously. The extreme peaks in battery depletion are now gone, and the depletion looks more constant throughout the year.

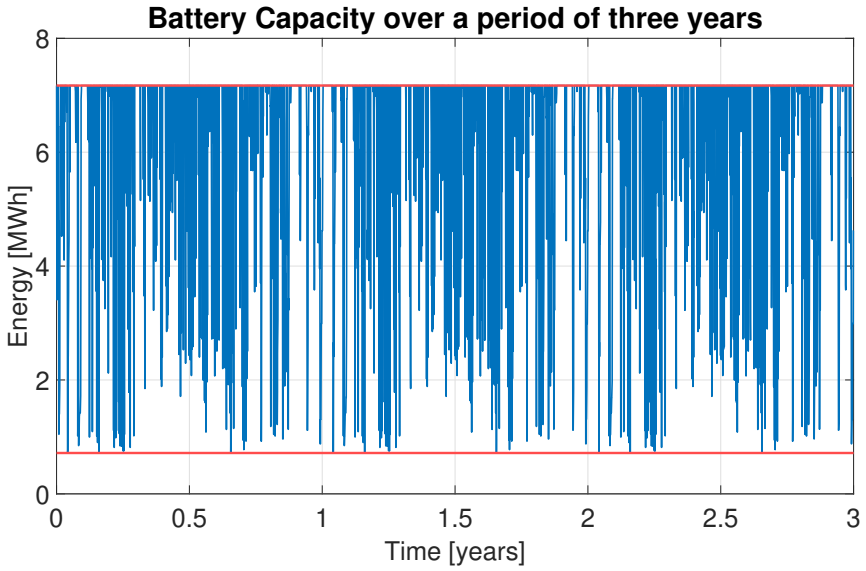

Figure 4.6: The hourly battery capacity for an optimally optimised HPP containing solar energy, AWE, diesel generation and batteries.

Another possibility would be that the diesel generators would supply all the electricity for the off-grid location. While maintaining the diesel price of the Netherlands in 2021 (at 1.37 €/L) and the carbon tax at 0.125 €/kg, the LCoE is equal to 719 €/MWh. The battery capacity and the installed solar and wind power would be zero since diesel is a controllable generation source. The LCoE of only using diesel is 2.5 times higher than the optimally sized HPP. This shows that, in the future, optimised HPPs with diesel generators will yield the lowest LCoE, as can be seen in figure 4.7.

By 2050, in Europe, the goal is to remove carbon-emitting electricity generators altogether. Therefore, diesel generators in a HPP will not even be an option anymore. However, that does not have to be a problem since the HPP without the DGO (and therefore the diesel generators) still has a very competitive LCoE of 388 €/MWh, which is 1.8 times lower than using just diesel generators.

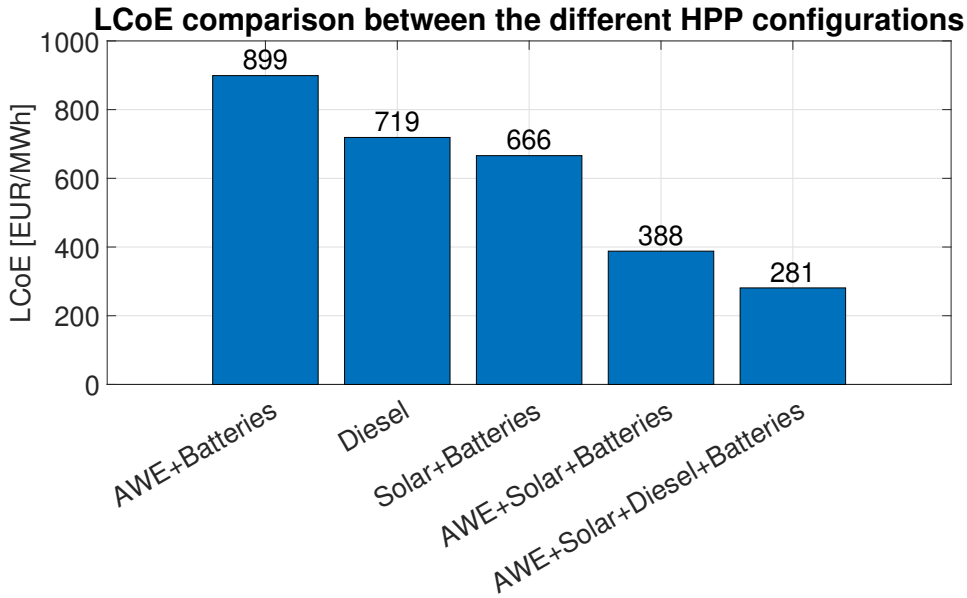

Figure 4.7: The LCoE of the five different HPP configurations.

The shared land use could play a significant part in cost reduction and optimisation of the land area. However, for this research, it is assumed that the users of the HPP already own the land, and therefore, no extra costs for using the land are investigated. Research into the shared land use and the effect on the cost of the HPP is outside the scope of this research.

4.2 Sensitivity Analysis

Many factors play a role in determining the LCoE of the optimally sized HPP. In this section, a sensitivity analysis is made to investigate how the LCoE changes with changing variables. First, the sensitivity to the security of supply is analysed. Then, the diesel price is varied to investigate what that does for the component sizing and LCoE. Finally, since the component costs are estimations, the individual component costs are varied to analyse and evaluate the component sizing and LCoE of the HPP.

4.2.1 Security of Supply

The sensitivity of the HPP to the loss of load is investigated in this section. Here, the loss of load, opposed to the DGO, will not be generated by the diesel generators. For the calculation of the LCoE, the annual energy use will decrease as the loss of load decreases. In table 4.4, increasing loss of load with increments of 5% is given, with the battery capacity of the optimally sized HPP and the corresponding LCoE. The results in this table cannot be compared to the results of section 4.1 because, in that situation, the delivered load is always constant.

Table 4.4: The sensitivity to the loss of load with the optimally sized components of the HPP.

Loss of Load [%]	Solar Power [MWp]	Wind Power [MW]	Battery Capacity [MWh]	LCoE [€/MWh]
0	10.1	0.5	25.3	388
5	5.4	0.7	10.5	285
10	6.4	0.6	9.0	283
15	6.0	0.6	7.4	282
20	**5.4**	**0.6**	**6.6**	**281**
25	5.0	0.6	5.6	286
30	4.7	0.6	5.3	296
35	4.0	0.6	5.5	306
40	5.0	0.4	6.7	309

In the beginning, the LCoE decreases while increasing the loss of load. However, after it reaches the minimum, it increases again because less and less energy is used (and therefore, less energy is used in calculating the LCoE). At the same time, the component sizing stays relatively the same. The optimal is found at a loss of load of 20%, solar power of 5.4 MWp, wind power of 0.6 MW, and a battery capacity of 6.6 MWh. This HPP configuration yields a LCoE of 281 €/MWh.

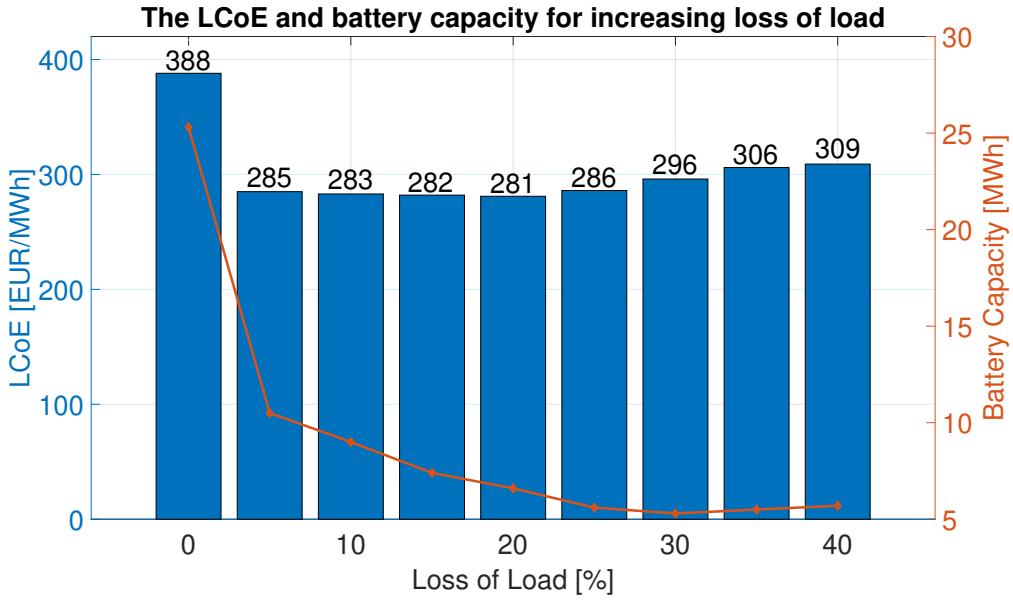

Figure 4.8: Increasing the loss of load with increments of 5% with the corresponding LCoE and battery capacity of the optimally sized HPP.

The battery capacity for an optimised HPP with a loss of load of 20% is given in figure 4.9. As can be seen from the figure, the battery capacity data is not neatly in between the minimum and maximum of the battery. There are hours, especially in the winter months, that go far below zero capacity. The trend of the solar modules peaking in the summer is still a little visible, resulting in the fact that during this season, the load is still kept within the state of charge limits of the battery.

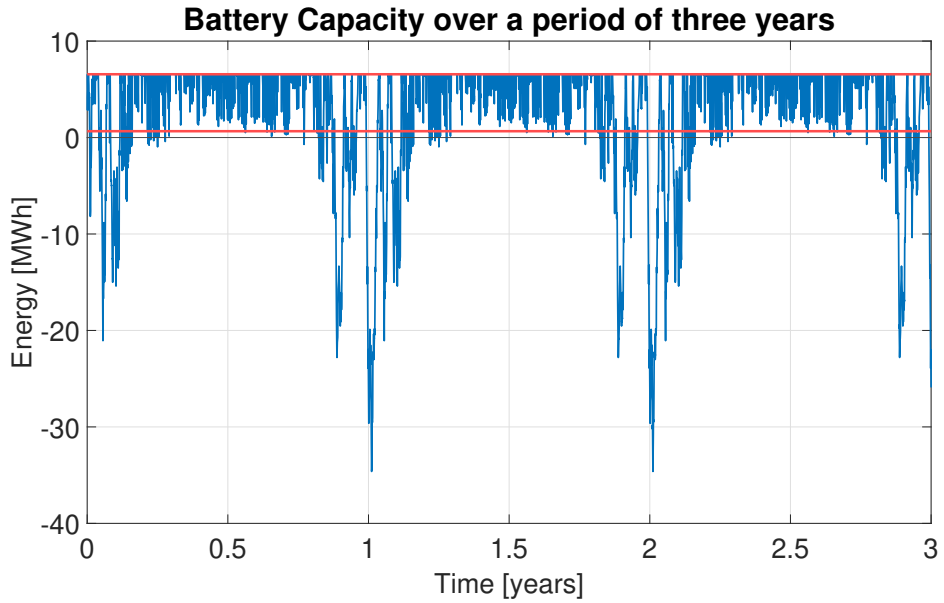

Figure 4.9: The hourly battery capacity for an optimised HPP and 20% load loss.

Figure 4.10 gives an impression of how the hourly battery capacity looks like for a loss of load of 40%. As can be seen now, the battery is far below the minimum capacity for the whole winter season. So far below that, the data for the rest of the year is barely distinguishable. The LCoE has not gone further down from the loss of load case of 20% since the system uses less and less energy. Therefore, the optimal loss of load, which decreases the LCoE by about 28%, is 20%.

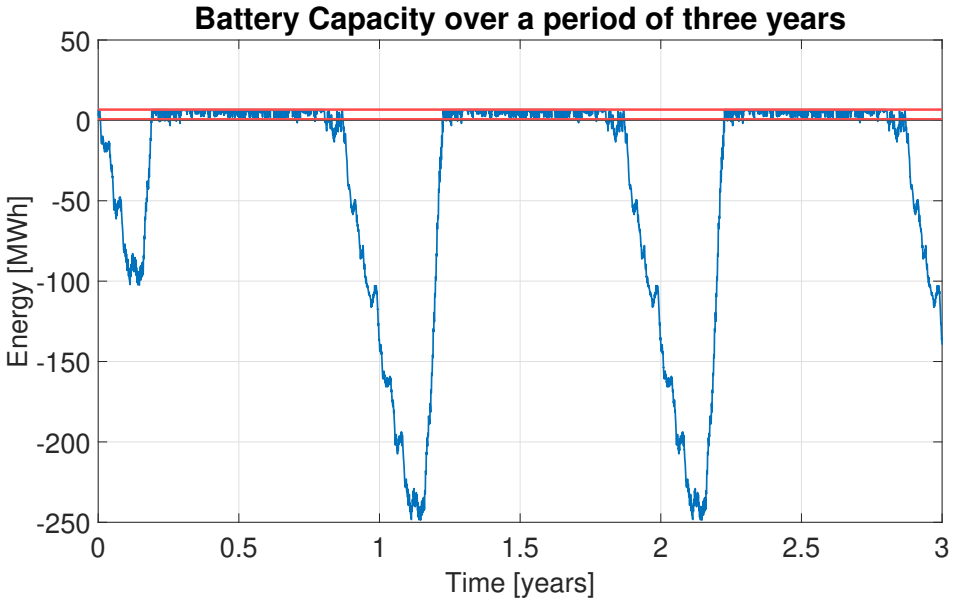

Figure 4.10: The hourly battery capacity for an optimised HPP and 40% load loss.

4.2.2 Diesel Price

The diesel price varies from country to country and with time. Therefore, it is still highly uncertain what the diesel price will be in 2030. An analysis of what the optimal sizing of the HPP components will look like for various diesel prices is done in this section. It is expected that the share of diesel generation will increase when the price decreases. The carbon tax will not be considered to make the approach more relatable for any location worldwide. The analysed location is again Marseille with the corresponding load and resource data. Moreover, since diesel generation is investigated, an off-grid situation is assumed.

The first analysis is done by optimally sizing the components of the HPP for different diesel prices, as can be seen in table 4.5. With a decrease in diesel price, the diesel use increases; therefore, the battery capacity decreases. Which makes sense, since it becomes cheaper to use the diesel generator. At a diesel price of 0.75 €/L, the batteries are not used anymore because all electricity is generated by the renewable components of the HPP or the diesel generator.

Table 4.5: The sensitivity of the LCoE to the diesel price for a HPP.

Diesel Price [€/L]	Diesel Generation [%]	Solar Power [MWp]	Wind Power [MW]	Battery Capacity [MWh]	LCoE [€/MWh]
2.00	6.3	5.0	0.6	8.1	290
1.75	7.0	5.0	0.6	7.2	283
1.50	7.0	5.0	0.6	7.2	275
1.25	8.2	5.0	0.6	5.9	267
1.00	13.2	3.4	0.6	5.2	250
0.75	30.5	1.3	0.5	0	211
0.50	44.4	1.3	0.3	0	173
0.25	74.8	1.0	0	0	101
0.00	100.0	0	0	0	7

In the final range of figure 4.11, a diesel price between 1.00-2.00 €/L, the LCoE of the HPP does not increase that quickly due to relatively cheap renewable generation methods. Moreover, at 0.25 €/L, no wind power is used anymore, yet some solar power is still installed since the LCoE of solar energy is lower than wind energy. Finally, a diesel price of 0 €/L is added to do a sanity check for the model. The LCoE is not zero in this case because, even though the cost of fuel is zero, there is still some investment cost in the generator itself.

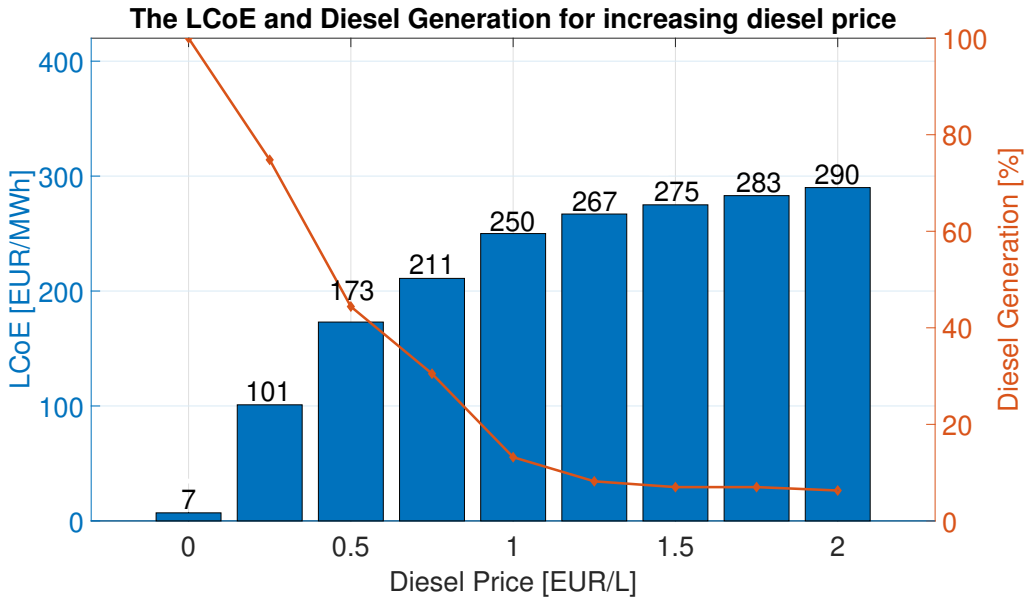

Figure 4.11: The LCoE and diesel generation of the optimally sized HPP for increasing diesel prices.

In figure 4.12, the battery capacity of the HPP is given for a diesel price of 1.00 €/L. What stands out is that the battery stays at maximum capacity during the winter periods. This is because electricity is generated through diesel generators during those periods. The diesel price is already so cheap that the diesel generators supply the electricity in that period. There is still some renewable electricity generation, especially in the summer periods of the years. The effect of solar energy generation is not that visible anymore since the installed capacity is relatively tiny as opposed to previous configurations.

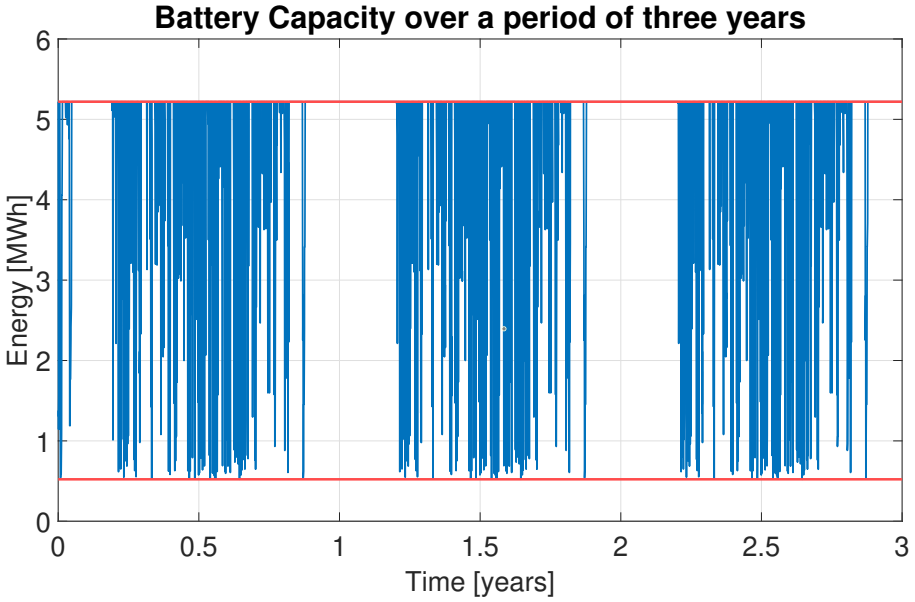

Figure 4.12: The hourly battery capacity for an optimised HPP and a diesel price of 1.00 €/L.

When the diesel price is 0 €/L, no other method of electricity generation is used anymore. Moreover, since diesel generators are a controllable energy generation source, the need for storage becomes zero too. Therefore, the battery capacity is zero throughout the whole period, as can be seen in figure 4.13. This figure is another sanity check for the model.

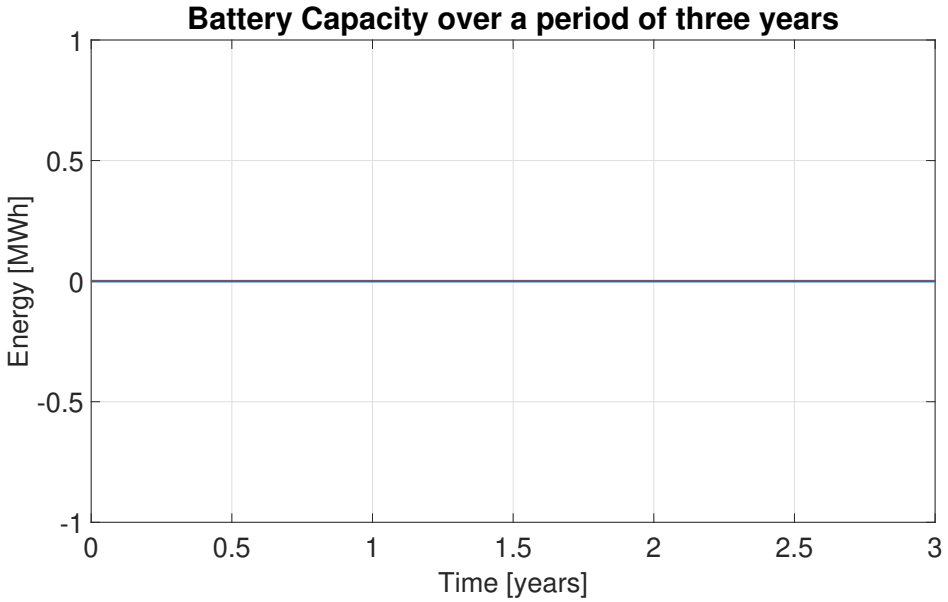

Figure 4.13: The hourly battery capacity for an optimised HPP and a diesel price of 0.00 €/L.

In most remote, off-grid locations, diesel generators are used to supply 100% of the load. Therefore, the LCoE will be dependent on only the cost of the initial investment cost, diesel price and usage, and the carbon tax. In this analysis, the carbon tax is set at zero to make the analysis applicable to any location around the world. However, the load data from section 3.5 is still used in this analysis.

Figure 4.14 gives the diesel price and the corresponding LCoE for a system that only consists of a diesel generator. The LCoE increases by 105 €/MWh for every 0.25 €increase in diesel price. As was seen in figure 4.11, when the diesel price is zero, the LCoE is not zero since investment costs into the diesel generator still have to be made.

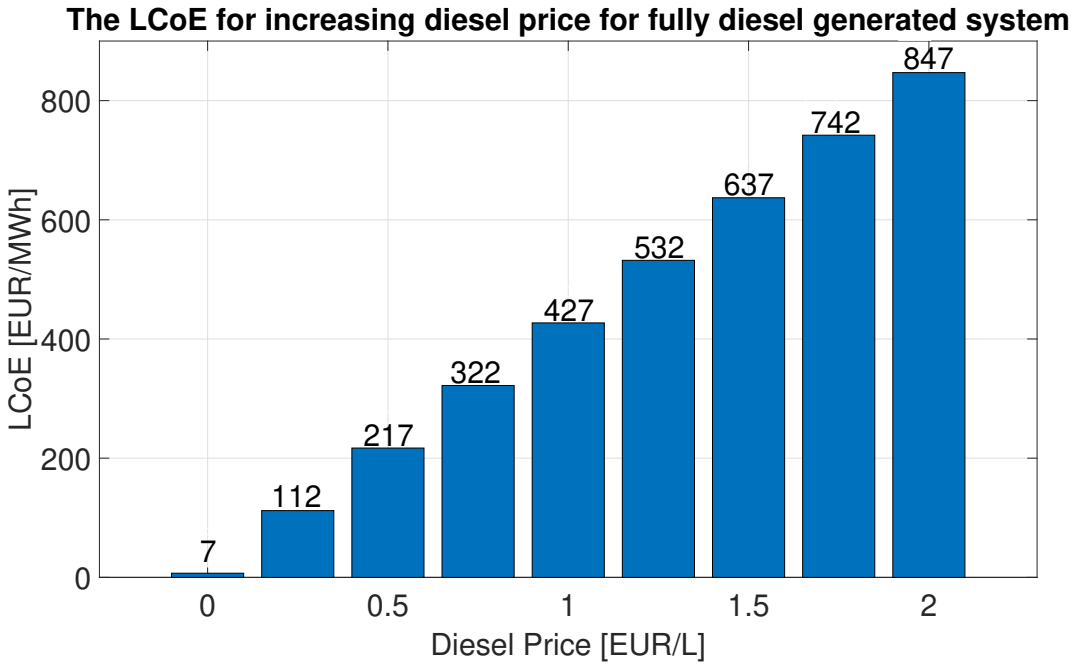

Figure 4.14: The sensitivity of the LCoE to a variation in the diesel price for a 100% diesel generated system.

Comparing figure 4.11 and figure 4.14 of this section, it can be seen that for high diesel prices, the LCoE for a 100% diesel-generated system is exceptionally high. At the same time, the LCoE of the HPP remains below 300 €/MWh. Even when the diesel price is extremely low, at 0.25 €/L, the LCoE of the HPP is still lower than the LCoE of the fully diesel-generated system. The LCoE of solar energy is very low; therefore, even when it is only used a little bit in a HPP, it still drives the cost down. The added value of AWE in an HPP is visible at a diesel price of 0.50 €/L and higher up.

4.2.3 Cost components

By calculating the cost of the different components of the HPP, assumptions have been made based on the literature. These assumptions give a good indication of the actual values of each of the components. However, these costs vary for different systems, locations and times. In this section, the sensitivity to percentage changes in cost is analysed.

A breakdown of the cost of the optimally sized HPP of section 4.1.4 is given in figure 4.15. The four cost components in a HPP are related to: wind, solar, battery, and diesel. All four components have the same order of magnitude cost in an optimally sized HPP. The total costs of the HPP consist of the initial investment cost, the cost of renewing certain parts of a component, and the O&M costs. For the last two cost components, discounting is taken into consideration.

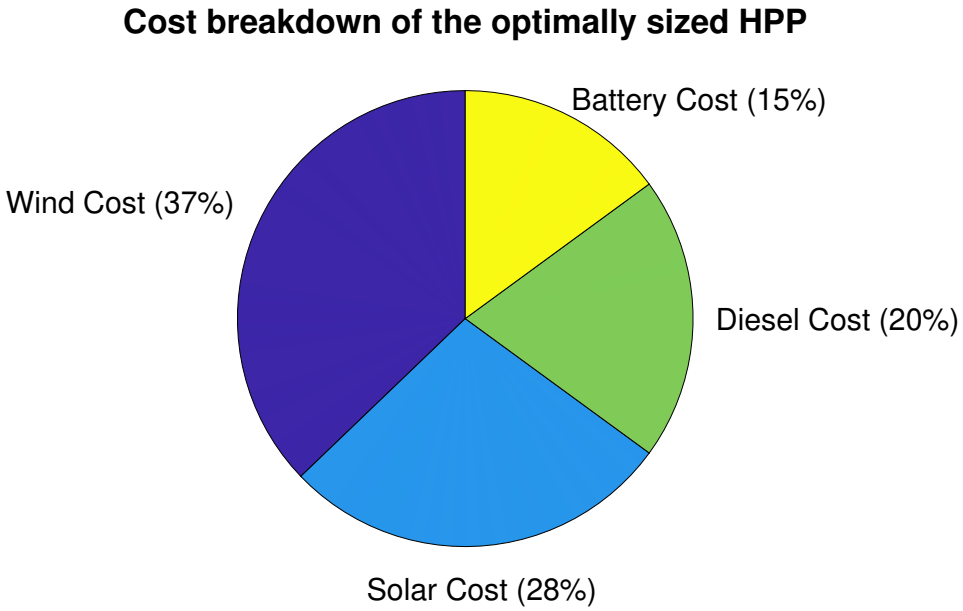

Figure 4.15: The cost breakdown of the optimally sized HPP.

The most significant cost component of the optimised HPP is wind energy, which makes up 37% of the total cost. Since it is the biggest component, it will affect the LCoE of the most. All other variables are kept constant to analyse the effect of the change in the cost of one component on the LCoE of the optimised HPP. The component sizing will vary when optimising the system, but the diesel price and carbon tax are kept constant, as in section 4.1.4.

With an increase in wind cost, a decrease of the component is seen in the optimal component sizing of the HPP, as can be seen in table 4.6. In the range of a price of -10% to +25%, the component sizing of the optimally designed HPP does not vary at all, only the LCoE changes. This is because only an integer number of kites for wind power is possible. When the AWES becomes very expensive, with a price increase of 50%, one kite is used less in the optimal sized HPP. With the price decrease in wind energy cost, the number of kites changes at -25% and -50%. When the wind power capacity increases, the solar power capacity decreases.

Table 4.6: The sensitivity of the LCoE to a variation in the cost of the AWES.

Price Vary [%]	Solar Power [MWp]	Wind Power [MW]	Battery Capacity [MWh]	Diesel Generation [%]	LCoE [€/MWh]
+50	6.0	0.5	6.9	8.6	333
+25	5.0	0.6	7.2	7.0	307
+10	5.0	0.6	7.2	7.0	292
0	5.0	0.6	7.2	7.0	281
-10	5.0	0.6	7.2	7.0	270
-25	4.7	0.7	7.4	5.6	254
-50	4.4	0.8	7.7	4.5	220

Moreover, the use of diesel decreases while the battery capacity increases. This is because wind energy becomes cheaper in the HPP, and therefore, the other generation methods are used less. Because of the intermittency of wind compared to the controllable diesel generators, the battery capacity has to increase. With a 50% increase in wind energy cost, the LCoE increases by 19%. With a 50% decrease in wind energy cost, the LCoE decreases by 22%. A graphical representation of table 4.6 is given in figure 4.16.

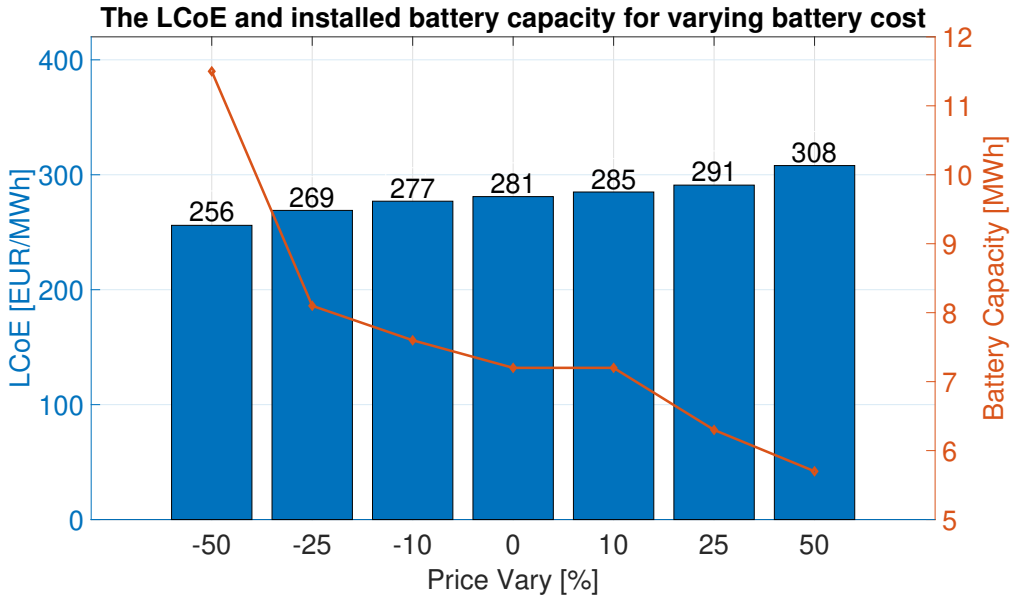

Figure 4.16: The sensitivity of the LCoE to a variation in the cost of the AWES.

The same analysis as done for the wind cost is done for the solar cost, which results are given in table 4.7. The price variation of the solar energy system affects the LCoE of the HPP less than the price variation of the AWES. This makes sense since the wind cost was the most significant share of the total cost of the HPP. The price variation has the most substantial effect on the trade-off between the installed solar power and the use of diesel.

Table 4.7: The sensitivity of the LCoE to a variation in the cost of solar energy.

Price Vary [%]	Solar Power [MWp]	Wind Power [MW]	Battery Capacity [MWh]	Diesel Generation [%]	LCoE [€/MWh]
+50	3.4	0.7	7.0	9.0	312
+25	3.4	0.7	7.0	9.0	300
+10	5.0	0.6	7.2	7.0	288
0	5.0	0.6	7.2	7.0	281
-10	5.0	0.6	7.2	7.0	273
-25	5.0	0.6	7.2	5.1	262
-50	6.7	0.6	7.8	3.9	237

The more expensive solar electricity generation gets, the more electricity generated by the diesel generator. Wind power seems unaffected by the price decrease of solar energy. Even when solar energy becomes very cheap (-50%), the installed wind power stays at 0.6 MW. At the price decrease of -50%, the solar power is more and more oversized, resulting more curtailment and a decrease in diesel use, as can be seen in figure 4.17. However, the battery capacity is still increased to use more of the oversized solar power.

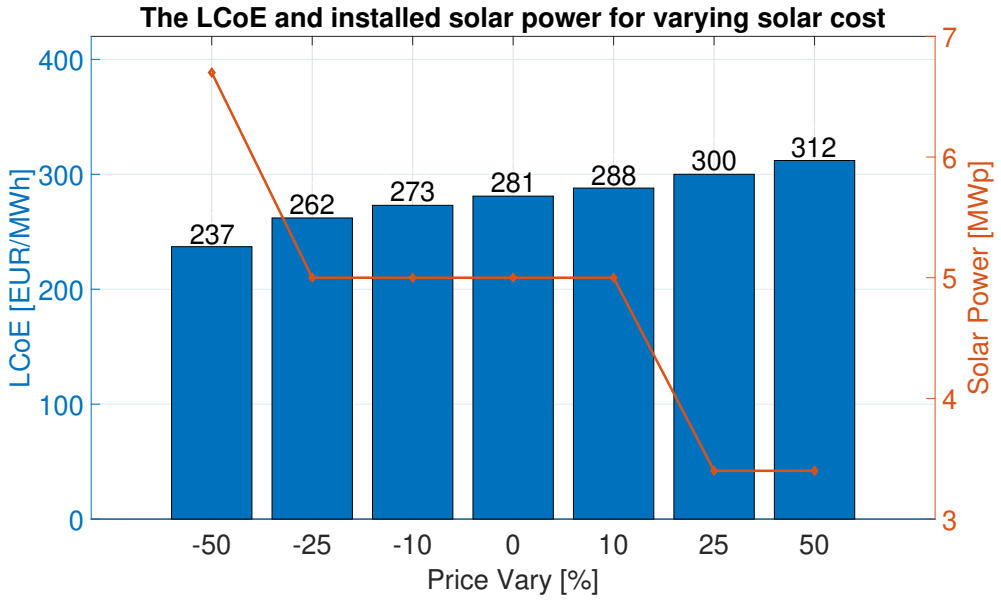

Figure 4.17: The sensitivity of the LCoE to a variation in the cost of solar energy.

The smallest cost component of the HPP is the battery cost, which makes up only 15% of the total cost. Therefore, the effect of varying the price of the battery has a smaller effect on the LCoE than the varying price of the wind and solar costs. Table 4.8 gives the sizing and LCoE of the HPP for various price variations of the battery cost. When storing energy becomes cheaper, the use of diesel decreases.

Table 4.8: The sensitivity of the LCoE to a variation in the battery cost.

Price Vary [%]	Solar Power [MWp]	Wind Power [MW]	Battery Capacity [MWh]	Diesel Generation [%]	LCoE [€/MWh]
+50	6.0	0.5	5.7	10.0	308
+25	5.0	0.6	6.3	7.8	291
+10	5.0	0.6	7.2	7.0	285
0	5.0	0.6	7.2	7.0	281
-10	5.0	0.6	7.6	6.6	277
-25	5.0	0.6	8.1	6.3	269
-50	5.4	0.6	11.5	4.0	256

As can be seen in figure 4.18, with an increase in battery cost, the battery capacity decreases. Moreover, the LCoE remains close to the zero price variation LCoE since the effect of varying the battery cost has the smallest effect on the LCoE.

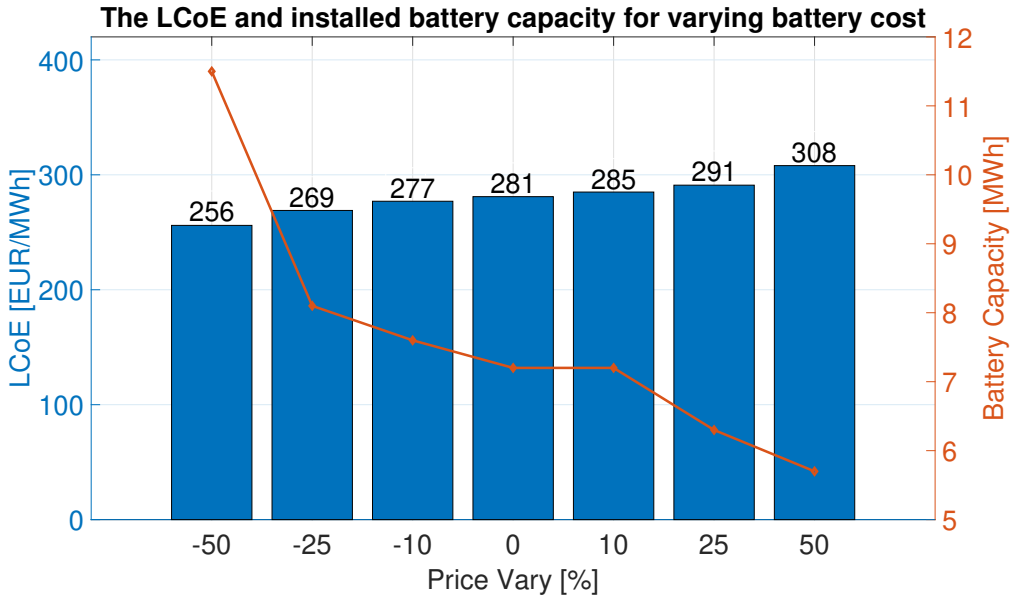

Figure 4.18: The sensitivity of the LCoE to a variation in the cost of the batteries.

What can be seen from these three cost evaluations is that the LCoE varies with varying prices. If all components (including the diesel generation cost) increase by 50%, the LCoE increases to 422 €/MWh. The HPP would still produce a lower LCoE than a 100% diesel-generated system with a diesel price of 1 €/L. The location that is used for all the analyses is Marseille in France. This location has substantial resources compared to other locations in Europe. However, the energy yield could be even higher when compared to the rest of the world, especially the solar resource. This shows how competitive these HPPs are.

Power blackouts due to a dunkelflaute scenario or breakdown of the HPP's components are omitted for the model's simplicity at this stage. However, an off-grid energy system is particularly vulnerable to these scenarios. By downloading real-life data for the resources and the load, extremes in the data are considered in the calculations, and the components of the HPP are sized accordingly. The components of the HPP are expected to produce power throughout their whole lifetime. For future research, a thorough investigation of the sizing of how the HPP's components would change in case of breaking down of the system is necessary to include power blackouts in the model.

5 Business Case

In this chapter, three locations are evaluated for the use of the hybrid power plant (HPP) as a business case. In section 5.1, the outline of the business case is given. The next step in the business case is to analyse the location in section 5.2. Since each location has new solar and wind resources, the AEP of each location is calculated in section 5.3. In section 5.4, the HPP is optimally sized for each location. To conclude this chapter, an evaluation is given in section 5.5.

5.1 Business Outline

Currently, in remote off-grid locations, electricity is primarily generated using diesel generators, which are expensive and have significant carbon emissions. Alternatively, these remote locations have a massive potential for utilising renewable energy sources. In such locations, airborne wind energy systems (AWESs) could have an advantage over conventional wind turbines. Since the AWESs operate at higher altitudes, stronger and more consistent wind energy can be harnessed. Moreover, they are more compact and have higher mobility, which can reduce installation, operation, and maintenance costs.

The mobility of the AWESs has another significant advantage over wind turbines. In some remote locations, temporary electricity is needed, from a few months to fifteen years. Once they are built in a specific location, Wind turbines have a lifetime of 25 years. Breaking down the wind turbine and building it up somewhere else is very expensive and inefficient. A 100 kW AWES fits in a 20 ft container and is transportable by a semi-truck. Therefore, for these temporary electricity grids, AWES are the perfect solution. The other components of the HPP are easily transported as well.

Examples of locations where a (temporal) microgrid is installed are mines and oil and gas fields. These sites are usually in operation for fifteen years before depleting resources. Currently, almost all electricity is generated using diesel generators at these sites. As can be seen in section 4, the HPP has already a strong case for a location within Europe. These mining and drilling sites are usually situated around the equator, where even more solar resource is available. Locating the sites where much wind is available at operating altitude could offset diesel generators entirely by installing HPPs.

An example of how an abundant supply of cheap electricity could help the energy transition is through electrification of the haul trucks used at the mines, image shown in figure 5.1. Most of these haul trucks are propelled using diesel-electric propulsion. Multiple diesel engines drive an electric generator to produce the electricity to drive the electric engines [62]. Electric engines are used because they produce more torque than fossil fuel engines. When abundant electricity is available, the diesel engine and electric engine in the haul trucks can be replaced with batteries that will drive the electric engines. Companies are already considering making a zero-emission vehicle fleet to produce carbon-neutral raw materials [63].

Figure 5.1: Image of a haul truck used at the mine sites [63].

5.2 Location Analysis

In collaboration with Enerwhere [64], three locations in Africa and the Middle East are identified using the global solar and wind atlas, where mining/drilling sites have abundant resources. Enerwhere invests in temporary micro-grids, offsetting diesel by replacing its electricity generation by solar electricity generation. Currently, Enerwhere is investigating the opportunity of using AWESs in the micro-grids. The three locations, shown on a map in figure 5.2, are:

A Basra - Iraq (30.56N; 47.25E)

B Haima - Oman (19.97N; 56.27E)

C Mako - Senegal (12.86N; 12.39W)

Figure 5.2: Map of Africa and the Middle East indicating the locations. A: Basra - Iraq, B: Haima - Oman, C: Mako - Senegal [65].

Locations A and B are oil drilling sites, while location C is a gold mine. The diesel prices differ from location to location. This affects the use of diesel generators in the HPP and, therefore, also on the overall component sizing. The diesel price in Oman is 0.69 €/L, while in Iraq and Senegal, the diesel price is 1.10 €/L [66]. The carbon tax is only valid for Europe. Therefore in these cases, it will not be considered. The cost of the AWES is kept the same as for Marseille, while the solar cost for all three locations is decreased to 644 €/kWp [66].

5.2.1 Load Data

Drilling happens 24/7, 365 days a year at most oil drilling sites. A land rig, seen in figure 5.3, is constantly drilling for oil while the operating crew takes shifts. To create a load case for all three business cases, a constant load of 1 MW is assumed. This number gives a good estimation and is easily scaled up and down. As just mentioned, a constant load can be assumed [66].

Figure 5.3: Image of a land oil rig used in the onshore oil and gas industry [67].

5.2.2 Resource Data

The solar and wind resource data is downloaded for 2017-2019 for all three locations. These three years represent all the years over the lifetime of the project, which is equal to25 years, the lifetime of the solar modules and the ground station of the AWES. Commonly, the lifetime of a mine or oil field is less than these 25 years. However, the HPP can be packed up and moved to the next location where it is necessary. The resource data is not averaged over the three years because the peaks in data due to a storm or a few consecutive days without wind make the HPP sized for more real-life situations.

In figure 5.4, the total solar irradiance for all three locations is given. It can be seen that for all three locations, but mainly in Iraq, there is still a seasonal trend. The fact that the peaks in irradiance are halfway through the years indicates that all three locations are in the northern hemisphere. Moreover, the difference between summer and winter is least present in Senegal, the country closest to the equator, and most present in Iraq, the most northern country of the three.

The solar irradiance of different locations can be compared by the equivalent sun hours (ESH). The ESH is equivalent to the average GHI of a location given in kWh/m^2/day [21]. The ESH of Iraq is equal to 5.3, of Oman 6.4 and the location in Senegal 5.6. This means that when a HPP is sized for the different locations only containing solar modules, Oman would need the tiniest amount while Iraq would need the most. More could be said about combining the two different generation methods when the wind data is added.

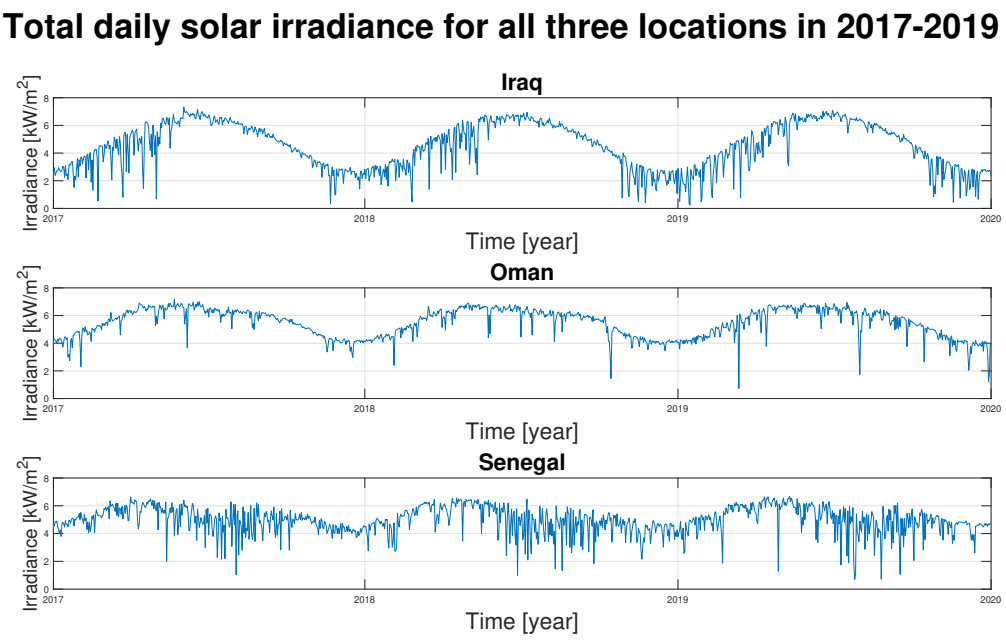

Figure 5.4: The daily solar irradiance for all three locations for three years.

Figure 5.5 gives the hourly wind speed for the three locations from 2017 to 2019. The seasonal variation is not as present as it was with the solar irradiance graph in figure 5.4. The average wind speeds are calculated to compare the different locations on their wind resource. In Iraq, the average wind speed is 7.5 m/s, in Oman 6.3 m/s, and in Senegal 5.6 m/s at an altitude of 320 m. For the wind resource comparison, more information is necessary than crude averages. The fraction of time the wind is below cut-in or above cut-out and the fraction between rated and cut-out wind speeds are all interesting values to evaluate the three locations further. This is done later in the chapter when the HPP is sized.

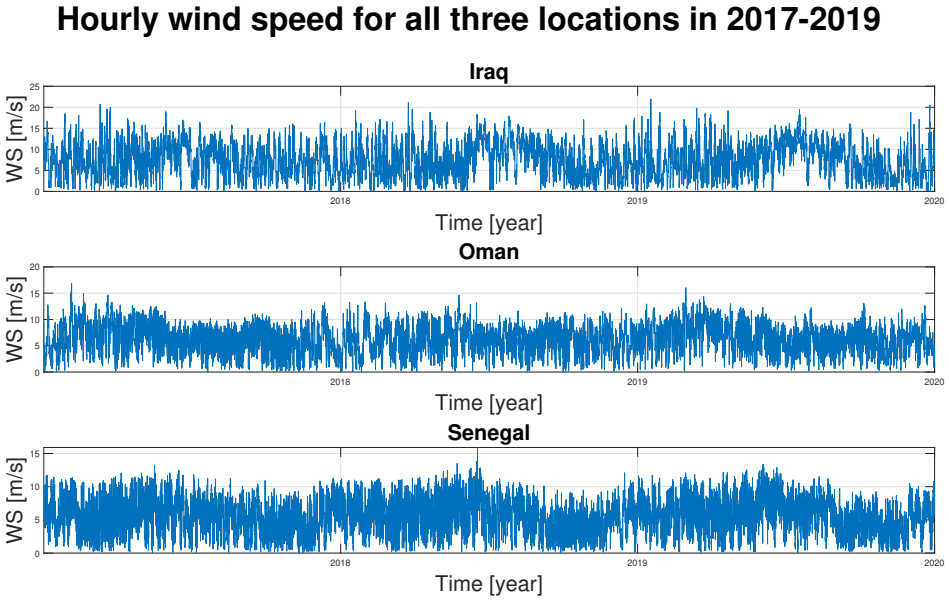

Figure 5.5: The hourly wind speed for all three locations for three years.

To compare the seasonal variation in the solar and wind resource, trend lines have been made to see the seasonal (anti-)correlation between the resources. As can be seen in figure 5.6, actually, for all three locations, on a seasonal resolution, the resources are significantly correlated. The fluctuations in the solar resources are not as strong as they were in the location analysis of section 3.2.2 since the locations analysed in the business case are closer to the equator. The fact that the resource data is positively correlated on a seasonal resolution means that the batteries and diesel generators need to fill in the gap left by the resources.

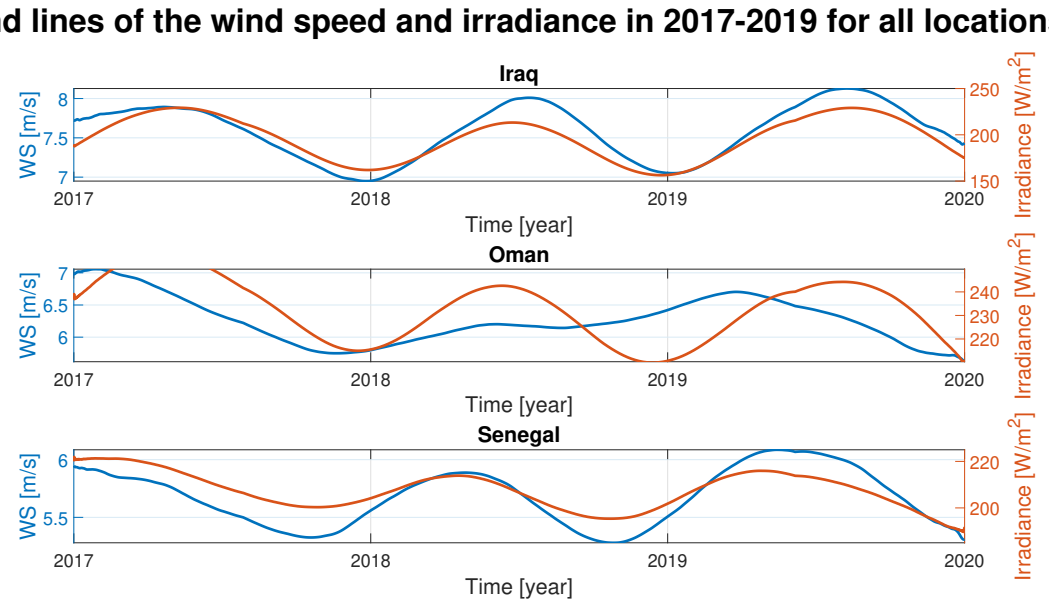

Figure 5.6: The trend lines of the wind speed and irradiance in all three locations for three years.

5.2.3 Pearson Correlation Coefficients

The Pearson correlation coefficients are calculated for the three locations for an hourly and daily period, given in table 5.1. What can be seen is that the correlation is negative for all three locations on an hourly resolution. Especially in Senegal, there is a strong anti-correlation between wind and solar resources. This strong anti-correlation will contribute to a decrease in the oversizing of the components. Since the load data is constant, Pearson correlation calculations cannot be done because the variance is equal to zero.

Table 5.1: The Pearson correlation coefficients between wind and solar on an hourly and daily resolution for all three locations.

Location	Resolution	Wind & Solar
Iraq	hourly	-0.13
	daily	0.24
Oman	hourly	-0.34
	daily	0.13
Senegal	hourly	-0.41
	daily	0.12

5.3 Annual Energy Production

The annual energy production for both solar and wind energy is evaluated in this section. The complete analysis is given in section 3.3 and section 3.4. Therefore, the analysis results are given, and some crucial differences between the business locations and Marseille are highlighted.

5.3.1 Solar Energy

It is expected that solar energy will be higher for the three business-case locations than what was seen with Marseille. Comparing the ESH of Marseille, which is 4.1, with that of the business-case locations, it can be seen that they are a bit higher. Therefore, fewer modules are needed to produce the same electricity output.

As was analysed in section 3.3.3 and section 3.3.4, the electricity output of the modules is also dependent on the temperature and the irradiance levels. In the business-case locations, the ambient temperature is significantly higher than in the evaluated case of Marseille. This higher ambient temperature negatively affects the energy production of the modules, which is the case for Oman, as can be seen in figure 5.7. The irradiance levels are higher than in the Marseille case. However, the temperature difference dominates the effect on efficiency and, therefore, energy production.

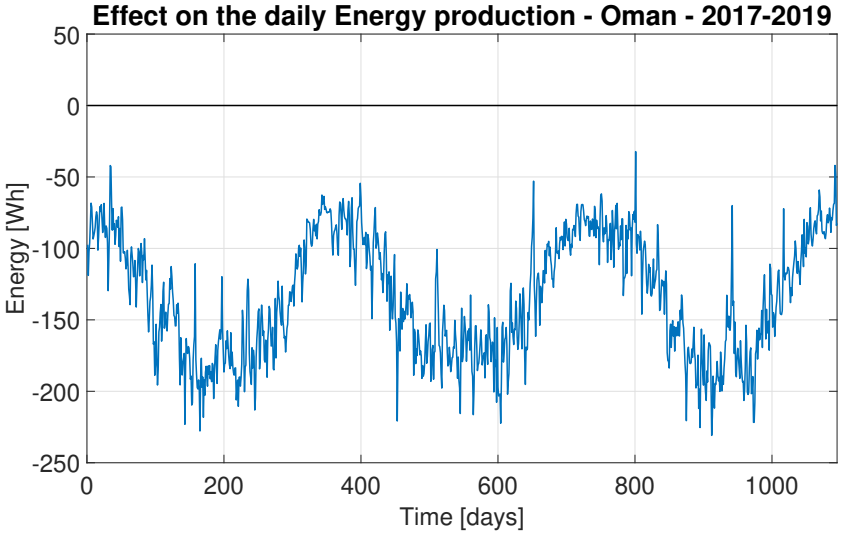

Figure 5.7: The effect of the temperature and irradiance on the daily energy production of one solar module.

The AEP of one solar module for the three different locations, with the corresponding capacity factor (CF) and levelized cost of electricity (LCoE), is calculated and given in table 5.2. It can be seen that the location with the highest ESH yield the highest AEP and CF and, therefore, the lowest LCoE. Different solar modules react differently to the effect of temperature. In this research, only one type of module is considered. Changing the modules for a type that is better suited for these hot conditions would yield an even higher AEP. The LCoE of all three locations is very low but sounds sane compared to the literature [49]. The LCoE calculation is done for a grid-connected case. When the solar modules are used in the off-grid situation, the LCoE will increase since batteries and diesel generators are considered.

Table 5.2: The ESH, AEP, CF, and LCoE of one solar module for the three different locations.

Location	**ESH [kWh/m^2/day]**	**AEP [kWh/year]**	**CF [%]**	**LCoE [€/MWh]**
Iraq	5.3	436	14.9	36
Oman	6.4	531	18.1	30
Senegal	5.6	481	16.4	33

5.3.2 Wind Energy

Similar calculations that were done for the annual solar energy production are done for the wind energy, and the results are given in table 5.3. Even though it has a lower mean wind speed than Marseille, Oman shows a higher AEP. This probably has to do that the wind speed being more constant at high altitudes, resulting in less negative energy yield when the wind speed is below the cut-in wind speed. Moreover, looking at the wind speed for all three locations, the wind speed never exceeds the cut-off wind speed of 25 m/s. It is clear that the location with the highest mean wind speed, Iraq, has the highest AEP and, therefore, the lowest LCoE. The following section determines how these results translate into the component sizing of the HPP for each location.

Table 5.3: The mean wind speed, AEP, CF, and LCoE of one Kitepower Falcon kite for the three different locations.

Location	**Wind Speed [m/s]**	**AEP [MWh/year]**	**CF [%]**	**LCoE [€/MWh]**
Iraq	7.5	549	62.6	139
Oman	6.3	492	56.1	155
Senegal	5.6	424	48.3	180

5.4 Optimised Hybrid Power Plant

Once the resources are analysed, the HPP can be sized. First, the electricity price is calculated based on the diesel price. The LCoE of a 100% diesel-generated system is used to compare the HPP, which is evaluated per location in the following subsections.

5.4.1 Diesel Generation

Before sizing the HPP, the LCoE is calculated for the stand-alone systems as if they only consist of diesel generators, as is still the case for most mining and drilling sites. This number is used as the value for calculating another economic KPI for the business case, the internal rate of return (IRR). The diesel price in Iraq and Senegal is 1.10 €/L, and in Oman, it is 0.69 €/L. Moreover, the carbon tax is not considered for these locations.

The power rating of the diesel generator is 1 MW for both a fully diesel-generated system and the optimal HPP. For the optimally sized HPP, the diesel generated electricity is produced when no/barely any power is generated with the renewable components. Hence the maximum mismatch is 1 MW (no renewable generation and the constant load of 1 MW).

In table 5.4, the diesel price with the corresponding LCoE for the three locations is given. Since Iraq and Senegal have the same diesel price, they have the same LCoE of 469 €/MWh. Oman has cheaper diesel, which results in a lower LCoE of 295 €/MWh. These LCoE values will be used as electricity prices when comparing the HPP with these 100% diesel generation systems.

Table 5.4: The diesel price and LCoE for an all diesel generated system for all three locations.

Location	Diesel Price [€/L]	LCoE [€/MWh]
Iraq	1.10	469
Oman	0.69	295
Senegal	1.10	469

5.4.2 Iraq

The first analysed location is Basra in Iraq. The result of optimising the HPP with all components, including diesel generation optimisation (DGO), which is partly supplied by the diesel generators, is given in the first row of table 5.5. The LCoE of this optimised HPP is 169 €/MWh, which is super competitive when compared to the 469 €/MWh of purely diesel generation given in section 5.4.1. Moreover, the IRR of the project is 27.8%, which is a reasonable rate of return for angel investors [68].

The amount of electricity generated by the diesel generator for three years is equal to 1,297 MWh, which is around 5%. Due to the introduction of the diesel generator, the battery capacity can go under the state of charge limit, resulting in a higher energy yield from the renewable generating components of the HPP.

When no use of diesel is allowed, the LCoE increases to 251 €/MWh, a 49% increase. The most significant change can be seen in the battery capacity, which more than doubles, an increase of 130%. Moreover, the battery power for the optimally sized HPP is 10.5 MW, and in the no diesel case, 11.1 MW. Finally, the result shows that in Iraq, when diesel is not used in the HPP, AWES will take over that part of the electricity generation.

Table 5.5: A comparison in the component sizing between a system in Iraq with zero and optimal diesel generation with corresponding LCoE and IRR.

Sized for	Solar Power [MWp]	Wind Power [MW]	Battery Capacity [MWh]	Diesel Generation [%]	LCoE [€/MWh]	IRR [%]
Optimal	14.7	0.1	18.1	5	169	27.8
No Diesel	15.0	0.5	41.0	0	251	19.2

5.4.3 Oman

As was determined in section 5.3.1, the solar irradiance, and therefore the annual solar energy production, in Haima, Oman, is the highest of the three locations. This leads to the fact that the optimally sized HPP only consists of solar modules, batteries, and diesel generators, as can be seen in table 5.6. Compared to the Iraq case, less solar energy and battery capacity are installed, yet the load loss is also smaller. Moreover, the diesel price is the lowest out of the three locations, which, together with the high solar AEP, yields a very low LCoE of 109 €/MWh. The electricity generated with the diesel generator, in this case, is equal to 1,029 MWh, or 4%.

The LCoE is the lowest out of the three locations. However, the IRR is, although still high, not the highest. This is because the electricity cost savings, calculated in section 5.4.1, is lower than the other two locations. Even when there is 100% diesel offset, no airborne wind energy (AWE) is used. The solar and the battery capacity are almost doubled, resulting in an increase of LCoE to 193 €/MWh, a 77% increase. The battery power for the HPP with and without diesel generation is 5.7 MW and 11.3 MW, respectively.

Table 5.6: A comparison in the component sizing between a system in Oman with zero and optimal diesel generation with corresponding LCoE and IRR.

Sized for	Solar Power [MWp]	Wind Power [MW]	Battery Capacity [MWh]	Diesel Generation [%]	LCoE [€/MWh]	IRR [%]
Optimal	8.0	0	17.9	4	109	27.0
No Diesel	14.7	0	36.9	0	193	13.2

5.4.4 Senegal

The final evaluated location is the gold mine in Mako, Senegal. The strongest anti-correlation of -0.41 on an hourly resolution was determined for this location. This anti-correlation on an hourly resolution shows in the optimisation of the HPP. Although Senegal had the lowest mean wind speed, the optimised HPP has the highest installed wind power of 0.3 MW, as is given in table 5.7. The installed solar power is the same as in Oman, but the battery capacity and diesel generation are smaller because more wind power is installed now. The amount of electricity generated by diesel is only 543 MWh, which is 2%.

The LCoE is 127 €/MWh, and the IRR is 38.9%, the highest of the three business cases. When no diesel is used, the installed solar power decreases a little while the installed wind power is used. The battery capacity increases by 43%, which results in a LCoE increase of 61%, to 205 €/MWh. Moreover, the necessary battery power increases slightly from 5.4 MW to 6.4 MW. The IRR is still an excellent rate of return at 29.3%.

Table 5.7: A comparison in the component sizing between a system in Senegal with zero and optimal diesel generation with corresponding LCoE and IRR.

Sized for	Solar Power [MWp]	Wind Power [MW]	Battery Capacity [MWh]	Diesel Generation [%]	LCoE [€/MWh]	IRR [%]
Optimal	9.4	0	18.6	2	127	38.9
No Diesel	8.4	0.9	26.5	0	205	29.2

5.5 Business Case Summary

This chapter evaluates three different locations with the same load profile but different resource data. For all three locations, it can be seen that the combination of solar modules and batteries can take over most of the electricity generation. Even when no diesel generation is allowed, the LCoE for all locations is below the LCoE of 100% diesel generation. This leads to the conclusion that significant investments should be made in solar energy for all locations, which are profitable and benefit the environment. An overview of the LCoE of the three business case locations is given in figure 5.8, where the blue bar is the optimally sized HPP, and the orange bar represents the HPP without diesel generation.

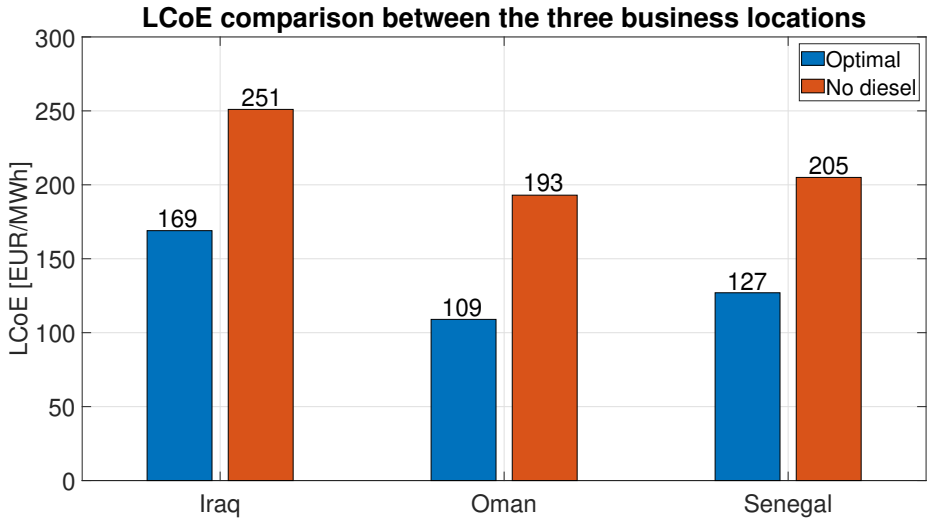

Figure 5.8: The comparison in LCoE for the three business case locations; the blue bars indicate the optimally sized HPP and the orange bars the HPP with diesel generation excluded.

When looking at the added value of AWE in a HPP, it follows that in two out of the three locations, the addition of AWE drives the LCoE down and increases the IRR. Where the added value of AWE in Iraq for an optimally sized HPP was only marginal, the added value in Senegal was clearly showing when diesel generation is not considered. It is concluded that a strong anti-correlation on an hourly resolution increases the use of AWE, even though it is generally more expensive than solar energy. However, although there is anti-correlation between the resources on an hourly resolution, there is a point for which solar energy is so cheap that there is no use for AWE in a HPP, as was the case for Oman.

The optimally sized HPP in Oman achieved the lowest LCoE, as can be seen in figure 5.8. However, that is not the best location to roll out this business case. If not by the HPP, the electricity in Oman would have been generated by super cheap diesel. This results in still high but a lower IRR than is the case for the gold mine site in Senegal. Therefore the best locations for the HPP are locations where the diesel price is not too low, the solar energy is abundant but not extremely high, a strong wind resource, and there is a noticeable anti-correlation between the solar and wind resource. Nonetheless, the HPP makes a strong case in all three locations and shows the potential in the energy transition that could be achieved for these three remote, off-grid locations.

6 Conclusions

This thesis aimed to model and size a hybrid power plant (HPP) using airborne wind energy (AWE) as one of its components. In the model, which was made in MATLAB, the performance and cost of the four components of the HPP were evaluated, which are AWE, solar photovoltaic (PV) energy, diesel generators, and a storage solution in the form of batteries. A system optimiser was built to optimise the component sizing of the HPP for the minimal levelized cost of electricity (LCoE). The model results were evaluated and reflected upon, after which a sensitivity analysis was done to the cost of the most critical aspects of the HPP. To evaluate the HPP, a business case where the HPP was used in three different locations was analysed.

In this research different combinations of the four components of the HPP are evaluated. The batteries play a role in both the short-term and long-term energy storage. In most cases, the HPP was dominated by solar energy, which resulted in an intense day and night energy generation difference. The batteries were primarily used to cover this intermittency. Moreover, the solar generation showed a solid seasonal dependency too. This meant that the sizing of the batteries and installed solar capacity was based on days with the lowest irradiance, usually during the winter.

The added value of AWE in a HPP was visible in locations with strong hourly anti-correlation between the solar and wind resources and where the solar LCoE was sufficiently high. The airborne wind energy system (AWES) made it possible to significantly reduce the battery's capacity and, therefore, the LCoE of the HPP for most locations. The essential advantage of the AWES over conventional wind turbines is the mobility of the HPP, which is vital for the HPP to be used in locations where temporary electricity is desired.

The anti-correlation between the wind and solar resources was analysed for the different locations. In Europe, a strong anti-correlation was visible between the resources on a seasonal time scale. On a daily scale, all four European locations showed a negative correlation. However, a weak positive and negative correlation was observed on an hourly resolution. The opposite was true for the business case sites in Africa and the Middle East. A strong correlation was observed on a seasonal time scale. On a daily scale, all three locations were mildly positively correlated, while all three were negatively correlated on an hourly resolution. It was concluded that a strong anti-correlation on an hourly resolution is the most beneficial for using both AWE and solar PV while driving the LCoE down.

A HPP sized for off-grid markets is entirely different from a grid-connected utility-scale HPP when sizing for the LCoE. Solar energy was at least three times cheaper than AWE in all evaluated cases when storage was not considered. When a grid-connected HPP was evaluated, storage would not be considered. The configuration would always show a 100% solar energy configuration since the LCoE of solar energy was cheaper. Moreover, the cost savings due to shared infrastructure were only a tiny fraction (about a per cent) of the total cost due to the weak anti-correlation between the resources. Even with a perfect anti-correlation, the cost savings on shared infrastructure were minimal.

For an off-grid HPP, the configuration of the HPP would be utterly different from a grid-connected HPP. In this case, all electricity demand needed to be supplied by the HPP, which resulted in the need for batteries. The two different electricity generation types, depending on different resources, would complement each other, resulting in a decrease in component sizing and, therefore, LCoE. The business case locations have shown that a 100% renewable HPP is most definitively competitive with diesel generated plants. Moreover, the LCoE was even further decreased when a diesel generator was added to the HPP.

The LCoE of almost every evaluated HPP would significantly decrease if a combination of solar and wind energy was used. The battery's capacity was greatly reduced, and the generating components of the HPP were less oversized. By introducing a diesel generator to the HPP, the LCoE would further decrease, and the HPP optimised. Therefore, the value of a HPP is significantly higher than the stand-alone systems. By setting different objectives for the HPP, the sizing of the components changed. The most significant difference was experienced whether diesel generation was considered or not. In case diesel was considered, the other components of the system would be significantly oversized, increasing the LCoE. The most significant LCoE increase for the business case was found in Oman, where the LCoE increased by 77% if diesel generation was not considered.

Future research
This thesis gave the first insights into the modelling and sizing of a HPP using AWE. The results are promising and encouraging to continue the work done in this thesis. For further research, this study recommends three things. Firstly, it would be interesting to investigate how the LCoE and other objectives of the HPP would change when different component types are used. For the business case, the only key performance indicators evaluated were the LCoE and the internal rate of return. Future research could investigate sizing for optimal capacity factor or maximum levelized profit of electricity.

Secondly, the analysed locations are based on a crude calculation of the solar and wind resources and the necessity of temporary electricity. Locations with abundant anti-correlated solar and wind resources show the most promise. By identifying these hot spots, the more optimal configurations of the HPP can be achieved, resulting in the decrease of curtailment and battery capacity. By placing and sizing the HPP for optimal locations, the LCoE can be further minimised. Moreover, for the AWES, when there are consecutive hours of wind speed between zero and cut-in, the kite stays up in the air, resulting in negative energy production. For these longer periods of negative energy production, landing and relaunching of the kite should be considered.

Finally, many estimations have been made with the calculations of this thesis. The input variables could be improved with more time, and more confident results can be evaluated. For example, since diesel generation plays a significant role in most of the optimal HPP configurations, more extensive research in the electricity yield per liter should be done. This will yield a more accurate use of diesel and the optimal configuration can be improved.

References

[1] Ryan Wiser et al. "Expert elicitation survey predicts 37% to 49% declines in wind energy costs by 2050". In: *Nature Energy* 6 (2021), pp. 555–565. DOI: 10.1038/s41560-021-00810-z.

[2] Philip Bechtle et al. "Airborne wind energy resource analysis". In: *Renewable Energy* 141 (Oct. 2019), pp. 1103–1116. ISSN: 18790682. DOI: 10.1016/j.renene.2019.03.118.

[3] Antonello Cherubini et al. *Airborne Wind Energy Systems: A review of the technologies*. Aug. 2015. DOI: 10.1016/j.rser.2015.07.053.

[4] Antonello Cherubini et al. "Airborne Wind Energy Systems: A review of the technologies". In: *Renewable and Sustainable Energy Reviews* 51 (2015), pp. 1461–1476. DOI: 10.1016/j.rser.2015.07.053.

[5] Roland Schmehl. *Airborne Wind Energy PowerWeb webinar lecture*. Available at https://airbornewindeurope.org/wp-content/uploads/2020/06/20200520-Powerweb.pdf (29-06-2022). 2020.

[6] Dan Tong et al. "Geophysical constraints on the reliability of solar and wind power worldwide". In: *Nature Communications* 12 (2021). DOI: 10.1038/s41467-021-26355-z.

[7] Kitepower. *Kitepower Falcon*. Available at https://thekitepower.com/product/ (22-05-2022).

[8] Józef Paska, Piotr Biczel, and Mariusz Kłos. "Hybrid power systems - An effective way of utilising primary energy sources". In: *Renewable Energy* 34.11 (Nov. 2009), pp. 2414–2421. ISSN: 09601481. DOI: 10.1016/j.renene.2009.02.018.

[9] WindEurope. *Database for wind + storage co-located projects*. Available at https://windeurope.org/about-wind/database-for-wind-and-storage-colocated-projects/ (03-06-2022).

[10] Wind Logger. *How Does Cold Weather Affect Wind Speed?* Available at https://www.windlogger.com/blogs/news/how-does-cold-weather-affect-wind-speed (09-02-2022).

[11] Robert Fajber, Adam H. Monaham, and William J. Merryfield. "At What Time of Day Do Daily Extreme Near-Surface Wind Speeds Occur?" In: *Journal of Climate* 27.11 (2014), pp. 4226–4244. DOI: 10.1175/JCLI-D-13-00286.1.

[12] F.M. Mulder. "Implications of diurnal and seasonal variations in renewable energy generation for large scale energy storage". In: *Journal of Renewable and Sustainable Energy* 6.3 (2014), pp. 033105-1–033105-13. DOI: 10.1063/1.4874845.

[13] Ashkan Edrisian et al. "The New Hybrid Model of Compressed Air for Stable Production of Wind Farms". In: *International Journal of Emerging Technology and Advanced Engineering* 3.11 (2013), pp. 37–43.

[14] Starlight Generator. *What Is the Difference Between AC Gensets And DC Gensets?* Available at https://medium.com/@dieselgenerator/what-is-the-difference-between-ac-gensets-and-dc-gensets-72fc330b1841 (07-06-2022).

[15] Noun Project Inc. *Icons and Photos For Everything*. Available at https://thenounproject.com/ (23-05-2022).

[16] R. de la Garza Cuevas. *Kite power in a microgrid*. Master Thesis at Delft University of Technology. 2018. URL: http://repository.tudelft.nl/.

[17] European Commission. "Study on Challenges in the commercialisation of airborne wind energy systems". In: (). DOI: 10.2777/933106. URL: http://europa.eu.

[18] Udo Zillmann and Philip Bechtle. "Emergence and economic dimension of airborne wind energy". In: *Green Energy and Technology*. Vol. 0. 9789811019463. Springer Verlag, 2018, pp. 1–25. DOI: 10.1007/978-981-10-1947-0{_}1.

[19] James Conca. *Do We Have The Raw Materials For The World To Become 80% Renewable by 2050?* Available at https://www.ourenergypolicy.org/do-we-have-the-raw-materials-for-the-world-to-become-80-renewable-by-2050/ (10-02-2022).

[20] Elena C. Malz et al. "The value of airborne wind energy to the electricity system". In: *Wind Energy* 25.2 (2022), pp. 281–299. DOI: 10.1002/we.2671.

[21] Arno Smets et al. *Solar Energy: The physics and engineering of photovoltaic conversion, technologies and systems*. English. UIT Cambridge Limited, 2016. ISBN: 978-1-906860-32-5.

[22] Christos Chalkias, Antigoni Faka, and Kleomenis Kalogeropoulos. "Assessment of the Direct Sun-Light on Rural Road Network through Solar Radiation Analysis Using GIS". In: *Open Journal of Applied Sciences* 3.2 (2013), pp. 224–231. DOI: 10.4236/ojapps.2013.32030.

[23] Tesla. *Powerpack - Commercial and Utility Energy Storage Solutions*. Available at https://www.tesla.com/powerpack (06-05-2022).

[24] V.M. Fthenakis and T.Nikolakakis. "1.11 - Storage Options for Photovoltaics". In: *Comprehensive Renewable Energy* 1 (2012), pp. 199–212. DOI: 10.1016/B978-0-08-087872-0.00106-2.

[25] Wesley Cole, A. Will Frazier, and Chad Augustine. *Cost Projections for Utility-Scale Battery Storage: 2021 Update*. Tech. rep. Golden, CO, 2021.

[26] Catherine Lane. *Are lithium ion solar batteries the best energy storage option?* Available at https://www.solarreviews.com/blog/are-lithium-ion-the-best-solar-batteries-for-energy-storage (06-05-2022).

[27] Jordan Hanania et al. *Energy Education - Diesel generator*. Available at https://energyeducation.ca/encyclopedia/Diesel_generator (06-05-2022).

[28] Eurostat. *Average prices of diesel fuel in the Netherlands from 2000 to 2021*. Available at https://www.statista.com/statistics/603745/diesel-fuel-prices-netherlands/ (06-05-2022).

[29] Lazard. *Lazard's levelized cost of energy analysis — version 8.0*. Available at https://www.lazard.com/media/1777/levelized_cost_of_energy_-_version_80.pdf (12-05-2022).

[30] IMP. *The lifespan of your diesel generator: How long will it last?* Available at https://www.impcorporation.com/blog/the-lifespan-of-your-diesel-generator-how-long-will-it-last (19-05-2022).

[31] PBL. *EU Emissions Trading System: effective and credible way to reduce greenhouse gas emissions, PBL researchers conclude*. Available at https://www.pbl.nl/en/news/2020/eu-emissions-trading-system-effective-and-credible-way-to-reduce-greenhouse-gas-emissions-pbl-researchers-conclude (06-05-2022).

[32] Elke Asen. *Carbon Taxes in Europe*. Available at https://taxfoundation.org/carbon-taxes-in-europe-2021/ (06-05-2022).

[33] PWC. *Green Deal Monitor #4 - National or European taxation of CO2 emissions?* Available at https://www.pwc.nl/en/topics/sustainability/green-deal-monitor/green-deal-monitor-4.html (06-05-2022).

[34] *GLOBAL SOLAR ATLAS*. Available at https://globalsolaratlas.info/map (11-02-2022).

[35] *GLOBAL WIND ATLAS*. Available at https://globalwindatlas.info/ (11-02-2022).

[36] NREL. *NSRDB Data Viewer*. Available at https://maps.nrel.gov/nsrdb-viewer/(21-03-2022).

[37] Mark Z. Jacobson and Vijaysinh Jadhav. "World estimates of PV optimal tilt angles and ratios of sunlight incident upon tilted and tracked PV panels relative to horizontal panels". In: *Solar Energy* 169 (2018), pp. 55–66. DOI: 10.1016/j.solener.2018.04.030.

[38] H. Li, J. Harvey, and A. Kendall. "Field measurement of albedo for different land cover materials and effects on thermal performance". In: *Building and Environment* 59 (2013), pp. 536–546. DOI: 10.1016/j.buildenv.2012.10.014.

[39] Sandia National Laboratories. *$pvl_g etaoi$*. Available at https://pvpmc.sandia.gov/PVLIB_Matlab_Help/ (09-04-2022).

[40] Dirk C. Jordan and Sarah R. Kurtz. *Photovoltaic Degradation Rates - An Analytical Review*. Available at https://www.nrel.gov/docs/fy12osti/51664.pdf (10-04-2022).

[41] Sami Ekici and Mehmet Ali Kopru. "Investigation of PV System Cable Losses". In: *International Journal of Renewable Energy Research* 7.2 (2017), pp. 808–815.

[42] Rte. *Solar power Generation*. Available at https://bilan-electrique-2020.rte-france.com/solar_power/(13-04-2022).

[43] Laura Rodriguez. *Breaking down solar farm costs*. Available at https://ratedpower.com/blog/solar-farm-costs/ (13-04-2022).

[44] Statista. *Average installed cost for solar photovoltaics worldwide from 2010 to 2020*. Available at https://www.statista.com/statistics/809796/global-solar-power-installation-cost-per-kilowatt/(26-04-2022).

[45] Zeeshan Hyder. *Utility-scale solar: what is it, how does it work?* Available at https://www.solarreviews.com/blog/how-does-utility-scale-solar-work(26-04-2022).

[46] William Driscoll. *PV plants lasting longer, with lower operational costs*. Available at https://www.pv-magazine.com/2020/06/03/pv-plants-lasting-longer-with-lower-operational-costs/(13-04-2022).

[47] IEA. *LCOE of utility-scale solar PV and onshore in 2020 and in the high commodity price scenario*. Available at https://www.iea.org/data-and-statistics/charts/lcoe-of-utility-scale-solar-pv-and-onshore-in-2020-and-in-the-high-commodity-price-scenario(13-04-2022).

[48] IRENA. *Renewable Power Generation Costs in 2019*. Tech. rep. Abu Dhabi, 2020.

[49] Manish Ram et al. "A comparative analysis of electricity generation costs from renewable, fossil fuel and nuclear sources in G20 countries for the period 2015-2030". In: *Journal of Cleaner Production* 199 (2018), pp. 687–704. DOI: 10.1016/j.jclepro.2018.07.159.

[50] Johannes Peschel. Private email correspondence. 2022.

[51] ERA5. *ERA5 hourly data on pressure levels from 1979 to present*. Available at https://cds.climate.copernicus.eu/(02-02-2022).

[52] Lavinia Thimm. *Contract Study - TU Delft and Uniper (20-05-2022)*.

[53] Mark Schelbergen and Roland Schmehl. "Validation of the quasi-steady performance model for pumping airborne wind energy systems". In: *Journal of Physics: Conference Series* 1618 (2020). DOI: 10.1088/1742-6596/1618/3/032003.

[54] Peter D. Yeh. *Six Degrees of Freedom (6DOF) Simulations of Supersonic Fragment Trajectories*. Tech. rep. Albuquerque, New Mexico, 2020.

[55] RenewablesFirst. *How much wind energy could I generate from a wind turbine?* Available at https://www.renewablesfirst.co.uk/windpower/windpower-learning-centre/how-much-energy-could-i-generate-from-a-wind-turbine/(27-04-2022).

[56] Pietro Faggiani. *Pumping Kites Wind Farm*. Master Thesis at Delft University of Technology. 2014.

[57] Alan McDonald and Leo Schrattenholzer. "Learning rates for energy technologies". In: *Energy Policy* 29 (2001), pp. 255–261. DOI: 10.1016/S0301-4215(00)00122-1.

[58] Edward S. Rubin et al. "A review of learning rates for electricity supply technologies". In: *Energy Policy* 86 (2015), pp. 198–218. DOI: 10.1016/j.enpol.2015.06.011.

[59] entseo. *Total Load - Day Ahead / Actual*. Available at https://transparency.entsoe.eu/load-domain/r2/totalLoadR2/show (12-03-2022).

[60] Energymag. *Daily energy demand curve*. Available at https://energymag.net/daily-energy-demand-curve/ (29-04-2022).

[61] IRENA. *Renewable Power Generation Costs in 2020*. Tech. rep. Abu Dhabi, 2021.

[62] Professional Mariner Staff. *Diesel-electric propulsion pushes ahead*. Available at https://professionalmariner.com/diesel-electric-propulsion-pushes-ahead/ (26-05-2022).

[63] Equipment Journal. *Teck and Caterpillar strike deal to deploy zero-emission large haul trucks*. Available at https://www.equipmentjournal.com/construction-news/teck-and-caterpillar-strike-deal-to-deploy-zero-emission-large-haul-trucks/ (26-05-2022).

[64] Enerwhere. *Enerwhere sustainable energy*. Available at https://www.enerwhere.com/ (29-06-2022).

[65] George Friedman. *5 Maps of the Middle East and North Africa That Explain This Region*. Available at https://www.mauldineconomics.com/editorial/5-maps-of-the-middle-east-and-north-africa-that-explain-this-region (26-05-2022).

[66] Daniel Zywietz. Private meeting conversation. 2022.

[67] Monitor Systems Scotland Ltd. *Land Rigs*. Available at https://www.monitor-systems-engineering.com/land-rigs.html (27-05-2022).

[68] Propel(x) Team. *What is the Internal Rate of Return (IRR) and why does it matter when investing in startups?* Available at https://www.propelx.com/blog/internal-rate-of-return-and-importance-when-investing-in-startups/ (29-05-2022).

[69] Panasonic. *Photovoltaic module HIT*. Available at https://www.europe-solarstore.com/download/panasonic/panasonic_VBHN335SJ53_datasheet.pdf(13-04-2022).

A Solar module data sheet

HIT® +
Photovoltaic Module

Panasonic

Photovoltaic module HIT® N340/N335

Panasonic's unique heterojunction technology uses ultra-thin amorphous silicon layers. These thin dual layers reduce losses, resulting in higher energy output than conventional panels.

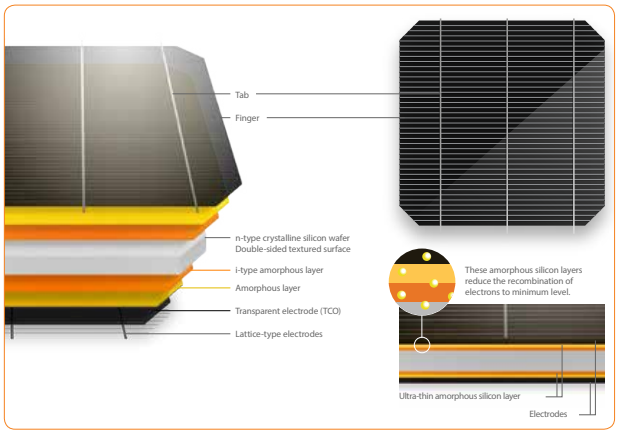

Our powerful Panasonic HIT® N340 features a high module efficiency of 20.4%, an industry leading temperature coefficient of -0.258% /°C and a sleek design. **Powerful and efficient, designed to get the most out of your roof!**

Our competitive advantages

High Performance at High Temperatures
As temperature increases, HIT® continues to perform at high levels due to the industry leading temperature coefficient of -0.258% /°C. No other module even comes close to our temperature characteristics. That means more energy throughout the day and particularly in summer.

25 Year Product and Performance Guarantee**
Industry leading 25 year product workmanship and performance guarantee is backed by a century old company - Panasonic.
Power output is guaranteed to 86.2% after 25 years.

Quality and Reliability
Panasonic's vertical integration, over 20 years of experience manufacturing HIT® and 20 internal tests 3-times beyond those mandated by current standards provide extreme quality assurance.

Higher efficiency of 20.4% through improved cells
The HIT+ cells boast an even cleaner junction between the layers of the cells. The cells are manufactured in Japan and offer you an even higher efficiency than the before.

Low Degradation
HIT "N-type" cells result in extremely Low Light Induced Degradation (LID) and zero Potential Induced Degradation (PID) which supports reliability and longevity. This technology reduces annual degradation, guaranteeing more power for the long haul.

Enhanced Frame Design
A 40mm frame increases durability and strength, being able to handle loads of up to 5400Pa. Also, the water drainage system gives rain water and snow melt a place to go, reducing water stains and soiling. Less dirt on the module means more sunlight getting through to generate power.

HIT® is a registered trademark of Panasonic Group

Panasonic [69]

HIT® + Photovoltaic Module

Panasonic

Photovoltaic module HIT® N340/N335

ELECTRICAL SPECIFICATIONS

Model	VBHN340SJ53	VBHN335SJ53
Maximum Power (Pmax)[1]	340W	335W
Maximum Power Voltage (Vpm)	59.7V	59.4V
Maximum Power Current (Ipm)	5.70A	5.65A
Open Circuit Voltage (Voc)	71.3V	71.0V
Short Circuit Current (Isc)	6.13A	6.08A
Module Efficiency	20.4%	20.0 %
Temperature Coefficient (Pmax)	-0.258%/°C	-0.258%/°C
Temperature Coefficient (Voc)	-0.235%/°C	-0.235%/°C
Temperature Coefficient (Isc)	0.055%/°C	0.055%/°C
NOCT	44.0°C	44.0°C
Maximum System Voltage	1000V	1000V
Series Fuse Rating	15A	15A
Power Tolerance (-/+)	+10%/ 0%*	+10%/ 0%*

MECHANICAL SPECIFICATIONS

Model	VBHN340SJ53, VBHN335SJ53
Internal Bypass Diodes	4 Bypass Diodes
Module Area	1.67m²
Weight	19kg
Dimensions LxWxH	1590mm x1053mm x40 mm
Cable Length +Male/-Female	1020mm/1020 mm
Cable Size / Type	No. 12 AWG / PV Cable
Connector Type	SMK
Static Wind / Snow Load	5400 Pa
Pallet Dimensions LxWxH	1618mm x 1071mm x 2356mm (double stack)
Quantity per Pallet / Pallet Weight	48 pcs. (2x24 pcs.) (960 kg)
Quantity per 40' Container	672 pcs.

OPERATING CONDITIONS & SAFETY RATINGS

Model	VBHN340SJ53, VBHN335SJ53
Operating Temperature	-40°C to 85°C
Safety & Rating Certifications	IEC61215, IEC61730-1, IEC1730-2
Fire Classification	Class Uno
Limited Guarantee	25** years workmanship and power output (linear)***

NOTE: Standard Test Conditions: Air mass 1.5; irradiance = 1000W/m²; cell temp. 25°C

* Maximum power at delivery. For guarantee conditions, please check our guarantee document.

** Registration necessary on www.eu-solar.panasonic.net, otherwise 15 years apply based on guarantee document).

*** 1st year 97 %, from 2nd year -0.45 %/year, in 25th year 86.2%.

[1] STC: Cell temp. 25°C, AM1.5, 1000W/m²

NOTE: Specifications and information above may change without notice.

LINEAR PERFORMANCE GUARANTEE

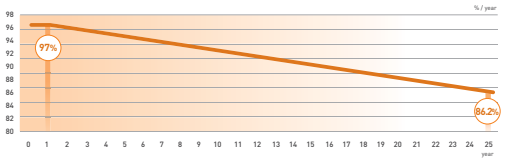

DIMENSIONS

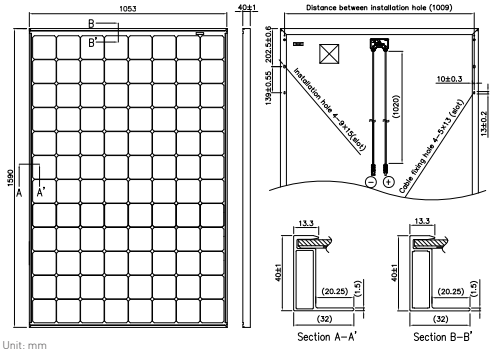

Unit: mm

CERTIFICATES

CLASS UNO
UNI 8457
UNI 9174
UNI 9177

IEC61215
IEC61730-1
IEC61730-2

Electrical Protectio n Class II

DEPENDENCE ON IRRADIANCE

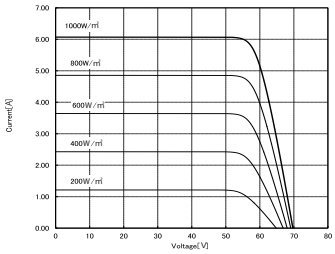

Reference data for model: VBHN340SJ53 (Cell temperature: 25°C)

⚠ CAUTION! Please read the installation manual carefully before using the products.

Used electrical and electronic products must not be mixed with general household waste. For proper treatment, recovery and recycling of old products, please take them to applicable collection points in accordance with your national legislation.

Panasonic

Panasonic Eco Solutions Europe, Panasonic Electric Works Europe AG
Robert-Koch-Straße 100, 85521 Ottobrunn, Germany
Tel. +49 89 45354-1000, Fax +49 89 45354-2111
info.solar@eu.panasonic.com www.eu-solar.panasonic.net

All rights reserved. © 2019 Copyright Panasonic Electric Works Europe AG

03/2019

Panasonic [69]

Introducing The Kitepower Falcon

System Components & Space Requirements

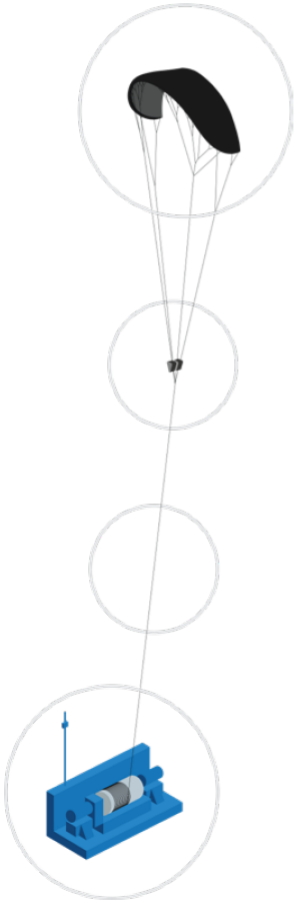

Kite
Consists of an inflatable membrane wing with reinforced tubular frame, forming the best combination for a strong and lightweight wing.

Kite Control Unit (KCU)
Used to steer the kite, control its pulling force and wirelessly connect the sensor unit placed on the kite to the GS.

Tether
Dyneema® line for a lightweight and strong connection between the kite and the GS.

Ground Station (GS)
Converts the mechanical energy of the kite into electrical power and reels the kite in by using the generator as a motor.

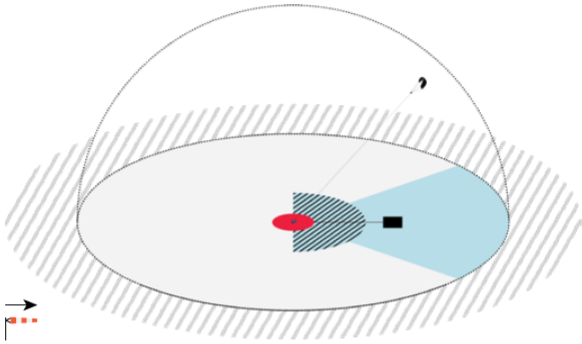

Zone	Dimensions	Dual Land-use[1]
Restricted Zone	30 m (r)	
Flight Zone	300 m (r)	√
Potential Flight Zone	300 m (r)	√
Safety Buffer	400 m (r)	√
Landing Zone	100 m (r)	
Launching Corridor	150x2 m	
Launch Pad	24x12 m	

Obstacles' height within operational envelope:
1m allowance every 10m of distance from the GS

[1] Land can be used for alternative activities while Kitepower is deployed.
(r) = Radius

The Kitepower Falcon

Technical Summary

General Information

Nominal Power Output[1]	100 kW
Yearly Power Output	450 MWh/year
Rated Wind Speed	7 m/s
Cut-in wind Speed	2 m/s
Max Operating Wind Speed	15 m/s
Min Launching Speed	5 m/s
Airborne Wind Range	0-25 m/s
Max Flight Altitude	300 m
Ground Space Required[2] (radius)	300 m

[1] Power output potential might differ depending on the kite variant
[2] The ground space must be free of obstacles

Kite

Variant	V9.60
Size flat (m²)	60 m²
Size projected (m²)	47 m²
Force (t)	3,5 t
Lifetime (hours)	4000h
Avg. Flight Speed (km/h)	110 km/h
Air Traffic Lights	√
Airborne Pump	√
Field Pump	√
Sensor Unit	√
Kite Bags	√
Safety Line	√
Landing Protection	√
Safety Attachment Points	√
Parachute Landing	√

KCU

Weight	23 kg
IP Rating	IP65
Wireless communication link	2 km
Built-in Alarm	90 dB
Airborne Power Supply	√
Protective Cover	√
Air Traffic Lights	√
Airborne Wind Turbine	√
Protection Cover	√
Safety Release	√
Health Supervisor	√

Tether

Type	UHMWPE Dyneema®
Length (default)	450 m
Passive Safety Release	√

Power Curves

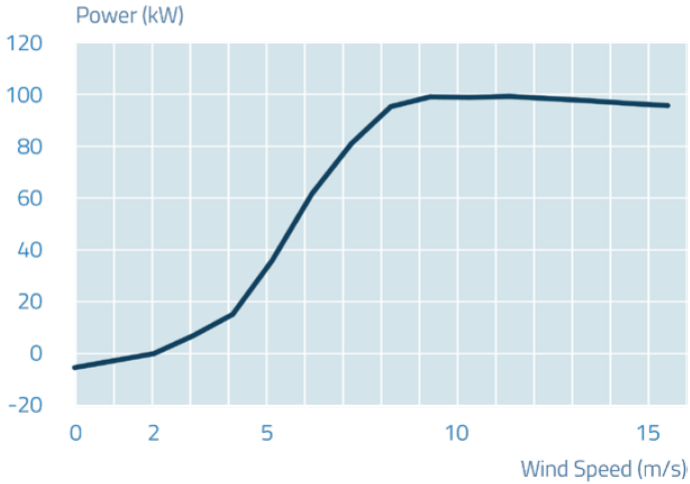

Ground Station

Main Dimensions	W: 2,44 m H: 2,60 m L: 6,06 m
Weight	9.6 t
IP Rating	IP64
Lifetime	25 years
AC Power output	400V AC 3 phase
DC power output	550-700 V
Nominal Power	100kW
Peak Power	120 kW AC / 250 kW DC
Connection mode	Power lock or screw terminals
Built-in Alarm	90 dB
Launch Unit	√
Safety Emergency Stop	√
Health Supervisor	√

+ More information can be found within *The Kitepower Falcon 100kW Technical Specification Document.*